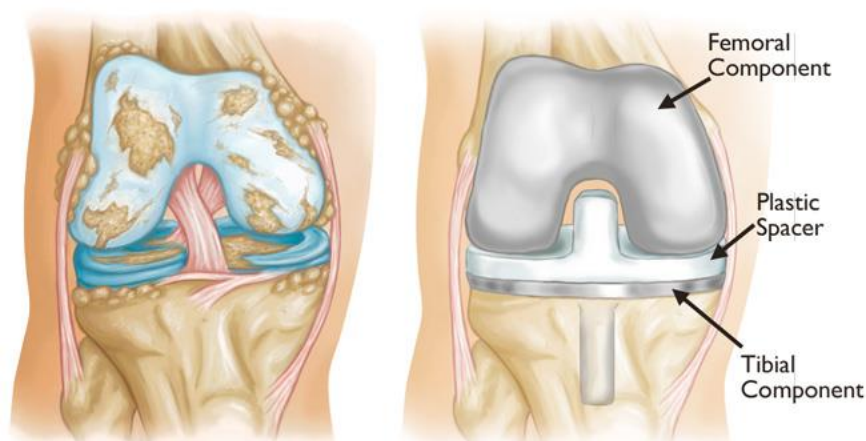


# HYBRID BCR TKA: A NOVEL PROPOSED TIBIAL DESIGN.

## Introduction

### Current TKAs and their limitations

Nowadays, standard procedures for TKR in patients with advanced osteoarthritis (OA) and rheumatoid arthritis (RA) of knee joint, consist in insertion of posterior cruciate substituting (PS) or cruciate retaining (CR) prosthesis.<sup>1,2</sup> Both implants require ACL sacrifice (Fig. 1).



**Figure 1: (Left) Severe osteoarthritis. (Right) A standard total knee arthroplasty TKA and its components.<sup>33</sup>**

Although PS and CR total knee replacements are well established worldwide, approximately 20% of patients who undergo TKA are unsatisfied, a consistently higher percentage than discontent patients after total hip arthroplasty (THA).<sup>3-6</sup> This is surely correlated to the higher expectations of young and active people experiencing TKR.<sup>7</sup> According to dr. Kurtz et al., a 17-fold increase in the number of TKAs in the 45-54 age category, from 59,077 procedures in 2006 to 994,104 procedures in 2030 is anticipated.<sup>3</sup> This young generation aim for a return to demanding activities such as cycling, running and sports trainings and competitions, even at high level, all exercises that strongly require a close to normal knee kinematics and proprioception. However, the current PS and CR prosthesis show many limitations in this direction. On the contrary, unicompartmental knee arthroplasty (UKA), which spares both ACL and PCL, has demonstrated kinematic and proprioceptive outcomes that more closely resemble the normal knee.<sup>8-10</sup> Therefore, it is clear that bicruciate retention might be the key to reduce the gap with satisfaction rates after THA.<sup>10</sup> In this optics, a different approach called bicruciate retaining (BCR) TKA offers a promising solution. BCR TKA, as the name suggests, is a specialized prosthetic implant which preserves both ACL and PCL. BCR prosthesis belongs to the “anatomical approach” aiming to recreate the physiological anatomy of knee joint, juxtaposed to CR and PS designs which focus on functionality instead, hence belonging to the so called “functional approach”.<sup>11,62</sup>

### BCR TKA advantages

Bicruciate retaining designs are supported over ACL-sacrificing ones by many reports in literature. In terms of kinematics,<sup>12-18</sup> BCR TKA demonstrates more normal posterior femoral roll back

during deep bending, compared to a CR TKA, which shows anterior femoral movement on flexion and exaggerated medial condyle translation on deep knee bend instead.<sup>19-21</sup> Anteroposterior laxity has also been shown to be closer to normal in BCR TKA than CR and PS TKA.<sup>19,22</sup> Stiehl et al reported a femorotibial contact close to the tibial midline in full extension in BCR designs similarly to healthy knee, while for CR implants the contact was significantly posterior.<sup>12</sup> Several studies univocally prove satisfying performance of BCR arthroplasties in gait and stair climbing analysis, where CR TKAs revealed extensor moment weakness with forward leaning and decreased stance phase knee flexion, typical of ACL-deficient knees.<sup>12,13,20,23-26</sup> At the same time, it has been shown that in absence of ACL, the PCL and collateral ligaments are abnormally loaded through the ROM, leading to a reduction in femoral rollback by an average of 36% and a 15% loss in extensor efficiency.<sup>27</sup> In posteriorly stabilized PS arthroplasties, both cruciates are extracted and compensated by a post-cam mechanism. This design demonstrated less abnormal kinematics than PCL-retaining TKAs<sup>2</sup>, but still Mahoney et al. shown a 12 % loss in rollback and an 11 % decrease in extensor efficiency.<sup>27</sup> Another kinematic study performed by Stacey M. Acker et al., assessing deep flexion daily activities performed by Asian patients, demonstrated a significantly higher femoral external rotation in PS knees with respect to the normal 20-30° range of normal joints. This is attributable to the absence of ACL constraint during knee motion in PS arthroplasties.<sup>28,29</sup> Furthermore, these functional designs are constraining and forcing the knee motion alone, resulting in higher stresses at the bone-implant interface and therefore possible prosthetic failures. On the other hand, a design which replicates the normal anatomy and spares the knee-stabilizing soft tissues will allow for physiological force transmission through ligaments, reducing the stresses on the implant.<sup>30</sup> In terms of proprioception, several recent researches reported superior outcomes in patients undergoing BCR TKAs rather than CR or PS procedures.<sup>2,8,31-34</sup> In addition to kinematics and proprioception and significantly linked to them are the patient reported outcomes (PROs), describing the patient satisfaction and feelings about the implant. In this context, dr. Pritchett reported that in 440 patients undergoing bilateral TKA with different prosthesis, with a minimum of 2-year follow-up, 89.1% preferred a BCR design in one knee to a PS in the other.<sup>2</sup> In a similar study, Pritchett, analyzing 50 patients, could show that 70% percent of them preferred the BCR knee, whereas only 10% preferred the posterior cruciate-retaining knee.<sup>26</sup> In addition, reduced joint awareness was observed in patients receiving a contemporary BCR implant with respect to PS prosthesis.<sup>35</sup>

Last but not least, Lombardi et al. found that if an intact ACL is removed during TKA the patient will have poorer postoperative results and more restricted ROM compared to patients who had an absent or dysfunctional ACL at operation time, strongly justifying a BCR arthroplasty for the former.<sup>10</sup> All these data firmly support BCR approach for patients with intact ACL, representing more than half of patients with knee OA undergoing TKA,<sup>36</sup> or at least with a functional anterior cruciate, findable in roughly 78% of knees at the time of TKA, according to Johnson et al.<sup>37</sup>

## **BCR TKA disadvantages**

Unfortunately, bicruciate retaining TKA doesn't come with advantages only. Some critical drawbacks have limited its wide-spreading on the market and made it outpaced by CR and PS techniques. Although BCR limitations will be discussed in details further on in this review, the main disadvantages carried by this approach are anticipated here.

The biggest drawback of BCR TKA is the more challenging knee surgery with respect to other designs such as PS and CR.<sup>9,30-32,39,40</sup> Indeed, in order to spare the ACL, the tibia eminence must be preserved and this make it impossible to sublunate the tibia intraoperatively, therefore narrowing the surgical space.<sup>10,30</sup> At the same time, the anatomical joint line (on average 3° of varus) should be restored, meaning that the exact amount of cartilage and bone resected should be supplemented by the implant.<sup>52</sup> Any significant discrepancy, will alter the normal kinematics and ligament tension. During BCR TKA, accurate balancing of the knee through the ROM is vital, but extremely

challenging at the same time.<sup>41,42</sup> Hence, fracture of the tibial eminence and rupture of the ACL are not infrequent intraoperatively under not experienced hands, making the surgical technique not easily reproducible.<sup>39,42-44</sup> Given the narrow space available intraoperatively, the size of fixation pegs or keels in the tibial component is constrained, while the application of a long stem as in PS and CR is out of question.<sup>10,45,143</sup> This might result in tibial tray loosening.<sup>31,46,47</sup> At the same time, as the tibial eminence must be retained, instead of fully covering the bone surface, the tibial baseplate must have a central cutout and a narrow bridge connecting the medial and lateral plateau, that therefore limits the bone-implant contact area, favoring instability and fatigue fractures of the anterior bridge.<sup>45,48-51</sup> Furthermore, patient selection criteria is considerably stricter for BCR TKA rather than bicruciate sacrificing knee replacements. It's obvious that ligaments must be present and functionally intact, a requirement not always fulfilled by elderly patients with advanced OA or RA. Concurrently, varus, valgus deformity and flexion contracture must be minimal.<sup>11,39,53</sup> Last but not least, BCR TKA is not only technically but also economically demanding. Design and development of these implants is usually associated with additional costs.<sup>1</sup>

To sum up, BCR arthroplasty represents a complex reality with weaknesses but strong benefits at the same time, that could finally bring the relatively high dissatisfaction rates after TKA to an end.

## **Project overview**

The Master Thesis project here described was comprised of three main parts.

- First, a detailed systematic review was initially performed over the major BCR designs from the historical to the contemporary ones, aiming for a deep understanding of their limitations in order to set some key design specifics which could help to overcome the latter.
- Second, a report of the author's clinical experience in Tarabichi center for joint replacement, Al Zahra Hospital, Dubai, UAE, is here presented. Tarabichi center of excellence for joint replacement, established in 2001 by dr. Samih Tarabichi is reputed the most famous joint surgeon in Middle East with more than 30,000 total joint replacement (knee and hip) performed to date. Tarabichi center is considered the most distinguished clinics in the Middle East providing the latest and most comprehensive medical services ranging from personalized conservative treatments to designing patient-specific artificial joint by 3D printing technology.<sup>1</sup> Within this highly motivating environment a close contact with the concrete problematics and patients dissatisfaction related to artificial knee replacement was experienced. The most powerful mean to get such an insight has been undoubtedly the patients interview, done TKA surgery. Thus, a special focus has been put on these in the author's clinical report. However, additional tasks like surgery witnessing, discussions and meetings with surgeons and physiotherapists were also undertaken. In this way, expertise advices and hints were collected and a direct involvement in the clinical activities of the orthopedic environment was experienced.
- Last but not least, after learning the lesson from the reviewed designs and the patients complaints, a novel "hybrid" BCR TKA implant was designed in 3D Studio Max software, with the aim to finally overcome the previous flaws and defects that prevented a widespread diffusion of ACL-retaining prosthesis.

Given the clear division of the project in these three different tasks, the report structure will reflect such a partition as well. Hence, the Results and Discussion, and Materials and Methods chapters will consist of subsections, specific for each project task. Additionally, the order in which the subsections will be presented is not random, but will follow the chronological succession, therefore with the systematic review chapters as first and the 3D design as last. Apart from the temporal perspective this organization also reflects the cause-and-effect relationship between the tasks, with the last one, the novel tibial component design, being tightly dependent on the results of the first two.

# **Materials and Methods**

## **Systematic review**

### **Research strategy**

A massive literature research was performed through 5 main online databases: Embase, Science Direct, Medline, Scopus and Google scholar. Arthroplasty journals, orthopaedic books, additional material provided by Tarabichi center (AZHD) and other sources were also consulted and included into this work. The research strategy did not follow a standard protocol because, contrarily to a conventional systematic review, this paper doesn't focus on a specific topic or aspect only, but covers a huge variety of themes, a significant number of different BCR designs, each one described in as much detail as possible, making it impossible to adopt a single, unique research plan. However, a personalized strategy was performed during databases consultation, to make the review as systematic as possible. Initially a broad investigation of BCR arthroplasties was performed in order to obtain basic knowledge about this field that was then exploited for the Introduction, Discussion and Conclusion paragraphs. Examples of search strings employed are: (BCR OR bicruciate retaining OR bi-cruciate retaining) AND (TKA OR TKR OR total knee replacement OR total knee arthroplasty OR implant OR implants OR prosthesis) AND (review OR systematic review) ; (ACL OR anterior cruciate ligament OR anterior cruciate) AND (preserv\* OR spar\* OR retain\*) AND (TKA OR TKR OR total knee replacement OR total knee arthroplasty OR implant OR implants OR prosthesis). In a subsequent step, more precise information about BCR designs was searched, with the aim to find all the major implants that have ever been developed until now. For this purpose, orthopedic books revealed to be more suitable than journal papers. The main research step comes now. After the individuation of all main BCR designs in TKA history, for each one a methodical research was performed in the databases, through every paper reference and images found online. For the contemporary BCR implants, the company website was consulted aiming to find product information and the design rationale.

### **Inclusion/exclusion criteria:**

Every study presenting BCR TKA approach was assessed in first place. Since, a basic knowledge of the field was initially sought, priority and preference was given to reviews and TKA books until collected data were considered enough by the author. In a second place, papers regarding each separate BCR design was read and evaluated. In this phase, studies not regarding directly the BCR design under consideration, in a non-English language, without an open institutional access or with low level of evidence (grey literature, conference abstracts, case reports and expert opinions) were excluded. On the other hand, every source providing reliable additional data to the already collected one was taken into consideration, resulting in a wide range of references. In this way, double checks could be performed between different publications to confirm the validity of most of the findings and therefore increase the solidity of the data provided in this work.

### **Clinical experience**

Between February and June 2021, the author attended different clinical activities within Tarabichi center, Al Zahra Hospital Dubai, UAE. Tasks like TKA and THA witnessing, patients interviews, implant measurements and qualitative analysis, personal meetings with surgeons and physiotherapists were undertaken. Between these, only the most relevant for this master thesis report (surgeries witnessing and patients interviews) will be described in details, while the others

will be occasionally mentioned when needed, especially within the 3D design sections as both tasks were mainly undertaken aiming for guidelines and hints for the novel BCR TKA design. Yet, before starting with the abovementioned tasks report, it's important to introduce the patients iter within Tarabichi center at Al Zahra Hospital Dubai, which could be partly observed during the author's clinical experience and partly confirmed by personal conversations with patients, surgeons and physiotherapists. Here is the procedure in steps:

- A first visit with the surgeon is undergone, during which joint stability tests (Lachman, anterior drawer..) and imaging examination (X-rays) are carried out on the patient. Based on them, a final diagnosis is disclosed as well as a treatment recommendation.
- If surgery is required and the patient accepts this solution, either his insurance or the patient himself has to bear the costs.
- Preoperative examinations such as blood tests, cardiology exams, anesthesia compatibility are performed.
- If the tests give a green (positive) result, the surgery is scheduled.
- The surgery is performed.
- Bilateral TKA patients are hospitalized for 7 days, while unilateral for 5.
- 1 week after surgery, stitches are removed.
- Starting from day one after surgery and lasting 2 months, physical rehabilitation sessions, both at home and at the clinics are undertaken.

The total iter duration can vary from patient to patient depending on his muscle strength, rehabilitation performances and perseverance, age, (BMI). Nevertheless, a 10 weeks total procedure for TKA patients is observed on average at Tarabichi center.

### **TKA surgeries witnessing**

During the first three months, bilateral and unilateral TKA surgeries were witnessed. Most of the time, Persona<sup>R</sup> TKA implants from Zimmer were implanted, either PS or CR dependently on PCL condition and functionality (Fig. 24).

One patient received custom-made Origin<sup>TM</sup> knee prosthesis by Symbios (Fig. 25). No bicruciate retaining TKRs were performed within Tarabichi center. Additionally, one THA was witnessed on 16/03/2021 where the patient received a cementless implant by Johnson & Johnson (**Supplementary Material**). The results of my surgeries witnessing, i.e. the notes taken within the operation room and during the meetings with the surgeons, will be reported later on in the results section ...in order to give a brief overview of the main steps of a total knee replacement performed within Tarabichi center, the biggest challenges faced during TKA and the future surgical breakthroughs in the knee replacement field.



**Figure 24:**  
**Figure 25:** Origin PS TKA.<sup>10</sup>



Persona

CR

TKA.<sup>9</sup>

## Patients interview

After the first months of surgeries witnessing, patients interviews were undertaken at Tarabichi center. A minimum of 3 and a maximum of 6 meetings with each patient were set, with the interviews done immediately before their routine rehabilitation sessions or during the final cycling exercise at the physiotherapy rooms within the clinics (Fig. 26). A first introductory conversation was willing to have a rough overview of patients experience with TKA. From the second meeting on, 17 specific questions about the degree of satisfaction, postoperative outcomes of the implant and so forth were asked (Table 2). A total of 4 TKA patients were interviewed, 3 women and 1 man. This limited number of cases was due to the increasing Covid-19 restrictions that precluded new patients to be accepted by the clinics at last.



**Figure 26:** a typical patient interview during the final cycling exercise.

Personal details and clinical data of the interviewed TKA patients are reported in Table 1. Average age is 66. Nationality and ethnicity is different between patients, with two Egyptians, 1 Italian (with Asian roots) and 1 patient from U.A.E. 3 out of 4 were “recent” patients (a few months after operation) while one was an “old” patient (2 years after operation) at interview time. The diagnosis was advanced osteoarthritis of knee joint for all cases. Two Bilateral TKAs (BTKAs) were performed applying Persona CR by Zimmer, while the other two cases were Unilateral TKAs (right knee) with the insertion of custom-made Origin™ PS by Symbios.

**Table 1 :** personal and clinical data of interviewed TKR patients

Patient's initials	Gender	Age	Nationality	Type of surgery	Time from operation*** *	Etiology	Implant received
N.O.A.G.D.	Female	58	Egyptian	RTKA**	50 days	OA	Origin PS
M.G.C.G.	Male	77	U.A.E	RTKA	5 months	OA	Origin PS
A.M.F.E.S.	Female	63	Egyptian	BTKA	2 years	OA	Persona CR
E.O.	Female	67	Italian	BTKA	2 months	OA	Persona CR

\*\*RTKA stands for right knee TKA. \*\*\*at the time of final interview.

**Table 2:** questions asked to interviewed patients

Question number	Question
1	When did you start feeling pain in your joint(s)?
2	Which was your ROM before surgery?
3	Which were the mostly limited activities by your joint disease?
4	When did you attend total knee surgery?
5	How did you feel the first days of hospitalization after TKA?
6	When did you start rehabilitation?
7	How frequently are you doing rehabilitation sessions at the clinics?
8	How stable do you feel your knee(s)? (from 1 to 10)
9	How painful is it you knee(s)? (from 1 to 10)
10	How natural does your prosthesis feel after TKA (also known as FJS)? (from 1 to 10)
11	Do you hear noise from your implant(s) (clunks, pops, clicks..)?
12	Which is you actual ROM?
13	Are you now able to do main motion tasks (walking, stair climbing, cycling..)?
14	Are you now able to do main daily activities (shopping, driving, praying, housekeeping..)?
15	How satisfied are you about your artificial joint(s)? (from 1 to 10)
16	Would you recommend this experience to a person in your same pre-operative conditions?
17	Do you have any suggestion regarding TKR patients care, prosthesis design and implantation?

In addition to TKA patients, the same THA patient whose surgery was witnessed was interviewed as well. However, since this report is centred on knee and not hip replacement, the results of his interview and details about hip surgeries at Tarabichi center will not be discussed in this instance **and could be found within the Supplementary Materials.**

### 3D implant design

Among different 3D CAD (computer aided design) software, 3D Studio Max (usually abbreviated to 3Ds Max) was chosen as the platform where to realize the novel “hybrid” BCR tibial implant. 3Ds max is one of the most famous and utilized three-dimensional vector graphics and animation programs, developed by Autodesk's Media & Entertainment division in 1990.<sup>18-19</sup> It offers a robust and wide range of tools to perform 3D modeling and rendering of premium designs, with full artistic control and precision down to the smallest details. An institutional access was obtained through ETH student credentials and the latest version of the software was then installed (2022). The 3D design task can be divided into three phases:

- The 3D design itself, including the 2D drawing and the three-dimensional modeling on it.
- The materials application.
- The rendering.

### Design and modelling

The entire designing process has been accomplished within 3Ds Max program, starting from the initial 2D spline drawing to the final 3D modeling of the prosthesis. Before actually starting with this phase, 3 weeks of online courses and official Autodesk tutorials were attended in order to master the software. After this introductory period, the 2D design steps were initiated. The designing process was not done unconsciously, but prior to the designing phase or in parallel to it,

an extensive literature review and frequent discussions with dr. Elfekky and dr. Tarabichi were carried out, aiming for a precise delineation of the design criteria for our novel tibial prosthesis. In this way, each design step was anticipated by a thoughtful research of the best option for its realization. The results of this design criteria investigation will be reported at the beginning of every design chapter, providing an precise insight of the thought behind each design stride. Throughout the whole design process, if the project resulted stuck in a complex step, either mr. Balu Sreehari (a designer expert) or Autodesk tutorials<sup>20</sup> or the Autodesk community<sup>21</sup> was consulted. Every time a new feature or design step was introduced, a new file was saved. This allowed the author to keep track of all the sequential modifications and, most importantly, offered the possibility to go back to previous files when some aspects had to be edited, without the need to start over with the initial steps. Nevertheless, this approach resulted in almost 200 files for the tibial component design. Considering that the latest versions, including thousands of design features and several complex operations (like booleans), weigh more than 8 Gigabytes, it's easy to understand that a computer with huge memory space was required. At the same time, high computational power was essential for the complex 3D modeling and rendering processes. In this case a 15 5000 Dell Inspiron notebook was utilized, with an 11th Generation Intel® Core™ i5-1135G7 processor and a 512 GB SSD.<sup>17</sup>

## **Materials application**

Subsequent to the design phase, materials were applied to the monochrome geometries. Arnold material editor was utilized with this aim. As will be better discussed later on in this report, for the tibial component a polished metallic material was chosen, resembling either CoCr or Ti-6Al-4V, while for the fixation components (hex pegs and hemisphere) along with the bottom surface of the tibial implant in contact with the underlying bone, a rough and highly porous material was applied, representing Tantalum, also known as “Trabecular Metal” by Zimmer Biomet. A significant amount of trials were made in order to find the best texture, matching the abovementioned materials, to apply to each design part. In order to do that, the material was firstly assigned to the model and then a quick Active-shade rendering was launched to see the result. Initially, ready-made materials were searched with poor results. No rough metallic bitmap was found. Poliigon website<sup>22</sup> offered only brushed metal textures that were leading to unsatisfactory rendering outcomes for the tibial component (Figure 27 **add this figure later on!**). Other online material libraries were either chargeable, or not compatible with Arnold renderer. Hence, both trabecular and polished metallic materials were realized from scratch within the Arnold material editor. For the former, no bitmap was utilized, and material data (base color intensity, index of refraction, metalness, reflection color intensity) provided by Chaos official website<sup>23</sup> were exploited to edit a standard surface Arnold material; for the latter, Photoshop software was exploited for the Tantalum bitmap editing. The detailed material production process will be described in section ....

## **Rendering**

Arnold renderer by Autodesk was utilized in this project. Arnold is an advanced renderer based on unbiased Monte Carlo ray tracing. Originally co-developed with Sony Pictures Imageworks, Arnold is nowadays one of the most widely used photorealistic rendering systems in computer graphics, with more than 300 studios relying on it worldwide.<sup>24</sup> Active-shade mode, a real time rendering approach, was utilized during material selection and trials, because it was allowing an instantaneously updated view of the rendering variations caused by every single modification made to the applied materials. In this way, it was possible to constantly observe the rendered scene, while working.<sup>25</sup> On the other hand, after completing the material editing and scene preparation, Production Rendering mode was launched. The latter provides full-scale, detailed and high resolution images at the expense of computational power and time. Therefore, it was used only for



final renderings.<sup>26</sup> A robust graphic card is then essential to withstand this highly demanding rendering sessions. For this project a 2 GB NVIDIA® GeForce® MX330 dedicated graphic card was used.

As for the materials, several trials of camera direction and lighting were carried out in order to set the scene. To illuminate the scene, Arnold lights with resolution intensity of 256 (without energy normalization) were initially introduced. However, the resulting renders had a non-uniform illumination, with dark regions alternated to bright spots. Consequently, instead of the artificial Arnold lights, a HDRI (high dynamic range imaging) bitmap was applied as a “fake” background for the 3Ds max scene, lighting up the geometries evenly and providing a more realistic touch to the rendered images. Several different HDRIs from HDRI Haven website<sup>27</sup> were tested, including both outdoors and indoors environments. Among these, the best result was given by “Photo Studio 01” (Fig. 28) and therefore the latter was applied to the final scene.



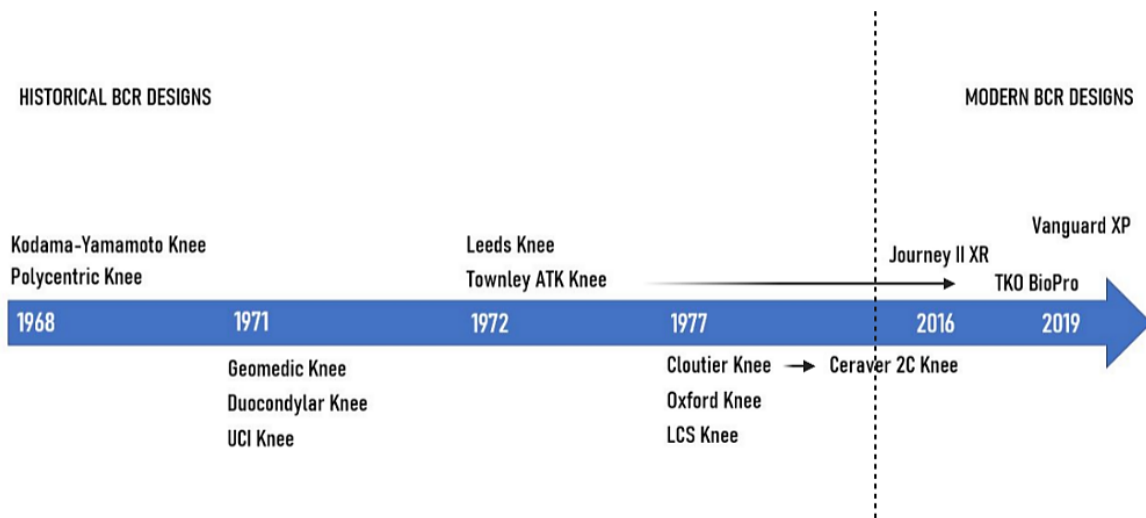
**Figure 28:** The HDRI bitmap “Photo Studio 1” applied as an environment for the rendered scene.

## Results and Discussion

### State of The Art

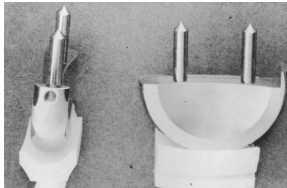

The concept of bicruciate retaining total knee arthroplasty was firstly introduced at the end of the 1960s, when dr. Gunston in the UK presented his Polycentric Knee. Despite the revolutionary idea carried by this implant, crucial design weaknesses unavoidably led to unsatisfactory clinical outcomes and the disuse of the latter. Inspired by the Polycentric Knee and aiming to improve it, many other BCR TKA designs were released to date. A chronological overview of these is presented below, with the prosthesis divided in two families according to the year of commercial release: historical and modern BCR designs (Fig. 2). While a highly detailed analysis of these implants is provided within the systematic review written at the beginning of this project, a briefer outline is here reported in order to relieve and better organize the information load and therefore smooth the reading process. With this purpose, historical designs will be merged in one single table, while modern ones will be described more thoroughly. At the same time, not all the historical implants will be discussed in the present paper, but only the ones that significantly contributed to the BCR TKA design evolution. Only key design features and the main drawbacks of the presented

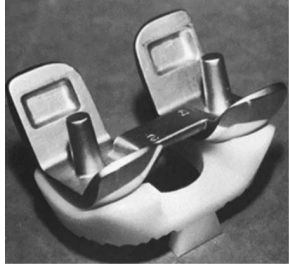
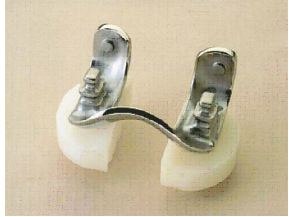
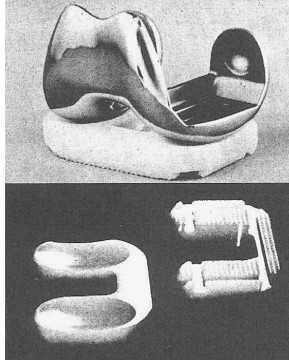
implants will be reported. For data regarding the other BCR designs not discussed here and more detailed information such as clinical limitations reported in literature and subsequent design modifications, readers can refer to the author’s systematic review entitled “BCR TKA designs: a systematic review of the literature”.





**Figure 2:** chronological representation of the historical and modern BCR designs assessed in this review.

**Historical BCR designs:**

Prosthesis, designer, date	Brief description	Key design features	Main design weaknesses*	Figure
Polycentric Knee, dr. Frank Gunston, 1968.	The cemented Polycentric Knee is recognized as the first bicompartamental knee arthroplasty without relying on any hinge, while retaining both cruciate and collateral ligaments instead. <sup>11,55-57</sup>	<ul style="list-style-type: none"> <li>- comprised of two unicompartamental implants (Fig. 3).</li> <li>- semicircular Co-Cr femoral components.</li> <li>- High density polyethylene (HDPE) tibial concave runners.</li> </ul>	<ul style="list-style-type: none"> <li>- too minimalistic design.</li> <li>- lack of anterior bridge led to implant misalignment.</li> <li>- narrow femoral components resulted in high contact stresses on PE inserts.</li> <li>- lack of metal backing in tibial component.</li> </ul>	 <p><b>Figure 3:</b> Gunston's Polycentric Knee prosthesis<sup>57</sup>.</p>
Kodama-Yamamoto Knee, Kodama and Yamamoto, 1968.	In 1968, the first cementless total condylar knee was invented by Kodama and Yamamoto at Okayama University, Japan. <sup>11,54,60-64</sup> The Kodama-Yamamoto Knee will then be called Mark I and subsequently develop in Mark II, Mark III and finally in the modern “New Yamamoto Mico Fit Knee”, manufactured and distributed by Corin company.	<ul style="list-style-type: none"> <li>- COP alloy (Co, Cr, Ni, Mo, C and P) femoral component with anterior flange.</li> <li>- horseshoe shaped HDPE tibial component, allowing the retention of ACL and PCL (Fig. 4).</li> <li>- slightly dished tibial surface.</li> <li>- two anterior staples in the tibia and fins on the femur for improved fixation.</li> </ul>	<ul style="list-style-type: none"> <li>- symmetrical femoral condyles.</li> <li>- lack of metal backing in tibial component.</li> <li>- poor tibial fixation components.</li> <li>- symmetrical tibial plateaus.</li> <li>- non-anatomical, symmetrical tibial component.</li> </ul>	 <p><b>Figure 4:</b> Mark I implant</p>

<p>Geomedic Knee, dr. Coventry, Averill, 1971.</p>	<p>Designed in 1971 at Mayo clinic, Minnesota, by a team of engineers and physicians led by dr. Coventry and mr. Averill, the so called Geomedic Knee is considered as the first cemented BCR bicondylar knee replacement.<sup>11,62,67</sup></p>	<ul style="list-style-type: none"> <li>- vitallium femoral component and HDPE tibial component comprised of two parts joined by a thin anterior bridge (Fig. 5).</li> <li>- pins and depressions in the femoral side for stable fixation.</li> <li>- two spherical condyle surfaces articulating against highly conformal, concave bearings on the tibial side.</li> </ul>	<ul style="list-style-type: none"> <li>- the highly conformal articular surfaces along with bicruciate retainment led to the so called "kinematic conflict".<sup>9,11</sup></li> <li>- too thin anterior bridges prone to fatigue breakage.<sup>118</sup></li> <li>- lack of metal backing in tibial component and femoral flange<sup>118</sup>.</li> <li>- symmetrical tibial plateaus, tibial component and femoral condyles.</li> <li>- poor tibial fixation components.</li> </ul>	 <p><b>Figure 5:</b> Geomedic Knee by Coventry and Averill.<sup>19</sup></p>
<p>Duocondylar Knee, dr. John Insall, 1971.</p>	<p>The cemented Duocondylar knee was developed in 1971 by dr. Insall in collaboration with drs. Ranawat and Walker. This design could be seen as a full-fledged thin anterior union of two unicompartamental implants (Fig. 6).<sup>11,57,62,78</sup></p>	<ul style="list-style-type: none"> <li>- two Co-Cr femoral condylar components linked by an thin anterior bar.</li> <li>- pillars on the femoral side for fixation.</li> <li>- tibial tray constituted by two separate, high density PE, nearly flat pads, allowing kinematics freedom (opposed to Geomedic knee).</li> </ul>	<ul style="list-style-type: none"> <li>- lack of femoral flange and metal backing in tibial component.</li> <li>- thin anterior femoral bar prone to fatigue breakage.</li> <li>- two separate tibial components difficult to align and balance intraoperatively and easily subjected to misalignment after surgery.</li> <li>- symmetrical tibial plateaus.</li> <li>- poor tibial fixation components.</li> </ul>	 <p><b>Figure 6:</b> Duocondylar Knee by dr. Insall.<sup>57</sup></p>
<p>Anatomical Total Knee (ATK), dr. Charles Townley, 1972.</p>	<p>1972 represents the birth of the Anatomical Total Knee, designed in Port Huron, Michigan, by dr. Townley (Fig. 7). This non conforming cemented BCR implant adopted a close to anatomy profile.<sup>62,84,85,87</sup> In 1973 a PE dome shaped patellar button was introduced, resulting in the first tricompartmental total knee prosthesis. Townley's Anatomical knee is now marketed as the Total Knee Original (Biopro, Port Huron, Mich), that will be discussed later on in this chapter.</p>	<ul style="list-style-type: none"> <li>- cobalt-chrome (Co-Cr) femoral component with three radii of curvature in the sagittal plane, resulting in a polycentric geometry.</li> <li>- smaller radius of femoral condyle curvature in the sagittal plane to allow normal anterior-posterior displacement and non-constrained rotation.</li> <li>- single piece PE tibial component with central cutout and cup-shaped concavities.</li> <li>- no intramedullary fixation pegs present on either femoral or tibial component.</li> </ul>	<ul style="list-style-type: none"> <li>- symmetrical femoral flange.</li> <li>- symmetrical femoral condyles.</li> <li>- lack of metal backing in tibial component.</li> <li>- symmetrical tibial plateaus.</li> <li>- poor tibial fixation components.</li> <li>- non-anatomical, symmetrical tibial component.</li> </ul>	 <p><b>Figure 7:</b> Anatomical Total Knee by dr. Charles Townley<sup>62</sup></p>

<p>Hermes Knee, J.M. Cloutier, 1977.</p>	<p>The first Cloutier's design was the Hermes AC TKR (actual name Hermes 2C), developed in 1977 in Montreal (Fig. 8).<sup>91,92</sup> The cemented design components were very similar to the modern BCR prosthesis.</p>	<ul style="list-style-type: none"> <li>- titanium (Ti) femoral component with asymmetrical condyles, an enlarged notch and a deep trochlear groove.</li> <li>- two independent carbon-reinforced PE inserts with a nearly flat surface.</li> <li>- U-shaped Ti tibial baseplate with two fixation pegs.</li> <li>- dome shaped PE patellar implant with a metal retainer and two pegs.</li> </ul>	<ul style="list-style-type: none"> <li>- non-anatomical, symmetrical tibial component.</li> <li>- symmetrical flat tibial plateaus.</li> <li>- suboptimal tibial fixation components.</li> <li>- sharp cutout-cruciate interface.</li> </ul>	 <p><b>Figure 8:</b> Hermes 2C implant.<sup>31</sup></p>
<p>Low Contact Stresses (LCS) Knee, Buechel and Pappas, 1977.</p>	<p>Influenced by a presentation of Goodfellow et al., dr. Buechel and Pappas started working on the LCS Knee system in 1977.<sup>30,95,96</sup> As the Oxford Knee, the LCS implant utilized mobile bearing surfaces to finally solve the orthopaedic dilemma of congruency vs. constraint. Yet, the LCS TKA provided a total knee replacement instead of the two separate unicondylar prosthesis of the Oxford one (Fig. 13).</p>	<ul style="list-style-type: none"> <li>- metal femoral component.</li> <li>- metal U-shaped tibial baseplate.</li> <li>- two separate concave mobile meniscal bearings of PE.</li> </ul>	<ul style="list-style-type: none"> <li>- symmetrical femoral flange.</li> <li>- symmetrical femoral condyles.</li> <li>- suboptimal tibial fixation components.</li> <li>- symmetrical tibial plateaus.</li> <li>- non-anatomical, symmetrical tibial component.</li> <li>- sharp cutout-cruciate interface.</li> </ul>	 <p><b>Figure 13:</b> Bicruciate retaining LCS tibial metal baseplate and mobile PE bearings.<sup>30</sup></p>

\* The “main design weaknesses” column refers to the initial proposed design, except for Kodama-Yamamoto Knee where it refers to Mark III design.

From the upper table it's clear that old BCR TKA designs, some more, some less, introduced promising alternatives to the functional prosthesis. Yet, it's even easier to infer that critical design flaws have been the main responsible for a limited success in joint replacement market. A recent study by dr. Ries et al. reported the main modes of failure of first-generation BCR designs being fracture of the anterior tibial bridge, insert dissociation, polyethylene wear and tibial component loosening.<sup>45</sup> The latter along with poor ROM (often <110° and sometimes even below 100°) are confirmed by the clinical reports around all the abovementioned BCR implants<sup>s.r.</sup>. All these complications are strictly interconnected and can be traced into suboptimal prosthetic design and insertion technique. Indeed, historical design defects led to abnormal joint kinematics that univocally resulted in higher stresses on the implant, provoking early failures.<sup>8</sup> The kinematic conflict observed with Geomedic knee is a prime example. Spurred by the stalemate associated to the historical implants, the orthopaedic industry recently endeavored to release new designs thought to overcome the old.

### Modern BCR designs:

#### Total Knee Original (TKO), BioPro., 2018

The BioPro TKO prosthesis is the third generation of dr. Townley's Anatomical Total Knee (Fig. 14).<sup>98</sup> The main difference with the original design of 1972 lies in the tibial component, which is no more a single PE piece, but is constituted by a metal tibial tray and a single piece polyethylene insert, both horseshoe shaped to allow ACL and PCL retention. The multiradius femoral

component is made of cobalt-chromium, is porous coated on the proximal surface to enhance adherence to the bone and has two pins for stable fixation (Fig. 15). The TKO tibial insert is a single piece ultra-high molecular weight polyethylene (UHMWPE) with a symmetric and slightly dished proximal surface articulating with the resurfaced femoral condyles. This insert can have variable thickness (8-11 mm in a study by Pritchett<sup>32</sup>) and lies on a metal tibial baseplate made of titanium, with a porous coating facing the underlying bone. The medial and lateral aspects of the prosthesis are reinforced by a long inferior flange while two pegs and a small keel are used for fixation (Fig. 16). When needed, a dome-shaped PE patellar component, articulating with the asymmetrical trochlear groove, might be implanted.<sup>32</sup>

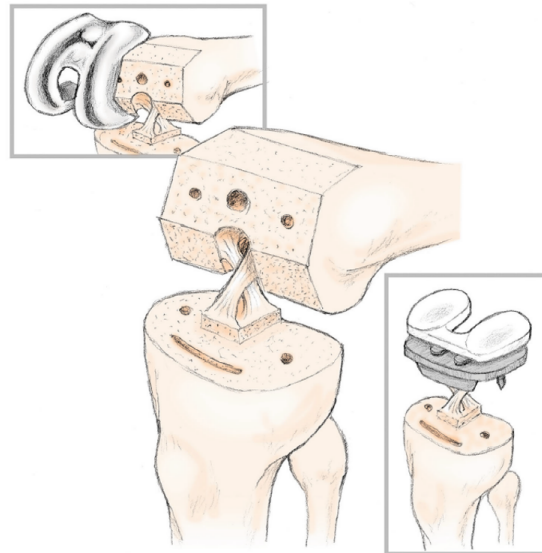


**Figure 14:** a schematic drawing of the BioPro TKO implant.<sup>32</sup>

Although a report of dr. James Pritchett showed the superiority of TKO implant with respect to CR design in terms of postoperative scores, kinematic performances and patient preferences<sup>26</sup>, another study revealed only 89% survivorship, a still suboptimal ROM of 117°, femorotibial instability and high rate of PE wear related to the BioPro BCR prosthesis.<sup>32</sup> The underlying reason of these complications is reasonably identified by a 2015 study conducted by a collaboration between Massachusetts General Hospital and ETH Zurich<sup>99</sup>.

In this research, dynamic simulations during a variety of daily activities revealed a non-restored differential medial and lateral rollback, seen in healthy knees. Even, the TKO prosthesis showed an abnormal and more posterior translation on the medial plateau than the lateral, contrasting with the medial pivot motion of knee during deep knee bend, demonstrated instead by the biomimetic BCR implant developed by the authors. These poor TKO performances are attributed to a non anatomical design of the tibial insert. Indeed, the symmetrical dished bearings do not reflect the medial concavity – lateral convexity of the normal tibial articular surface. Especially, the decreasing slope in the lateral bearing results in a posteriorly directed joint force opposing to the anteriorly directed ACL pull, therefore also representing a possible cause for the high wear rate observed on the PE insert for such prosthesis. In contrast, a lateral convex bearing surface provides a leveled anterior portion, allowing a more anterior femoral location in extension, and a gradually increasing slope, encouraging normal posterior rollback with flexion.



**Figure 15:** The femoral component of TKO prosthesis with (top) the porous coating on the inside surface<sup>98</sup> (bottom) view of metal backed tibial component with PE symmetrical TKO implant (bottom).<sup>98</sup>

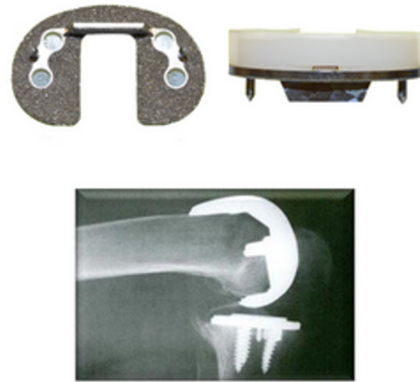


**Figure 16:** Bottom view of tibial baseplate (left). Frontal view of tibial baseplate (top right). A radiograph of an inserted tibial baseplate (bottom right).

### Vanguard XP, Zimmer Biomet, 2019

The modern Vanguard XP is the modified version of the well established Vanguard CR by Zimmer Biomet (Fig. 17,18).<sup>100,104,105</sup> While the patellofemoral joint is the same as in CR implant, the tibial component is significantly different, with a central cutout for the ACL attachment preservation. Since this is not allowing the employment of a central stem or a big keel, the cemented fixation is enhanced by two small pegs and two small keels on either side of the retained bone island.<sup>101</sup> The femoral component features asymmetric condyles to resemble the knee anatomy. A funnel-shaped narrowed anterior femoral flange ensures low shear stresses on the patella.<sup>19,35,102</sup> Both femoral implant and tibial baseplate are made of forged Co-Cr. On the other side, the vitamin E-infused antioxidant polyethylene bearings are independently designed, one for the medial and one for the lateral plateau and incorporate compartment-specific geometries, recognizing the difference in kinematics between the medial and lateral side (Fig 17).<sup>19</sup> Vanguard XP allows for different inserts thickness, with the lateral thicker than medial, making easier the ligament balancing.<sup>19,101</sup> 1 mm thickness increments represent another key feature of this implant.<sup>103</sup> Of high importance, it's possible to switch from the BCR to an ACL sacrificing solution intraoperatively. A considerable amount of short term studies on the contemporary Vanguard XP TKA have been performed, focusing on clinical results and kinematic outcomes.

In most of these, complications like aseptic tibial loosening and implant instability were still non-negligible.<sup>10,101,106,107</sup> The low survival rate of 88% at 3 years follow-up reported by Pelt et al.<sup>107</sup> along with the higher frequency of revisions with respect to CR implants reported by Christensen et al.<sup>106</sup> lead to the same conclusion of suboptimal tibial component design and cementation technique. Utilizing special surgical instrumentation and third generation cementation technique, Alnachoukati et al. could report great patient reported satisfaction, function, and short-term (mean 12 months) outcomes for 146 patients receiving Vanguard XP prosthesis.<sup>44</sup> However, one case of tibial loosening and a still far from ideality mean postoperative ROM of 121° were reported.

Finally, kinematic studies on Vanguard XP design revealed contradictory results. While researches on this implant reported greater knee stability during gait and downhill walking<sup>108</sup>, a better femoral component posterior offset ratio (lower femorotibial impingement in deep flexion)<sup>109</sup> and more natural screw-home mechanism in late extension<sup>110</sup> compared to CR TKA, other studies could show asymmetrical flexion-extension and internal-external rotation associated to Vanguard XP, indicating a still non-restored tibiofemoral kinematics.<sup>111-113</sup>



**Figure 18:** The modern Vanguard XP knee implant, frontal view.<sup>105</sup>

### **Journey II XP, Smith & Nephew, 2016.**

Journey II XP design was released on market in March 2016 by the American company Smith & Nephew (Fig. 19,20).<sup>8,46,53,114</sup> This contemporary implant aims to restore femorotibial joint line with an oblique three-degree angle and the shape of the asymmetrical joint surface.<sup>115,46</sup> For this reason, it features asymmetric femoral condyles made of Oxinium™ (oxidized zirconium) articulating with a metal backed tibial component. The tibial baseplate is forged Ti-6Al-4V, that having a lower E modulus than CoCr reduces the risk of stress shielding and bone resorption. It is asymmetrically shaped with a more anterior position medially to better replicate the anatomical profile and ensure higher bone coverage and therefore lower implant loosening. The central notch is asymmetric as well, providing enough space for bicruciate preservation. Good fixation is given by a continuous keel and four pegs. The keel is angled posteriorly by 20° to allow fixation depth and contains grooves to improve implant cementation (Fig. 21). Medial and lateral compartments are connected anteriorly by a reinforced bridge with increased thickness surrounding the cruciate notch that should prevent fatigue breakage. In order to have mismatched thicknesses between medial and lateral plateaus, two independent highly-crosslinked polyethylene (XLPE) bearings are used. They are designed with a medial concavity and lateral convexity with the aim to restore normal knee kinematic and tibiofemoral contact point through the ROM. Special surgical instrumentation is adopted and components are cemented separately. Upon cementation, the inserts are mated to the tibial tray by a fully captured lock detail with posterior and anterior locking interfaces. Like Vanguard XP, also Journey II XR allows for immediate intraoperative switch to ACL-sacrificing designs if the patient is no-longer a good candidate for BCR TKA.

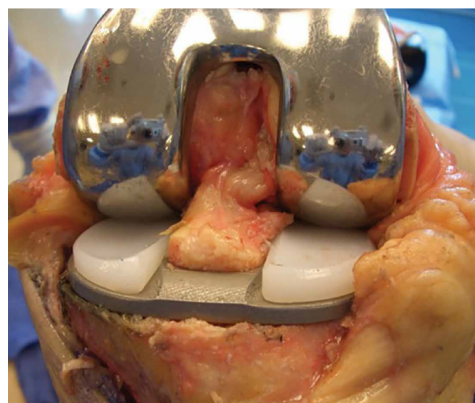


**Figure 19:** the Journey II XR prosthesis by S&N.<sup>114</sup> **Figure 20:** implanted Journey II XR TKA with the retention of ACL

and PCL.<sup>8</sup>

Laboratory tests performed by S&N reported promising results of Journey XP implant.<sup>114</sup> The tibial baseplate design revealed to have a fatigue resistance more than double the minimum recommended by ASTM F 2083-08 and the one documented in the Zimmer Biomet literature around VANGUARD XP's fatigue strength. The Oxinium on XLPE material combination (Verilast™ technology) has proven no measurable wear at 6 million cycles, a significantly lower rate than Vanguard prosthesis. On the other hand, however, tibial fixation testing reported significantly lower outcome than long keel implants, suggesting that further design adjustments may be essential to definitively close the fixation gap with ACL-sacrificing designs. Given the recent market release, limited follow up studies are available in literature and the picture that emerges from these is contradictory. While a few papers claim the superior kinematic performance of Journey II XR with respect to PCR and PS implants<sup>22,116</sup>, another highlight poor postoperative flexion and extension results associated to the BCR design from S&N.<sup>115</sup> More than that, another recent publication demonstrated that the kinematics of Journey II XR is still far from the one of UKA and healthy joint.<sup>117</sup> In particular, during early flexion, the medial side of BCR-TKA knees was significantly more anteriorly located and the femoral external rotation angle significantly greater than that of normal and UKA knees. Besides, from 30° to 120° of flexion, the lateral side of BCR-TKA knees was positioned more anteriorly than that of normal and UKA knees.

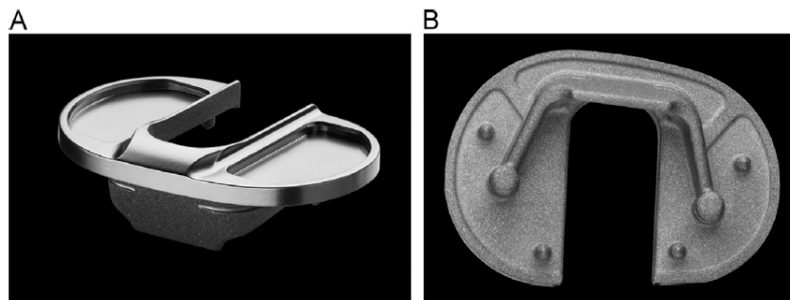


**Figure 21:** the forged Ti-6Al-4V tibial baseplate (A). Bottom view of the tibial component (B).<sup>53</sup>

Contemporary implants were designed in attempt to solve the complications associated to historical BCR prosthesis once and for all. Although several improvements have been certainly introduced, the early results of these modern designs suggest that the aim for a completely restored knee motion in BCR patients may not be definitely addressed yet and additional modifications are still required. Since the femoral component is almost identical to CR and PS designs whereas the tibial implant significantly differ from them, the latter represents the major concern for BCR TKA and the component modern designs have focused on and future modifications should pay the outmost attention to.

It's reasonable that given the high incidence of implant loosening, the tibial design still features suboptimal fixation components and cementation technique. At the same time, the inferior kinematic performance of modern BCR implants with respect to UKA knees and healthy joints suggests a femorotibial articulation still far from ideality, revealing design flaws in polyethylene inserts. Moreover, as the historical designs, the modern implants described above persist in having a sharp interface with the preserved cruciate ligaments, which may reasonably lead to high stresses at the soft tissues – implant interface inevitably causing tears and microdamages to ACL and PCL over time and therefore undermine their functionality and the prosthesis stability.

Last but not least, recently released implants seem to have failed in ultimately bridge the “complexity and reproducibility gap” of surgical technique with the standard ACL-sacrificing arthroplasties.<sup>10,101</sup>



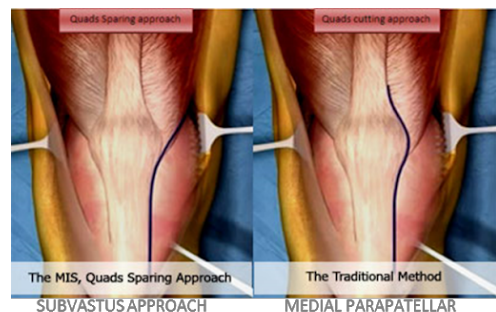
In the discussion chapter of author’s systematic review, a list of the key design features an ideal BCR design should feature is presented and considerations regarding the locking mechanism, implant fixation, component materials, surgical technique and contraindications of BCR TKA have been raised too. Based on this, the novel “hybrid” tibial component has been designed in Al Zahra Hospital Dubai and therefore the major project specifics will be discussed later on in section .....

To conclude, it’s important to highlight that the systematic review here reported in broad terms had a major limitation represented by the denied access to a few critical publications in literature, that have surely restricted the amount of details covered. However, most of the information and specifics of these restricted-access papers could be reasonably inferred their abstracts and all the related publications and references, providing a wide and often detailed overview of the design at issue.

## Knee surgery procedure at Tarabichi center

The hereafter listed steps are referred to the surgical implantation of Persona CR prosthesis, observed during the early experience in Tarabichi center. No patellar replacement was witnessed throughout the author’s permanence at the clinics. Therefore, only bicompartmental procedure is reported here.

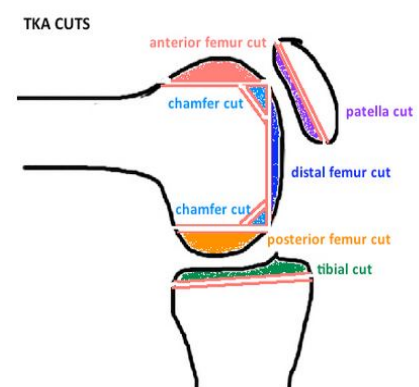
1. Spinal anesthesia. This is a regional procedure numbing the lower limbs only, while keeping the patient awake.
2. Longitudinal incision in the femorotibial direction to cut skin and adipose tissues.
3. Sub-vastus approach to access the joint space through soft tissues surrounding the knee (Fig. 22, left). This incision is following the more popular medial parapatellar approach (Fig. 22, right) until patellar location, but then, instead of proceeding longitudinally it is deviating medially, below the insertion point of the vastus medialis obliquus.




**⚠ Attention!** This procedure is a truly “quadriceps-sparing” surgical technique, where both muscles and patellar tendon are preserved. In this way, the extensor mechanism, guaranteed by medial parapatellar (right) and lateral

the abovementioned soft tissues, is not undermined.<sup>4-6</sup> Less pain parapatellar (left) approach.<sup>7</sup> and a faster recovery are consequences of this. Nevertheless, this approach is more demanding for the surgeon and can result in inadequate knee exposure and complicated patellar eversion.<sup>3</sup> For this reason, according to dr. Anas and Omar of Tarabichi center, sub-vastus approach is representing only the 4% of the worldwide performed procedures in TKA, against the 95% of medial parapatellar.


4. With knee in flexion, removal of synovium membrane and connective tissues that hinder a wide access to the joint.
5. Evaluation of functionality and intactness of cruciate ligaments. Removal of ACL and menisci (with PS implants, PCL is removed too).
6. Insertion of the intramedullary rod for placement of the guides for the 5 femoral cuts.




7. Distal cut, posterior cut, anterior cut, posterior chamfer, anterior chamfer.
8. Application of the extramedullary guide for the tibial cut (it tells the varus/valgus angle and slope).

 **Attention!** Since the cutting guide for the tibia is not intramedullary as the femoral one, the risk of malrotation of the tibial component is significantly higher than for the femur. **For additional information about this topic, readers can refer to Supplementary Figure 23: TKA cuts. (patellar cut was not material x, where one case of tibial malrotation author's clinical experience)<sup>8</sup>. witnessed during**  
**witnessed at the clinics is reported.**


9. After subluxation, tibial cut. Posterior slope is implant dependent (for Persona implant is 3° for PS and 7° for CR). Varus-Valgus angle is kept to 0°.

 **Attention!** The anatomical joint line is at 3° varus. Contemporary tibial implants like Journey II XR have a 3° medial-lateral inclination in the design itself in order to compensate for the 0° varus-valgus surgical cut and therefore restore the natural joint line.<sup>115</sup>

10. Placement of tibial guide for keel drilling.
11. Keel hole drilling.
12. Trialing of tibial and femoral components and inlays. This step ensures correct implant size is inserted. At the same time, surgeons test knee stability and soft tissue balance through ROM. In this direction, while continuously observing the femorotibial gap in flexion/extension, thickness of PE inserts is incremented from the initial 10mm size until the joint is stable, and the ligaments are neither too tight nor too loose. If the stabilizing tissues are too tight, the tibial cut is increased, if too loose the PE thickness.
13. Implantation of tibial component with cemented fixation and removal of the PMMA in excess.

 **Attention!** The bone cement is harmful for the surrounding tissues and if it overflows beyond the tibial-bone interface it can cause impingement after solidification.

14. Implantation of femoral component with cemented fixation and removal of the PMMA in excess.
15. Insertion of the PE bearings into the tibial locking profile.
16. Extension of the knee to position the implants under pressure.
17. Tests of knee stability, ligament balance, sizing and positioning of implants during flexion/extension movement.
18. Examination of the maximum degree of flexion/extension under anesthesia. The values reached at this stage represent the goal for the patient after the rehabilitation.

 **Attention!** The medical equipe of Tarabichi center targets more full extension as the primary goal for the artificial joint than full flexion, since the former is the precondition to entirely restore essential activities like walking, sitting on chair, while flexion angles beyond 120° are not required to accomplish these simple motion tasks.

19. Cleaning of the joint space.
20. Closure of the wound by stitches.

The surgical procedure described above doesn't fully apply to the custom-made Origin™ prosthesis by Symbios, also implanted within Tarabichi center. In this case, indeed, the trialing step is not conducted and significant disparities in the technical instrumentation is present. The reason for that

lies in the different designing principle between Origin™ and Persona<sup>R</sup>. While standard prosthesis rely on the size increments provided by the manufacturer company to fit patient’s measures, custom-made implants are based on the exact patient anatomy. The former are preferred when patient has a close to normal anatomy of the joint; the latter are applied when significant deformities of the knee prevent the surgeons from individuating landmarks or compromise correct cutting guides placement (case of patient N.O.A.G.D. is an example). Certainly, a custom-made design like Origin™ matches more accurately the patient’s geometry than standard Persona TKA. Indeed, although the 2mm femoral increments of Persona provide the most comprehensive femoral sizing scheme on the market,<sup>2</sup> this mm range of difference between one size and the other is not insignificant at the tissue level and can cause consistent over/underhang. This profile mismatch is instead avoided by Origin™ thanks to the CT scans of the patient joint acquired before TKA, that provide all the anatomical measurements needed to design a patient-specific implant. However, this undoubtedly more accurate method, requires more technical, economical and temporal effort with respect to standard TKA. At the same time, as dr. Tarabichi pinpointed, a customized prosthesis consistently limits the surgeon freedom and flexibility inside operation room. Indeed, along with the implant, the surgical instrumentation is patient specific too. Consequently, there is little to no room for mistakes in the bone cuts and implant alignment, with the doctor that has to follow precisely the guidelines provided by the manufacturer company. On the contrary, when implanting a standard prosthesis, the surgeon has a wide range of choices both for the components and the instrumentation, that can be exploited to correct any small mistake and therefore avoid any irreversible compromise of the arthroplasty success. Beyond this implant distinction, when asked which is the most challenging part of a standard TKA, dr. Anas pointed his finger at knee balancing. This step is even tougher for the surgeon when ACL is spared along with PCL.<sup>41,42</sup> However, recent publications suggest that novel design features and modern “smart instruments” (Fig. 26) can significantly simplify soft tissue balancing as well as the whole knee surgery and almost reset the complexity gap between BCR and ACL-sacrificing operations.<sup>7,9,39</sup> On the one hand, as will be discussed more in details in the 3D design results sections, PE inserts thickness mismatch between lateral (thicker) and medial (thinner) is facilitating a more anatomical joint alignment; on the other hand, gyros may be exploited for tibial alignment,<sup>129-131</sup> sensor devices for the gap balancing and haptic surgical robotic guides for precise tibial resection, eliminating the risks of eminence undermining in BCR TKAs.<sup>132</sup> It follows that patient specific designs combined to this smart instrumentation can finally provide an accurate and manageable replacement of the impaired joint in the nearest future.

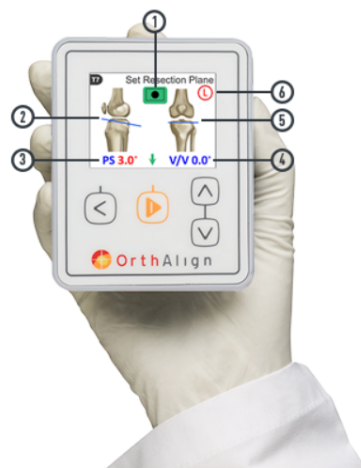


**Figure 26:** The gyro-guided KneeAlign<sup>R</sup> technology (OrthAlign, Aliso Viejo, CA) allows for accurate tibial and femoral cut during TKA.<sup>11</sup>

## Patients interviews

Table 3 shows the results of patients interviews, divided, for practical and space reasons, into three parts. For reading convenience, the questions table (Table 2) is reposed here so that the readers are not forced to jump constantly from one chapter to the other.

**Table 2:** questions asked to interviewed patients

Question number	Question
1	When did you start feeling pain in your joint(s)?
2	What did you try initially to deal with your knee(s) pain?
3	Which was your ROM before surgery?
4	Did you have significant deformities or previous trauma affecting your joint(s)?
5	Which were the mostly limited activities/motion tasks by your joint disease?
6	When did you attend total knee surgery?
7	How did you feel the first days of hospitalization after TKA?
8	How frequently are you doing rehabilitation sessions at the clinics?
9	How stable do you feel your knee(s)? (from 1 to 10)
10	How painful is it you knee(s)? (from 1 to 10)
11	How natural does your prosthesis feel after TKA (also known as FJS)? (from 1 to 10)
12	Do you hear noise from your implant(s) (clunks, pops, clicks..)?
13	Which is you actual ROM?
14	Are you now able to do main motion tasks (walking, stair climbing, cycling..)?
15	Are you now able to do main daily activities (shopping, driving, praying, housekeeping..)?
16	How satisfied are you about your artificial joint(s)? (from 1 to 10)
17	Would you recommend this experience to a person in your same pre-operative conditions?
18	Do you have any suggestion regarding TKR patients care, prosthesis design and implantation?

**Table 3.1:** patients answers to the first 6 questions related to the preoperative experience. The numbers in the top row are referred to the questions posed to patients (Table 2).

Patient	1	2	3	4	5	6
N.O.A.G.D.	1 year ago	Medications	5-120°	Previous fracture of distal femur of right knee 12 years ago. Mild varus deformity on right side	Walking, standing, stair climbing.	06/03/2021
M.G.C.G.	1 and half year ago	Physiotherapy, anti-inflammatories, hyaluronic acid injections	5-135°	Mild varus deformity on right knee	Walking, standing, stair climbing, kneeling, sleeping	23/11/2020 (5 months ago)
A.M.F.E.S.	13 years ago	Anti-inflammatory drugs	0-125° for right knee. 0-100° for left knee	Varus deformity of 20° on left side and 10° on right side. Flatfeet	Walking, sleeping, kneeling (and therefore praying)	21/04/2019 (2 years ago)

E.O.	6 years ago	PRP and corticosteroid injections, acupuncture, painkillers	Extension contracture 5°, flexion contracture 10°	No significant deformities	Walking, kneeling, bending over, stair climbing, sleeping	13/02/2021 (2 months ago)
------	-------------	---	---	----------------------------	---	---------------------------

**Table 3.2:** patients answers to the questions 6-12 related to immediate postoperative and actual experience. The numbers in the top row are referred to the questions posed to patients (Table 2).

Patient	7	8	9	10	11	12
N.O.A.G.D.	She had surgical pain, especially at night and felt the joint stiff	The first month, 3 times per week. Now one session per week.	9	6	8	She reported some clunks coming from the knee.
M.G.C.G.	He had stinging surgical pain, couldn't sleep properly	Irregular sessions for the first month. Then stopped for 4 months because of Covid-19. Now he will start again three times per week and later on undergo manipulation under anesthesia	6.5	10	2	No noise reported.
A.M.F.E.S.	She had stinging surgical pain, very slow in movements and needed significant support, felt discomfort in the operated knees	3 times per week for the first 2 months. Then stopped for 1.5 years because of Covid-19. Now she will start again three times per week.	2	7.5	3	After standing up for some minutes she feels the joint twisting and she hears some clicks in correspondence.
E.O.	She had stinging surgical pain, felt uncomfortable, couldn't sleep properly	The first month, 3 times per week. Now two sessions per week.	8	6.5	6	A few clunks and clicks heard while walking.

\*passively means with the physiotherapist's aid, actively without.

**Table 3.3:** patients answers to the last six questions related to the actual experience and personal thoughts about total knee replacement. The numbers in the top row are referred to the questions posed to patients (Table 2).

Patient	13	14	15	16	17	18
N.O.A.G.D.	0-135° actively. 0-145° passively.*	Yes, only bending is significantly painful.	Yes, only a bit slowed down because of the pain	9	Yes	No suggestions
M.G.C.G.	30-100° actively. 0-120° passively.	No, he is on a wheelchair.	No, he need assistance for all daily activities	5	No	"Future prosthesis should be able to provide a

						more normal feeling and higher ROM”
A.M.F.E.S.	0-125° actively. 0-135° passively	Limping on both sides when walking, inability to cross legs, kneeling is limited, bending is painful.	Daily activities are very limited. She cannot drive and pray. She need assistance for housekeeping and shopping	6.5	Yes	No suggestions
E.O.	0-120° actively. 0-140° passively.	Yes, only bending is significantly painful.	Yes, only a bit slowed down because of the pain	9	Yes	“TKA should preserve, as far as possible, the soft tissues stabilizing the knee in order to achieve a better feeling and a faster recovery”

Although the limited number of cases interviewed at Tarabichi center and reported in this work, some important conclusions can be drawn.

Patients consider Total Knee Replacement as the last resort for their joint impairment. Great concern is placed on the implantation of an artificial joint in place of the natural one and, most of the time, this distrust results in belated surgeries when the joint disease is in an advanced stage, and surrounding soft tissues are compromised.

The rehabilitation process is patient-dependent and certainly represents the key for a fast and optimal recovery after knee replacement, as supported by many publications in literature.<sup>12-16</sup> Indeed, as dr. Omar pinpointed, the first three months after surgery are known as the “golden period” when TKA patients can amplify their operated joint ROM window. Despite the consistent surgical pain, if the knee is trained perseveringly, there is high chance to restore a close to normal ROM spectrum. Otherwise, if a stationary condition prevails, soft tissues will scar and therefore block the joint, restricting its motion freedom. Physiotherapy sessions within the clinical environment generally starts with three appointments per week which then are reduced over time. Beyond these, home exercises must be done every day. If the rehabilitation route is executed correctly it lasts between 2 and 3 months dependently on patient’s age, muscular strength, efforts and so on. On the other hand, if patient’s ineptitude or external factors (like Covid-19) make this process irregular, it can extend up to years and generally leads to unsuccessful recovery (M.G.C.G. and A.M.F.E.S. cases).

The clinical outcomes of the implanted prosthesis are contradictory and do not lead to an univocal conclusion. Two patients (N.O.A.G.D. and E.O.) have an overall positive judgment of their TKA experience so far. They both expressed high satisfaction and great confidence for their future recovery. Instead, the other two patients revealed dissatisfaction (M.G.C.G. more than A.M.F.E.S.) and discontent. It’s difficult to uniquely establish the underlying reasons for this disparity. Yet, the implant design can be surely discarded as an option, since M.G.C.G and N.O.A.G.D. received the same PS Origin™ implant as well as E.O. and A.M.F.E.S. the same CR Persona<sup>R</sup>, but had totally different outcomes. There’s little to no possibility that the surgical procedure tipped the balance in this outcome disparity. Indeed, the exact same medical equipe performed the highly reproduceable TKA procedures for all the interviewed patients. What, instead, it’s likely to represent the main cause of dissatisfaction is the poor rehabilitation process, with both M.G.C.G. and A.M.F.E.S. that

had a troubled and inconstant physiotherapy, while E.O. and N.O.A.G.D. are attending sessions with regularity. It's reasonable that other explanations can lurk behind these contradictory results, like patient's lifestyle, BMI, age, body response to the artificial joint and many others. For time constraints it was not possible to deeply investigate these possibilities and therefore additional researches should be undertaken in order to safely determine the key factors for TKA success and patients satisfaction.

Beyond these considerations, the main take-home message that emerges from the patients interviews is that the current PS and CR implants are not able to completely restore the natural knee, especially in the joint awareness and feeling. Even the two patients who reported satisfaction and optimism around their implant admitted to feel the operated knee(s) as abnormal. All patients revealed discomfort coming from artificial joint(s) during daily activities or after being seated for some minutes. E.O also reported thermal sensibility and a stiffness feeling related to the operated knees. Most of the patients complained about noises such as clunks and clicks originating from the artificial implant(s). At the same time, when looking at the active ROM reached by the interviewed patients, three out of four cannot go beyond 125° (with high pain at late flexion), resulting in significant limitations in daily activities and religious habits (muslim kneel while praying). These aspects, reinforced by the patients suggestions reported in Table 3.3, suggest that kinematic and proprioceptive performances of CR and PS implants should be further improved by design modifications or a more anatomical approach like BCR TKA. What is actually present on the market offers valid and robust solutions to diseased and impaired knees. However, patients interviews at Tarabichi center totally reflects the dissatisfaction atmosphere around current TKR options and suggest that novel approaches are required to dissolve the latter.

## **Design of the hybrid BCR tibial component**

The three-dimensional design of the novel "hybrid" BCR tibial component was a long and winding path. All the steps constituting the latter are here reported in a chronological order, starting from the initial 2D spline drawing to the final materials application and rendering. For each design feature or stride, an initial discussion will provide readers with a detailed overview of the rationale behind it. After the delineation of the design step criteria, the proper design process within 3Ds Max software will be thoughtfully described and key images will be presented in parallel as well.

### **2D spline design**

#### **Reference framework and background**

The first step of the three-dimensional implant designing process was the profiling of the 2D proximal tibial contour. Before starting with the actual software drawing, literature investigation was undertaken in order to establish the level of asymmetry, anteroposterior (AP) and mediolateral (ML) measures and radii of curvature of the tibial 2D profile.

The asymmetry of the proximal tibial outline is a well-established concept nowadays in arthroplasty field. However, apart from Journey II XR prosthesis,<sup>46</sup> all BCR implants on the market feature a symmetric configuration <sup>s.r.</sup>. As already mentioned previously, the presence of a central cut-out dramatically reduces the bone coverage guaranteed by the tibial component, undermining the implant stability and fixation. Symmetric tibial designs simplify the manufacturing process and reduce inventory costs at the expense of bone coverage and implant alignment.<sup>28,29,123</sup> This configuration unavoidably produces over/underhang and therefore lead to impingement or loosening respectively, both finally resulting in implant failure (Fig. 29).<sup>28,29,33,34</sup> At the same time, when surgeons attempt to align the posterior aspect of a symmetric design on the smaller, lateral

tibial plateau, internal rotational malalignment is likely to occur. Such implant malrotation may cause rotatory subluxation with increasing edge loading and early failure of PE inserts, uneven patellofemoral tracking, translation and/or dislocation of the patellar component with subsequent PE wear<sup>32</sup> and consequently is responsible for over 50% of painful TKA cases.<sup>31</sup>

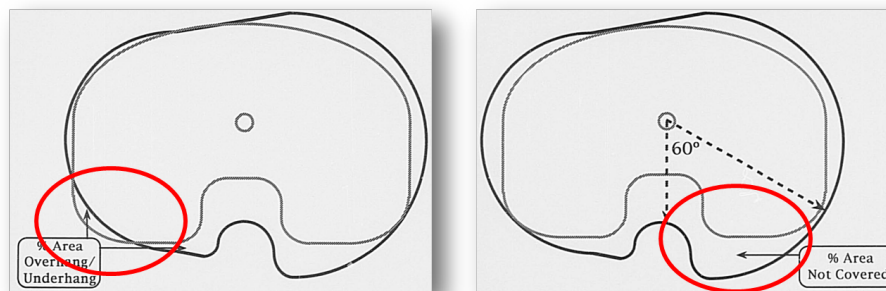


**Figure 29:** Symmetric tibial implant (grey profile) on asymmetric proximal tibial surface (black profile). A symmetric design can either cause overhang (left) or underhang (right), since its surface it's not matching the underlying bony one.<sup>30</sup>

On the other side, asymmetric, anatomic designs can closely fit the proximal tibial contour, ensuring maximal bone coverage and cortical support and proper implant alignment. In this way, it's possible to compensate for the BCR central aperture and reach a fixation rate akin to the standard ACL-sacrificing designs. Last but not least, the condyles inequality reproduced by asymmetric designs, allows, as in nature, normal knee valgus alignment, equalizing loads on medial and lateral compartments.<sup>35</sup> Given this, an anatomical tibial profile was chosen for the BCR implant of this project.

Regarding AP and ML dimensions and radii of curvature of the tibial outline, the significant joint size variability between patients and the recognized differences between genders and ethnicities, prevents implant designers from producing a universal prosthesis relying on a single measures set.<sup>29</sup> That's why each component should be either custom-made or offered in a sufficient sizing scheme to cover the whole population variations. Since our novel prosthesis was aimed as a proof of concept and not, at this stage, for commercial purposes, one single size set was utilized. It was reasonable then to utilize mean values reported in tibial plateau morphological analysis publications available in literature. Therefore, AP and ML dimensions along with medial and lateral anterior radii of curvatures were extracted from the male Caucasian average tibial measures divulged by Yifei Dai and Jeffrey E. Bischoff and exploited for the tibial design of Persona by Zimmer<sup>29</sup>. In addition, the 2D tibial proximal profile was delineated with reference to the resection specimen based drawings of dr. Geoffrey et al.<sup>28</sup> From this publication, the mean anteroposterior measurements at 10, 20, and 30, 50% of the width of the medial and lateral tibial plateau specimens were also exploited for our tibial design. In this way, data originating from two different anthropometric publications were merged aiming for a tibial contour as much representative and anatomical as possible. Nevertheless, due to the different methodology and specimen cohort of the two papers, expecting a perfect match between the data was totally unreasonable. Yet, the confidential intervals (c.i.s) provided by both publications allowed us to adjust the measures of one paper to the other's ones, without overturning the 2D profile.

**Table 1: AP Dimensions (mm) (Mean ± Standard Deviation)**

AP <sub>medial</sub> 10%	37,9 ± 4,2
AP <sub>medial</sub> 20%	47,4 ± 4,8
AP <sub>medial</sub> 30%	50,6 ± 5,8
AP 50%	42,9 ± 6,8
AP <sub>lateral</sub> 10%	34,8 ± 4,5
AP <sub>lateral</sub> 10%	41 ± 4,9
AP <sub>lateral</sub> 10%	41,6 ± 5,4

Initially, the exact mean 10, 20, 30, 50% AP measurements of Geoffrey's paper (Table 1) were faithfully reproduced and drawn on the x-y plane as reference (since no ML and AP dimensions were known at this stage yet, the placement of 10, 20, 30, 50% AP lines on x-y plane was rough at first instance) whereas ML, AP, and anterior radii values of Dai's paper were subsequently adapted accordingly, but never going out of their c.i.s. starting point of the 2D spline drawing was to create



a rectangular bounding box, similar to the one built by Dai and Bischoff (Fig. 30 A, solid grey line).

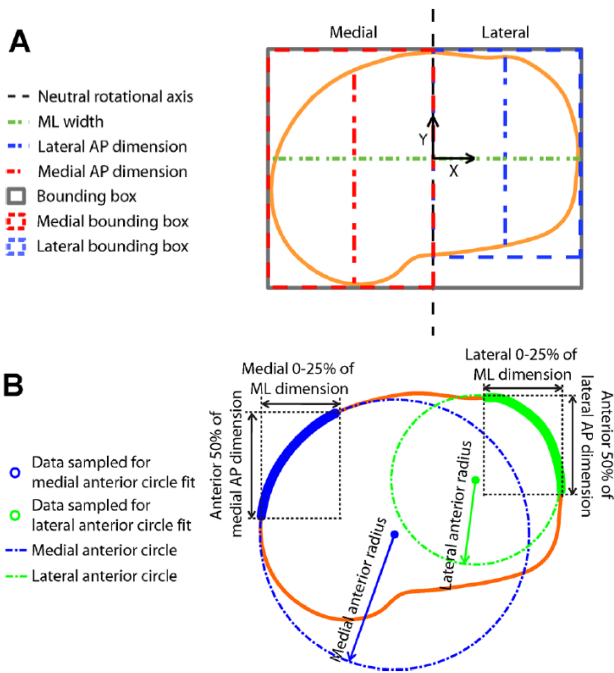


**Figure 30:** Schematic representation of (A) dimensional and (B) radius measurements by Dai and Bischoff.<sup>29</sup>

As ML width (the width of the bounding box), the mean male Caucasian ML dimension (78,13 mm)<sup>29</sup> was then summed with half of the c.i. of 3,91 mm resulting in ML = 80,085 mm.

$$ML = 78,13 + (3,91/2) = 80,085 \text{ mm}$$

ML dimension will be the width of the bounding box.

Once ML dimension was determined, it was possible to calculate the percentage values of the latter (Table 2) in order to precisely collocate the 10, 20, 30% AP splines (Fig. 32, red vertical lines).<sup>28</sup>

Table 2: Percentages values of ML width (mm)

$M_{10\%}$	8,009
$M_{20\%}$	16,017
$M_{30\%}$	24,026
$M_{50\%}$	40,043

In order to establish the AP dimension (the length of the bounding box), not directly provided by Dai's paper, the bounding box area was then divided by the ML width. However, before doing that, the mean area value (4670 mm<sup>2</sup>) was subtracted by half of the c.i. of 450 mm<sup>2</sup>. The resulting AP dimension was 55,504 mm.

$$AP = (4670 - 225) / 80,085 = 55,504 \text{ mm}$$

As anterior medial radius of curvature ( $AR_m$ ), the average value of 38,67 mm was subtracted by its c.i. (7,61 mm) resulting in a final  $AR_m = 31,06$  mm. As shown in figure 30 B, this radius is the fitting curve of the medial contour from the anterior 50% of medial AP dimension to the medial 0-25% of ML dimension. In our design, this area was identified by two splines (Fig. 32, blue lines):

- A vertical line positioned at  $x = 20,021$  mm (25% of ML medial side)
- An horizontal line positioned at  $y = 0,051$  mm (50% of medial AP)\*

$$AR_m = 38,67 - 7,61 = 31,06 \text{ mm}$$

As anterior lateral radius of curvature ( $AR_l$ ) instead, the average value of 24,16 mm was subtracted by the half of its c.i. (2,11 mm) resulting in a final  $AR_l = 22,05$  mm. As shown in figure 30 B, this radius is the fitting curve of the lateral contour from the anterior 50% of lateral AP dimension to the lateral 0-25% of ML dimension. In our design, this area was identified by two splines (Fig. 32, green lines):

- A vertical line positioned at  $x = -20,021$  mm (25% of ML lateral side)
- An horizontal line positioned at  $y = 0,475$  mm (50% of medial AP)\*

$$AR_l = 24,16 - (4,22/2) = 22,05 \text{ mm}$$

Once all these reference measurements were calculated, the resulting splines, rectangular bounding box (Fig. 32, black rectangular outline) and fitting anterior circles (Fig. 32, blue and green circles) were drawn in Top view ( $z = 0$ ). In order to do that, under the creation tab, 2D spline mode was utilized. The bounding box and the underlying reference plane were centred in the origin (0;0;0). After having these guidelines on the scene, the time had come to start with the actual 2D tibial profile design. As a background reference, the schematic representation based on analysed proximal tibial resection specimens provided by dr. Geoffrey et al. was employed (Fig. 31).

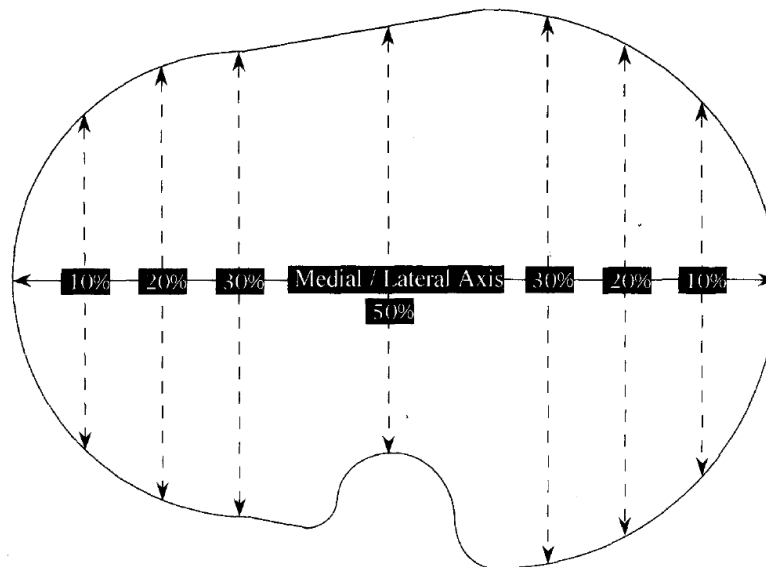


**Figure 31:** Drawing of a proximal tibial resection specimen, with his ML axis and the 10, 20, 30, 50% AP medial and lateral dimensions.<sup>28</sup>

It was decided to utilize Geoffrey's contour instead of Ray's one for two main reasons. First, no implant on the market ever based its design on such a profile yet. Second, according to dr. Tarabichi and his vast clinical experience, Geoffrey's tibial outline more closely represent the real anatomical shape of resected proximal tibia with respect to Ray's one. The key aspects emerging from such profile are:

- The medial condyle is larger than the lateral one and features a more symmetric radius of curvature with respect to the increasing posterior radius on the lateral side.
- Looking from the top view, the medial condyle reaches more posterior and anterior locations than the lateral condyle.
- The anteroposterior difference between the two condyles increases moving towards the joint centre.<sup>28</sup>

A rectangular plane matching exactly the ML and AP dimensions previously determined was created above the bounding box and Geoffrey's image was applied on it as a bitmap (Fig. 32).

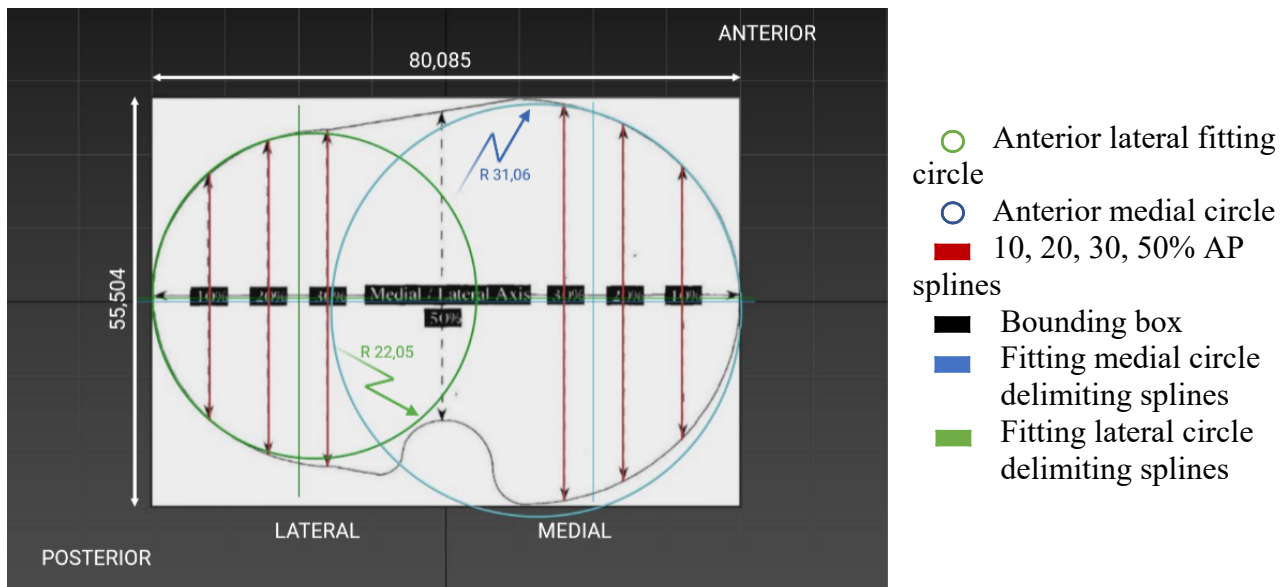


**Figure 32:** Reference framework and background image exploited for the subsequent tibial 2D contour design. Values in mm.

\*medial and lateral AP dimensions and central axis were estimated at a second stage from the reference tibial image imported into 3Ds max (Figure 31). Medial AP dimension was measured to be 54,956 mm. Since the minimum medial condyle point (in AP direction) was at  $y = -27,427$  mm the medial central axis was then located at  $y = -27,427 + (54,956/2) = 0,051$  mm. Lateral AP dimension was measured to be 45,963. Since the minimum lateral condyle point (in AP direction) was at  $y = -22,507$  mm the medial central axis was then located at  $y = -22,507 + (45,963/2) = 0,475$  mm.

### Fitting circles and transition lines.

With the reference tibial contour as a background, the best fitting circles for medial and lateral compartments were searched visually (Fig. 33). It was clear soon that more than one circles was needed for each condyle to match the curvature of the outline. Among these, the primary circles were initially sought. With this term, the curves fitting the majority of the medial and lateral contour excluding the closing regions (most anterior and posterior areas of the condyles) were meant.

After tens of trials, the best fitting primary medial/lateral radii and centres characterizing the primary circles were found to be:

- Primary medial circle.  $R = 26,2$  mm,  $C = (13,724; 0,026; 0)$ .
- Primary lateral circle.  $R = 22,05$  mm,  $C = (-17,876; 0,833; 0)$ .

Once the primary circles were determined, the secondary ones were investigated. The latter were divided into anterior closing circles and posterior closing circles, resulting in two secondary fitting circumferences per condyle.

The radii and centres defining the four secondary circles are here reported:

- Anterior closing medial circle.  $R = 31,94$  mm,  $C = (9,832; -4,432; 0)$ .
- Posterior closing medial circle.  $R = 30$  mm,  $C = (10,932; 2,621; 0)$ .
- Anterior closing lateral circle.  $R = 24,5$  mm,  $C = (-15,773; -1,095; 0)$ .

- Posterior closing lateral circle.  $R = 24,5 \text{ mm}$ ,  $C = (-15,615; 2,203; 0)$ .

Subsequent to the closing circumferences, the next step was to design the anterior and posterior oblique lines (Fig. 33). The former represented the transition between medial and lateral condylar contours; the latter bridges the posterior lateral closing circle to the cruciate cut-out. This transition was thought to imitate the increasing posterior radius of lateral side described by Geoffrey et al., but using a oblique line instead of a fitting circle. This simplification was reasonable because the degree of curvature in the posterior transition region was minimal and a little waviness would have been given to the line by subsequent editing.

The anterior transition line was then drawn with a  $9,2^\circ$  inclination in z direction, while the posterior with a  $-10^\circ$  inclination.

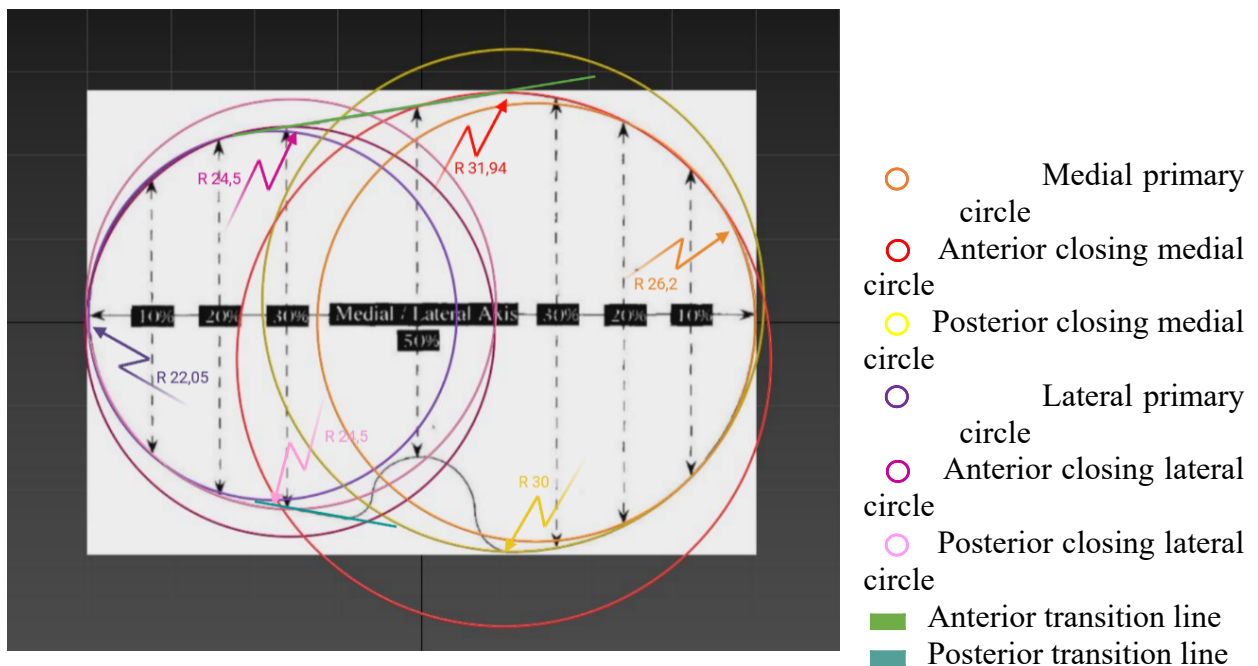


**Figure 33:** Fitting circumferences and transition lines for medial and lateral contours. Values in mm.

### Trim-weld-fillet operation

Upon plotting all the fitting circles and transition lines in 3Ds Max, the next step was to smoothly bridge one spline to the other in order to follow the background image contour. In this direction, all the abovementioned 2D geometries were initially converted into editable splines and then attached together. Now, with spline mode selected, trim tool was employed to firstly detect the intersection points between the attached geometries and secondly, to delete the unwanted segments. Trim operation leaves two distinct points at the intersection site that therefore needed to be welded in order to end up in a continuous curve starting from the posterior end of lateral condyle to the one of medial. The past intersection points, now turned into transition points between one spline and the other, presented a sharp and edgy changeover after trim operation. In order to smooth the latter, two operations were performed. The first option was to convert the transition points into bezier corners and then move the two independent tangent handles adjusting the degree of curvature of the section. Otherwise, fillet operation was applied to the transition points and, playing on the radius value, it

was possible to round up the previous acute corners to perfectly match the underlying reference contours. The resulting condylar outline is showed in Figure 33b. The sequence of trim, weld and fillet operations is a crucial process to design complex, multi-radius bidimensional splines starting from simple 2D geometries. For this reason, everytime a 2D spline editing was required throughout the project, the composed operation precisely described above was performed and will be then mentioned in this report by the term “trim-weld-fillet operation”.

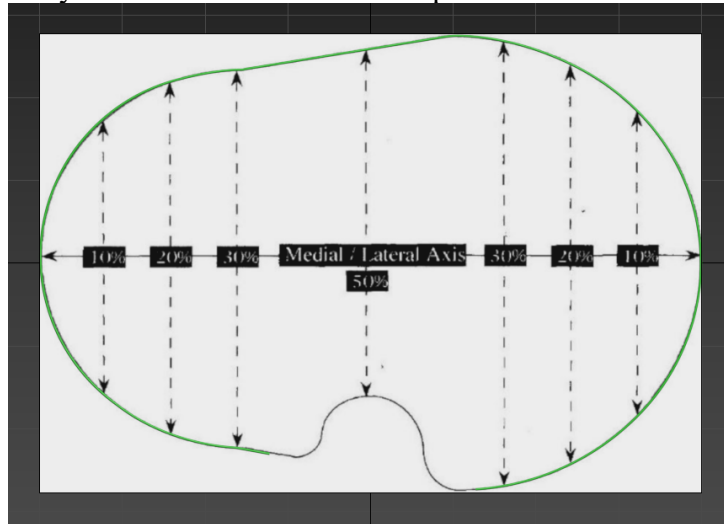


**Figure 33b:** the green curve above the background reference image contour (in black) represents the spline obtained after the trim-weld-fillet operation applied on the 2D geometries of Figure 33.

### Cruciate cutout

Dr. Geoffrey’s resection specimen schematic representation depicts the proximal, transverse, tibial profile, following the whole bony contour. Hence, it’s clear that this design does not account for a central aperture, essential for cruciate preservation in BCR TKA implants. Such cruciate cutout was therefore introduced from scratch by the author to the condylar profile, substituting in this way the small minor recess in Geoffrey’s image. As for the outer contour, even now for the central aperture a framework of reference lines were initially sketched. The first one to establish was the anterior limit of ACL attachment. In this direction, morphological studies of ACL attachments extension available in literature were contemplated. Among these, dr. Colombet et al. reported the distance between the anterior border of the ACL attachment area and the anterior border of the tibial plateau to be 13,1 mm on average (Fig. 34, segment ai)<sup>36</sup>, dr. Girgis et al. 15,2 mm<sup>37</sup>, Staubli et al. 15,2 mm<sup>38</sup> and dr. Dijk 15 mm<sup>39</sup>. Since Colombet study was even based on the least number of specimens analysed, a 15 mm distance between anterior tibial border and ACL attachment was decided for our cutout design. The most anterior medial point was individuated by an horizontal line positioned at  $y = 25,919$  mm (Fig. 36). Moving 15mm posteriorly from this upper line, the anterior cruciate cutout limit was drawn ( $y = 10,919$  mm).

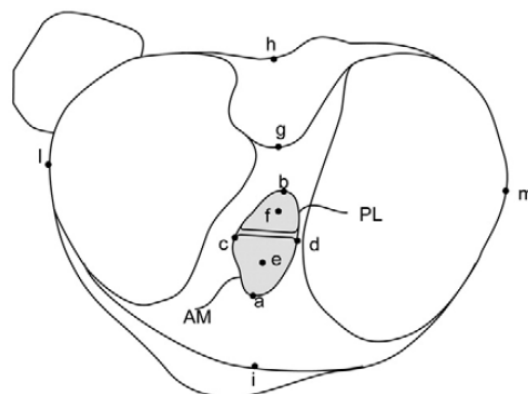


**Figure 34:** Morphological representation ACL attachment sites with the measurements points a-m by Colombet et al.<sup>36</sup>

Subsequently, it was necessary to establish the posterior and central width of the cruciate aperture. Significant variability in transverse dimensions of the intercondylar area between papers analysing different ethnicities was found in literature.<sup>40-42</sup> After a discussion with dr. Elfekky and dr. Tarabichi it was decided to follow the measures provided by Jacobsen, reporting a transverse measurement of intercondylar area at posterior end on Danish population of 16 mm on average.<sup>41</sup> Therefore, two vertical lines positioned at  $x = 8$  mm and  $x = -8$  mm were drawn at the beginning of the central aperture to delimit the posterior width (Fig. 36). The width of the intercondylar area beyond the posterior extremity then shrinks consistently at middle narrow region and finally widens up at the anterior end, correspondingly to ACL location (Fig. 35).

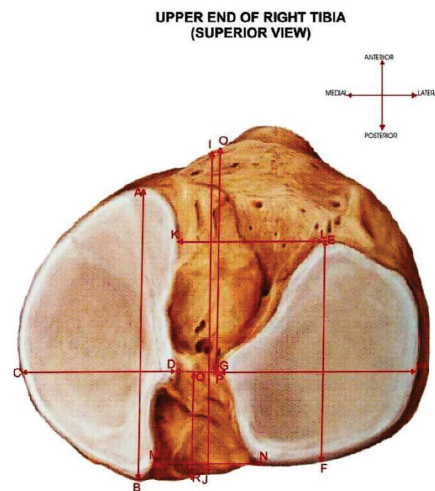


**Figure 35:** top view of right tibia.

As can be seen from the image, the anatomical intercondylar width reaches its minimum in the middle region (DG) and then gets wider going both anteriorly (KL) and posteriorly (MN), with the anterior region being the broader area.<sup>40</sup>

Reproducing such complex and asymmetric profile would bring more drawbacks than benefits. Indeed, a consistent boost in the design and manufacture difficulty would be introduced and the narrow central width would threaten the cruciate ligaments, whereas the increase of bone coverage would not be significant at the same time. For this reason, in our design, a simpler outline was drawn (Fig. 40). In order to guarantee enough action space for the ACL, the aperture width was increased from the 16 mm posteriorly to 20 mm anteriorly, differing from the constant notch width of the commercially available BCR TKAs. In this direction, two vertical lines positioned at  $x = 10$  mm and  $x = -10$  mm were plotted as anterior width boundaries (Fig. 36). It's important to pinpoint that, as suggested by dr. Tarabichi, it's not vital to perfectly match the anatomical cruciate attachments extension by the implant aperture, as during surgery the ligament base can be partly trimmed without compromising the cruciate functionality.

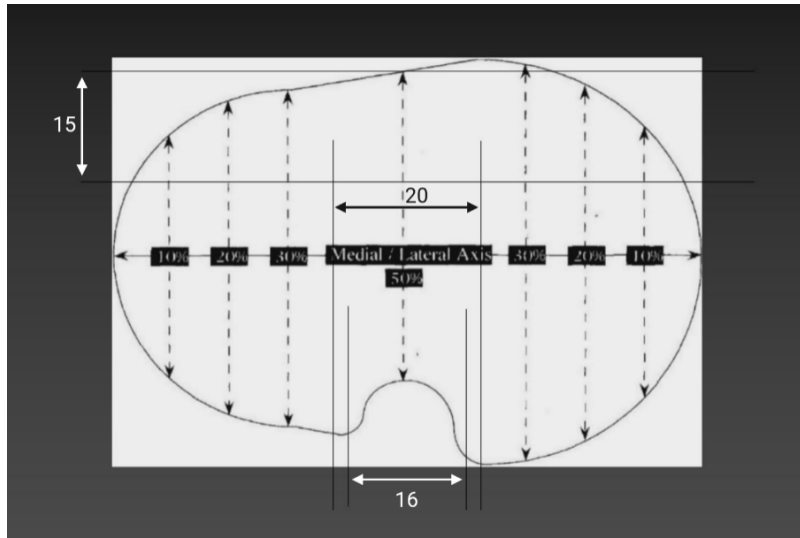


**Figure 36:** cruciate cutout delimitation lines and reciprocal distances (in mm).

Upon having sketched the margins, the following step was to draw the primitive 2D elementary geometries to start from for the central notch profile design. Laterally, a posterior circle of radius  $R = 3$  mm was created to link the medial tibial profile to the cutout. With this scope, the circle pivot was moved from its centre to the lateral vertex and then aligned to the posterior lateral margin line via tangent snap mode. Afterwards, the circle bottom vertex was aligned in the same way to the lateral tibial outline (Fig. 37). The resulting circle centre was positioned in  $C = (-11; -20,142; 0)$ . On the medial side, the same process was undertaken, with a 4,45 mm radius circle centred in  $C = (12,45; -22,885; 0)$ . Subsequent to this transition, the lateral cutout profile was thought to follow the vertical margin until  $y = -12,5$  mm and then move smoothly to the 20 mm wide ACL boundary. In order to accomplish this second changeover, a 40mm radius circle centred in  $C = (30; 0; 0)$  was plotted (Fig. 37). After trim-weld-fillet operation, a sinuous profile was obtained medially. Such contour was mirrored with respect to x axis leading to a symmetrical curve on the medial side (Fig. 38).

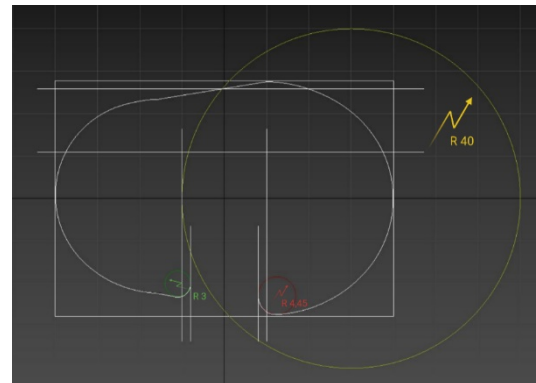
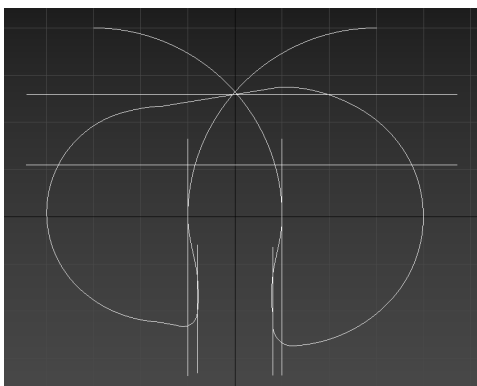


**Figure 37:** posterior medial (red) and (green) circle and profile transition lateral circle (yellow).



The final step for the cruciate aperture design was to delineate the anterior contour. In this direction, two 5 mm circles were plotted medially ( $C = (4,565; 5,645; 0)$ ) and laterally ( $C = (-4,71; 4,594; 0)$ ) as well as a bigger anterior transition circumference of  $R = 15$  mm, centred in  $(1,973; -4,017; 0)$ . The bridge between these curves was an oblique line featuring the same inclination of the anterior tibial border, resulting in two parallel, asymmetric profiles (Fig. 39). This more anterior location of the notch on the medial side, also present in Journey II XR design by S&N, reflects the natural more anterior medial position of the anterior

cruciate and therefore allows for safe acceptance of well fixed ACL footprint.<sup>46</sup>

**Figure 38:** posterior cutout profile after trim-weld-fillet operation.

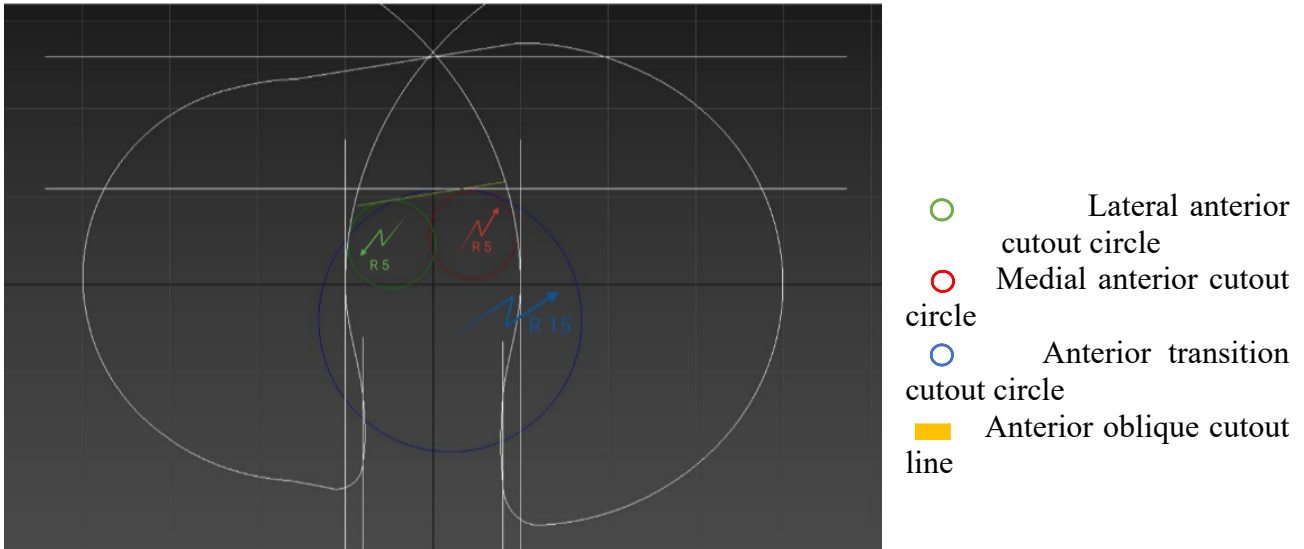


**Figure 39:** 2D starting geometries from which the anterior cutout contour was designed.

In the end, trim-weld-fillet operation was performed on the abovementioned 2D elementary geometries, resulting in a continuous outline, that was ultimately unified to the tibial profile. The final design of the 2D tibial profile is shown in figure 40.

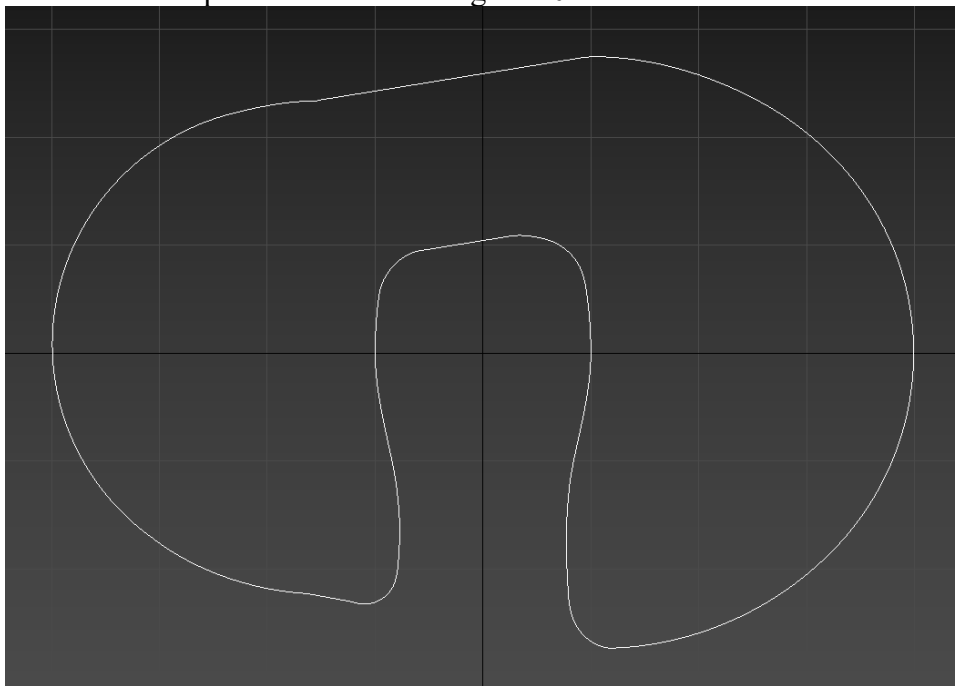


**Figure 40:** completed transverse 2D tibial profile.

### 3D extrusion

The second design step was to do an upper extrusion of the 2D tibial profile in order to give the third dimension to the geometry ( $z \neq 0$ ). Extrusion height, representing the tibial baseplate thickness, was initially investigated through online literature and discussed with the doctors. A recent publication could show that thick CoCr tibial tray (4mm) are associated to high incidence of proximal tibial bone resorption, leading to stress-shielding phenomenon, that can ultimately cause tibial instability and loosening.<sup>43</sup> These results are reinforced by a dr. Martin's research proving that 4 mm thick CoCr tibial tray results in significantly more medial tibial bone loss with respect to thinner CoCr baseplates (2,7 mm).<sup>44</sup> In addition to the higher mean bone resorption amount (1.07 vs



0.16 mm;  $P \frac{1}{4} .0001$ ) reported for thicker implant cohort, consistently higher prevalence of bone loss (44% vs 10%,  $P \frac{1}{4} .0002$ ) was found for the latter. Apart from the well-known influence of the high CoCr stiffness on surrounding bone resorption,<sup>45,127</sup> from Martin's results it's easy to infer that even material thickness is strictly correlated to this. Indeed, flexural rigidity of a plate increases by the cube of its thickness.<sup>45</sup> At the same time, a thin tibial baseplate increases the minimum polyethylene thickness<sup>46</sup>, resulting in a wear reduction over time.<sup>47</sup> For all the abovementioned reasons, a 2,5 mm extrusion height was agreed for our tibial tray design. In order to accomplish that, an extrusion modifier was applied on top of the selected tibial 2D spline and the extrusion amount was set to + 2,5mm in z direction (Fig. 41).

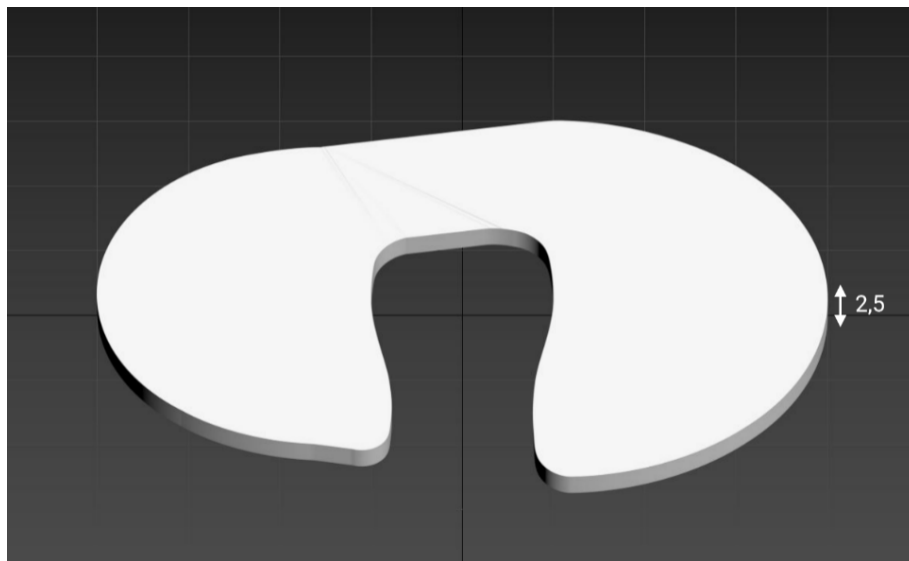


**Figure 41:** 3D tibial baseplate after the 2,5 mm upper extrusion. Values in mm.

### Anterior hemisphere

As mentioned before, one of the biggest limitations of BCR TKA designs is the fragility of the thin anterior tibial bridge that can lead to fatigue breakage over time. In order to address this problematic, the creation of a fixation anterior component was discussed. The ideal shape of the latter should be rounded to avoid stress concentration<sup>48</sup> and at the same time it should be easy to insert in the tibial bone during surgery. Therefore complex geometries that require challenging cuts and skillful preparation procedure should be avoided. Inspired by NexGen cementless implant (Zimmer Biomet, Warsaw, IN)<sup>50</sup> (Fig. 42), an hemispherical component was opted for.



**Figure 42:** Nexgen cementless tibial component featuring two hexagonal pegs and a central hemispherical pin.<sup>49</sup>

The underlying reason for such a geometrical shape is that a complementary groove can be easily dig into the proximal tibial bone by a spherical rasp once the transverse cut is done. Our aim was to design it in such a way the majority of the anterior bridge would be covered by this fixation component. In this way, it would be possible to both stiffen up this region and increase the thickness and therefore the robustness of the otherwise weak bridge. At the same time, the bone contact would be significantly increased by such spherical configuration, enhancing implant fixation. Moreover, this central element should act as a central pivot preventing unnatural implant rotation trough ROM.<sup>49</sup>

With this purpose in mind, a reference circle of radius 7,658 was drawn onto the bottom surface of the anterior bridge. This value was found to be the optimal fit to have maximum implant coverage, without any overhang. Any smaller radius would have led to some uncovered bridge areas (therefore prone to breakage), whereas any higher radius would have resulted in hemisphere overextension beyond tibial contours. Aiming to place the circle at the bridge centre, the upper and lower bridge lengths were calculated and their halves were exploited to position the circumference. In particular, the upper length was found to be 24,221 mm while the lower 8,696 mm. Knowing these dimensions, two reference lines were sketched halfway in both sides. The circle centre was finally moved in the middle of the x-distance between these two lines, resulting in  $C = (-2,459; 17,837; 0)$  (Fig. 43).

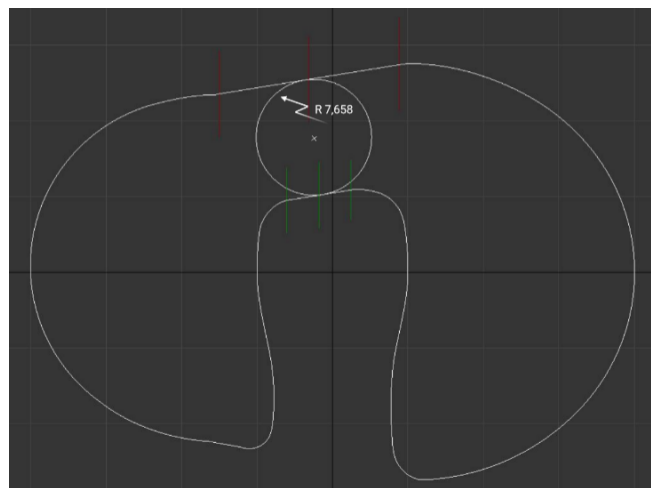


**Figure 43:** Upper bridge measurement extremities and their middle line (red) along with lower bridge measurement extremities and their middle line (green). The benchmark circle was positioned halfway of the distance between the middle red and middle green lines as shown by the tiny cross representing circle centre.

Once, the benchmark circumference was plotted and correctly positioned, the actual 3D sphere was designed on top of it, using the standard primitives pop-up in the creation tab. The sphere featured the same radius and centre of the circle. Upon its creation, an hemisphere value of 0,5 was assigned to the geometry and the maximum segments number of 100 was set to produce a smooth and rounded surface (Fig. 44).

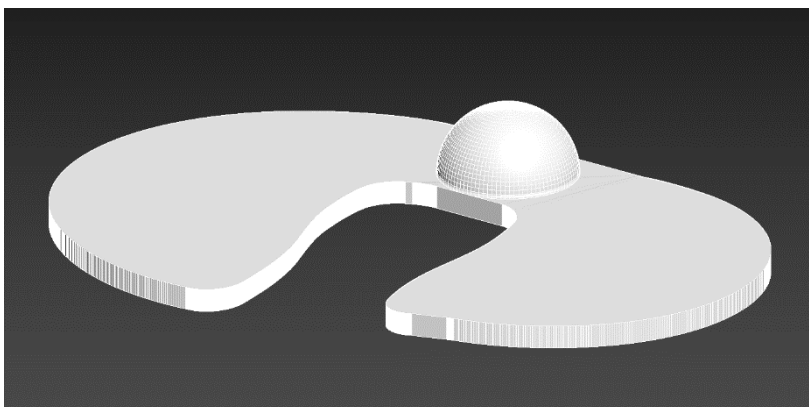


**Figure 44:** orthographic, bottom view of the 3D smooth hemisphere created below the anterior tibial bridge.

A final modification was applied to the hemisphere. After converting it into an editable poly, half of the hemisphere faces were alternatively selected and an inner extrusion of -0,5 mm was applied to these (Fig. 45 B). This modelling step produced a highly grooved structure, thought to have an increased bone contact surface and entrapment with respect to the previous smooth geometry, thanks to the recesses introduced (Fig. 45 A). However, dr. Tarabichi pinpointed that if the hemisphere was made of trabecular metal, the grooving effect would be already present thanks to the high porosity level of this rough biomaterial and therefore it wouldn't be worth to apply such highly manufacturing demanding design step. Yet, it could be argued that the Tantalum microchanneling does not exclude or overwhelm the macrogrooving of the selective negative extrusion modification, but rather these two architectures can coexist and amplify each other resulting in a highly interconnected texture, intricately embedded and fixated within the surrounding bone environment. Further investigations are therefore required in this direction.

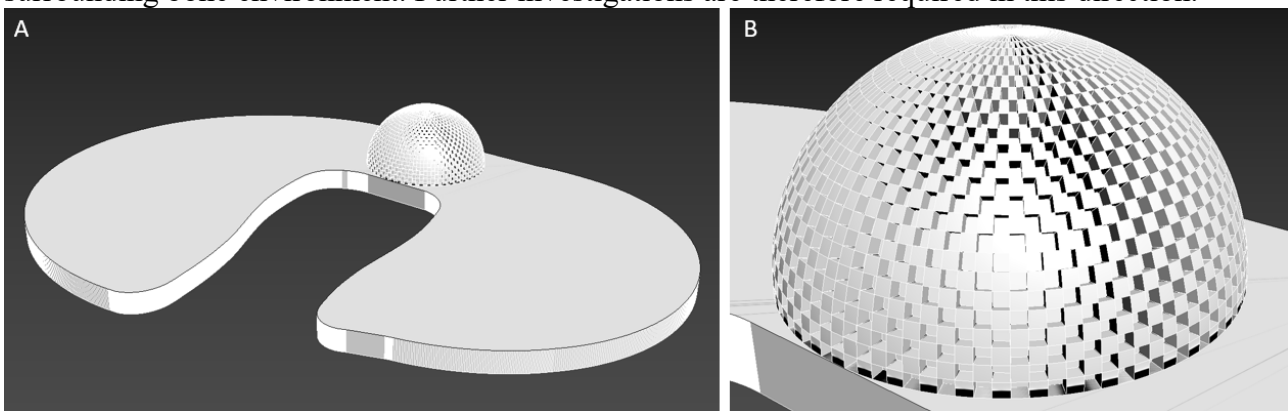
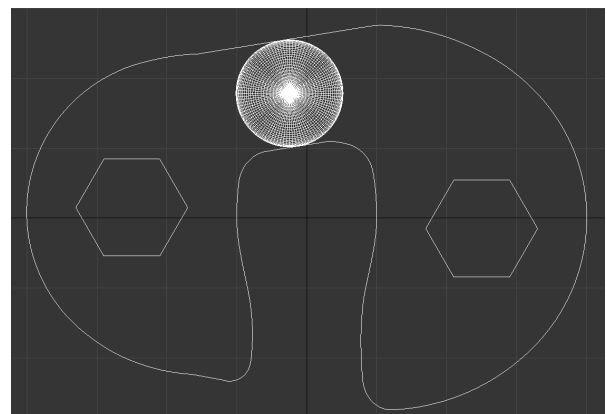


**Figure 45:** orthographic, bottom view of the 3D grooved hemisphere created below the anterior tibial bridge (A) and a close-up of the 0,5 mm negative extrusion performed on the hemispherical geometry (B).

### Hexagonal pegs

Persona<sup>R</sup> cementless TKA by Zimmer Biomet has a well proven fixation reached by the employment of two press-fit, 16 mm long hexagonal pegs.<sup>52-54</sup> These two components, made of Trabecular Metal, engage the area of highest tibial bone density in line with condylar loading, ensuring great prompt cementless fixation.<sup>49</sup> The hexagonal shape at the same time guarantee exceptional stability and locking once the pegs are impacted inside the circular hole drilled to make room for them, due to this shape mismatch. Providing a robust implant stability was a key goal for our BCR design. Hence, assured by Persona<sup>R</sup> successful results, two hex-pegs were added as fixation components to the tibial design. Initially, two hexagonal polygons were plotted on the bottom tibial surface, one on medial and one on lateral side. The radius was agreed with the doctors to be 7 mm. These geometries were initially positioned at  $y = 0$  and then moved on the  $x$  axis to the condyles respective middle points. The latter were previously calculated to be at  $x = -25,013$  mm for the lateral and at  $x = 25,02$  mm for the medial compartment. The resulting hexagons centres were at  $C_l = (-25,013; 0; 0)$  laterally and  $C_m = (25,02; 0; 0)$  medially. Nevertheless, as suggested by recent unpublished researches by Zimmer Biomet, an asymmetrical placement of the hex-pegs is more likely to prevent insertion mistakes.<sup>55</sup> Indeed a slightly more anterior lateral and a more posterior



medial position of the pegs better reflects the anatomical asymmetry in the tibial epiphysis and therefore should guarantee a correct centred implantation without any peg overhang outside the tibial cortical bone. For this reason **Figure 46:** asymmetrically placed hex-pegs on the bottom face of the lateral hex-peg was finally translated anteriorly to  $y = 1,5$  tibial tray. mm, while the medial was moved posteriorly to  $y = -1,5$ mm (Fig. 46). On top of that, a lower extrusion of + 15 mm was ultimately applied to the hexagons (Fig. 47).

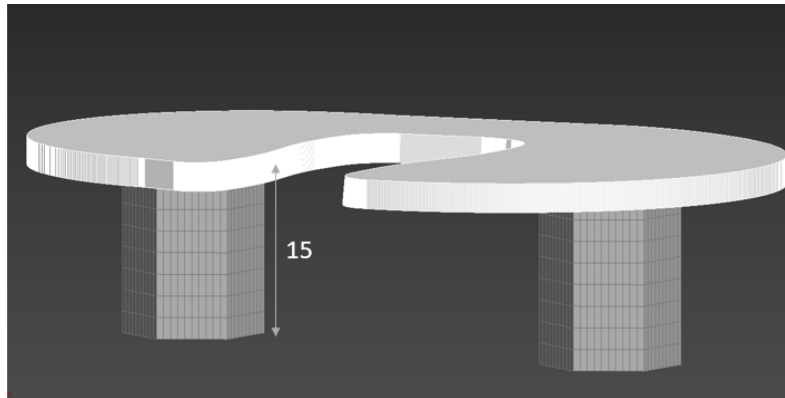
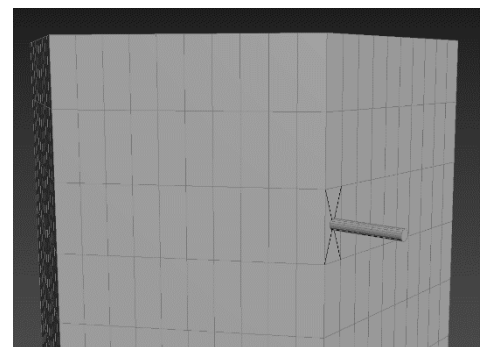


**Figure 47:** 15 mm long hexagonal pegs.

### Perimetral spikes

As can be seen from Figure 47, 8 extrusion segments (horizontal) were assigned to the geometry, as well as 9 vertical division lines, created by “connect” operation. In this way, each hexagonal face was parted in 10 horizontal x 8 vertical subparts. This modelling step was added in order to pave the way for the application of spikes around the pegs surface. These new fixation features were introduced at the suggestion of dr. Tarabichi, under the influence of **who?** Report presented at ..... Thin metal anchors are indeed thought to improve not only the long term but even more significantly the immediate implant fixation, reducing the initial instability associated to cementless implants in the first weeks after surgery, before osseointegration and bone ingrowth start.<sup>56-57</sup> Obliquely upwards directed spikes (Fig. 48) allow the insertion of the tibial component thanks to their internal collapsing, while implant retraction is hampered as the anchors will hook to the surrounding bone network and therefore fixate the prosthesis. A simple wire-like configuration for the spikes was decided, ensuring low manufacturing complexity. Two perimetral rows of equally spaced anchors were considered sufficient to guarantee the aimed tibial fixation, without significantly altering the peg size. In a certain way, these spikes could be seen as tiny “hairs” coming out in multiple directions from the hex-peg faces.



Coming to the designing process, a cylinder of radius  $R = 0,15$  mm and height  $H = 2$  mm was created on one of the third row (from the top) subfaces of the peg, by Autogrid mode. The cylinder base was then positioned at the face **Figure 48:** cylinder placed at the centre of a subface on the third row from the top.

Now the geometry was rotated by  $60^\circ$  around the z axis, with the pivot being at point P on the base in contact with the peg surface (Fig. 49A). Thereafter, a box of 1,5 mm length, 1,5 mm width and 0,5 mm height was created. Upon rotating it by  $30^\circ$  in z direction, it was placed on top of the cylinder tip at point P' as shown in figure 49 A.

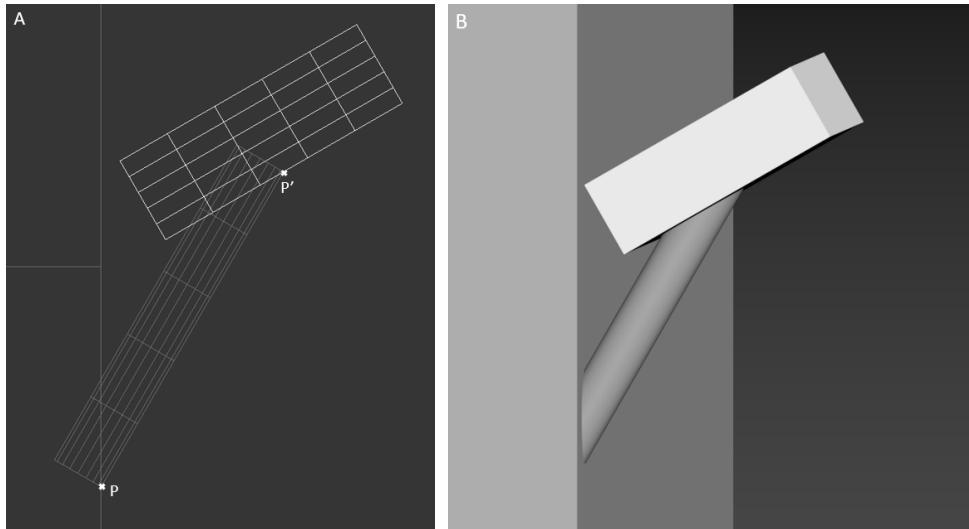


**Figure 49:** Wireframe front (A) and default shading orthographic (B) view of the obliquely upwards directed cylinder, intersecting the peg on the left and the box on the top. The tiny crosses indicate the position of point P and P' which represent the cylinder pivot and the inferior z-limit of the box respectively.

The subsequent step was to remove the intersection areas between the cylinder, box and peg. This task was accomplished by applying a boolean subtraction operation to the geometries, that finally produced the desired wire-like anchor configuration (Fig. 50).

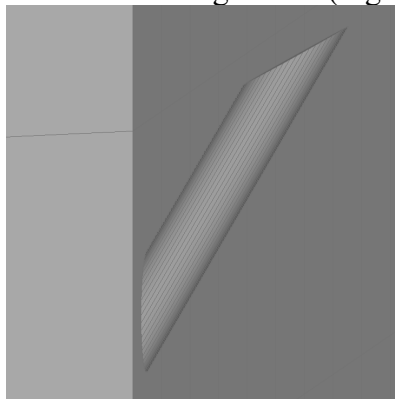


**Figure 50:** wire-like spike created by boolean subtraction operation.

At the end, 5 copies each hexagonal face were cloned and alternatively placed, thanks to the vertex snap tool, at the subfaces centres, covering the entire third row. The same procedure was reproduced on the sixth row, but in a half staggered way, in order to increase the hooking probability and anchoring degree. As a last step, the identical process was applied to the other peg, with the result that can be seen in figure 51.

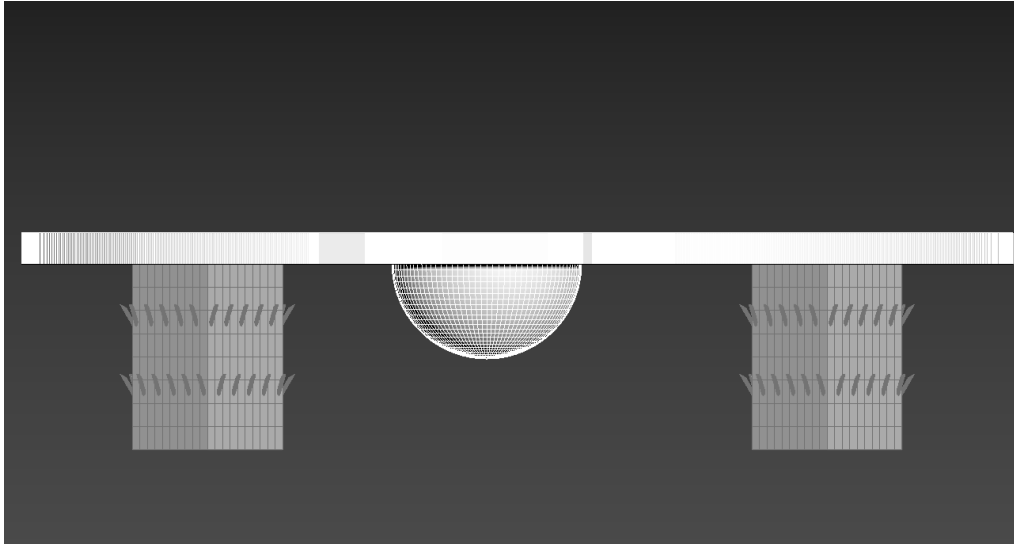


**Figure 51:** front view of the two spiked pegs. The third and sixth rows are staggered by one subface.

### Hybrid locking mechanism

It's within the locking mechanism design process that the key breakthrough introduced by our novel BCR tibial component took place. However, before describing it, it's necessary to take a step back.

Nowadays, total knee replacement prosthesis on the market are either fixed (FB) or mobile bearing (MB) designs. For the former, a locking mechanism on both medial and lateral side fixes the PE inserts to the tibial baseplate. For the latter, no locking mechanism is present and freedom in motion is conferred to the inlays.<sup>58</sup> An endless debate about which approach is superior to the other is drawing the global orthopaedic community attention on itself over the past decades, without reaching a definitive solution yet. Both currents of thoughts comes with advantages and drawbacks, that ultimately lead to similar clinical outcomes.<sup>70</sup> Briefly, FB designs secure the inlays to the tibial tray proving a stable articulation with no risk of bearing dislocation. However, in order to

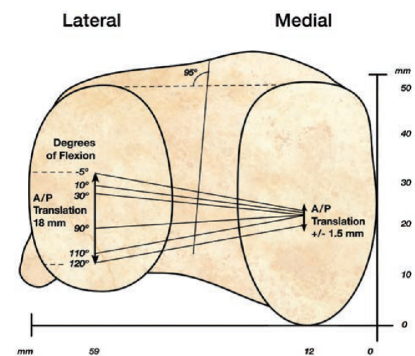


**Figure 52:** mean AP translations in medial and lateral compartments throughout knee flexion.<sup>61</sup>

provide rotational freedom on lateral side a nearly flat lateral insert upper surface is implemented resulting in small contact area with the convex femoral condyle, high contact stresses and therefore massive the PE wear. MB designs, on the contrary, decouple translational and rotational inserts motion solving in this way the congruity/mobility conflict of FB designs.<sup>71</sup> The fully congruent femorotibial interface featured by MB prosthesis dramatically reducing polyethylene wear, but the absence of a locking profile rises the risk of bearing dislocation. Nevertheless, this eternal quarrel may not require a conclusive verdict. Both MB and FB TKA designs were born as exclusive and unique joint replacement, however, with a change in perspective, these two approaches are not incompatible. Indeed, if one thinks about the natural knee kinematics, a substantial difference between the two compartments exists that cannot be represented by a single implant category. It's well recognized that the concave medial knee side is stable through ROM, with a limited mean AP translation of barely +/- 1,5 mm corresponding to the femoral external rotation on the tibial plateaus.<sup>59,60</sup> On the other hand, the convex lateral compartment is significantly more mobile, experiencing a mean AP translation of 18 mm (Fig. 52)<sup>61,67,68</sup>.

In particular, during deep flexion the femorotibial lateral contact moves so far posteriorly to require a consistent translation of the meniscus exceeding the tibial contour (Fig. 53 2d, bottom right)<sup>62,69</sup>.

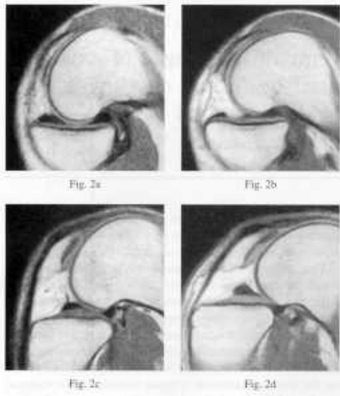


**Figure 53:** radiographic images of medial (top) and lateral (bottom) knee compartments at middle (left) or deep (right) flexion. The concave medial plateau along with a rigid meniscus provide stability, while the convex lateral plateau and a more mobile meniscus allow for freedom of motion.<sup>62</sup>

Trying to perfectly reproduce this anatomical and kinematics disparity with just a single either mobile or fixed bearing solution is impossible and conceptually incorrect. Even medial pivot designs which attempt to replicate this natural difference in motion, provide a fixed bearing solution for both sides, which unavoidably doesn't reflect the decisive lateral meniscus mobility found in human knee joint.<sup>65-67</sup> The here presented BCR TKA is offering a novel, revolutionary "hybrid" approach, featuring a stable, fixed bearing on medial side and a mobile bearing on the lateral. Following the hints of great forerunners like dr. Gunston and dr. Insall, the total knee arthroplasty is not seen anymore as just a single unit implant, but rather as the robust union of two separate unicondylar replacements, providing specific designs and solutions for each compartment as it is in the normal knee joint. This "bi-UKA" perspective is supported by the better kinematic and clinical outcomes as well as the higher satisfaction rate associated to unicondylar replacements with respect to TKRs.<sup>8-10,63,64</sup> At the same time, the decoupling present in our prosthesis, together with some key design features, allow to combine and enhance the advantages of both FB and MB approaches, while dampening their weaknesses, as will be highlighted later on during the designing process report.

The first step for the realization of this hybrid configuration was the design of the so called "hybrid locking mechanism". This features a proper locking interface on medial side for fixed bearing, while a simple medial AP guiding wall characterizes the lateral compartment for mobile bearing. As for the tibial baseplate, an initial 2D profile design was required.

## 2D design of the hybrid locking profile

### *Medial compartment*

Starting with the medial compartment, the two main design criteria of the locking mechanism were robustness of the capture and ease of inlays insertion. Indeed, the biggest complication associated to fixed bearing, as mentioned before, is polyethylene wear. In addition to the articular interface wear, in many instances, an even larger amount of PE wear and debris particles can be produced by the non-articulating tibial bearing undersurface lying on the metal baseplate.<sup>73-74</sup> While the first type of wear can be significantly reduced by a conforming articular interface, like in medial pivot designs,<sup>61,75</sup> the second, called "backside wear", represents a very complex interplay of factors which considerably threaten both cemented<sup>76,77</sup> and cementless<sup>78,79</sup> implant success.<sup>80,81</sup> It has been proved that with new biomaterials<sup>82-83</sup>, polished tibial baseplates<sup>72,89</sup> and correct surgical component positioning<sup>84-86</sup>, backside wear can be significantly reduced. Yet, coming to the designing aspect, many researches reported a strict correlation between backside wear and locking mechanism.<sup>87,88</sup> Among these, dr. Zachary's publication could show that a polished baseplate featuring a partial peripheral rim-capture with an anterior constraint and dovetail locks produced minimal backside damage and linear wear, whereas weak locking interfaces loosened over time causing backside PE

wear, that may surely lead to osteolysis in patient's body.<sup>89</sup> The take home message is that a robust and strong locking mechanism is essential to prevent micromotion between inserts and tibial tray, consistently attenuating the risk of backside wear in FB TKAs. At the same time, bearing insertion and capture into tibial tray should be an easy and reproducible task for the surgeon. However a logical trade-off between the latter and locking robustness exists. For instance, a complete peripheral lock theoretically ensures the highest stability and integrity for the bearing capture, however, its extended rim reasonably complicates inlays insertion inside operation room. For the abovementioned reasons, a semi-peripheral locking mechanism with anterior/posterior lips and medial dovetail capture was reputed the best trade-off between locking robustness and insertion ease. Hereafter the designing procedure for the realization of the medial locking profile is reported.

Initially a 1,5 mm inwards outline of the tibial 2D profile was created. The posterior internal segment of the medial outline was then mirrored with respect to the y axis resulting in an "orange slice" contour on medial side (Fig. 54).

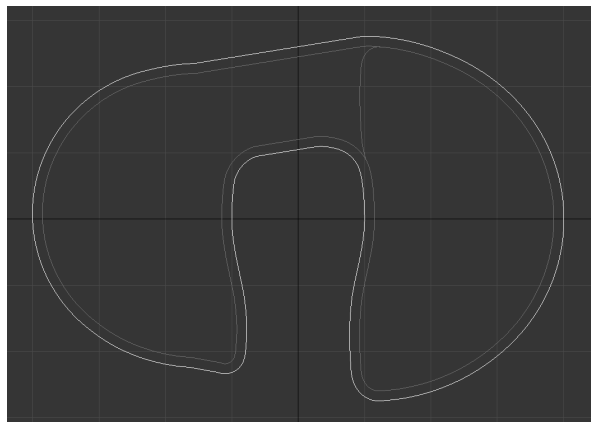


**Figure 54:** The 1,5 mm inwards outline (grey) of the tibial contour (white). On the medial compartment an "orange slice" like profile was sketched by mirror operation.

Upon this medial profile, a posterior lip was designed to provide posterior robust constraint. The lip was projected to delve inside the tibial plateau by a max of 3,75 mm from the outer border. A 50 mm radius circle centred in (13,764; 26,459; 0) was employed to produce such posterior recess and a transition line bridged this upper curvature to the lower outline in correspondence to the lower circumference extremity P and the outline notable vertex V (Fig. 55). Trim-weld-fillet operation was finally applied to the lip profile.

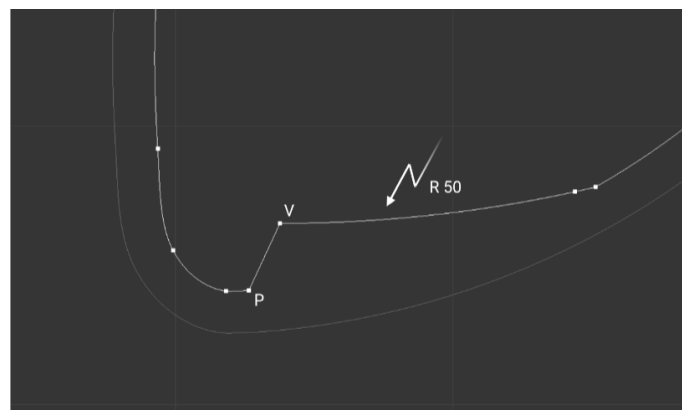


**Figure 55:** close-up of the posterior 50 mm radius lip (after trim operation) with points V and P highlighted in vertex mode.

In order to strengthen the posterior locking mechanism, a medial dovetail lock was added, similar to the one present in Genesis II TKA (Smith and Nephew, Memphis, TN, USA)<sup>90</sup>, which could be



precisely analyzed and measured during the author's clinical experience. This dovetail is a robust locking mechanism consisting of a beveled groove within the tibial wall which hosts a beveled lip of the fixed inlay blocking it against a less pronounced metal rim (Fig. 56)<sup>72</sup>.



**Figure 56:** Genesis II TKA and its dovetail capture mechanism detail indicated by the black arrow.<sup>90</sup>

Coming to the dovetail 2D profile design, a 10 mm radius circle centred in (1; -12,619; 0) and a 3 mm one in (8,023; -12,983; 0) were utilized for the opening lower and closing upper curvature respectively (Fig. 57 A). After the application of trim-weld-fillet operation an inverse S-shape, smooth, internal recess of approx. 3mm from the outer contour was finally obtained (Fig. 57 B).

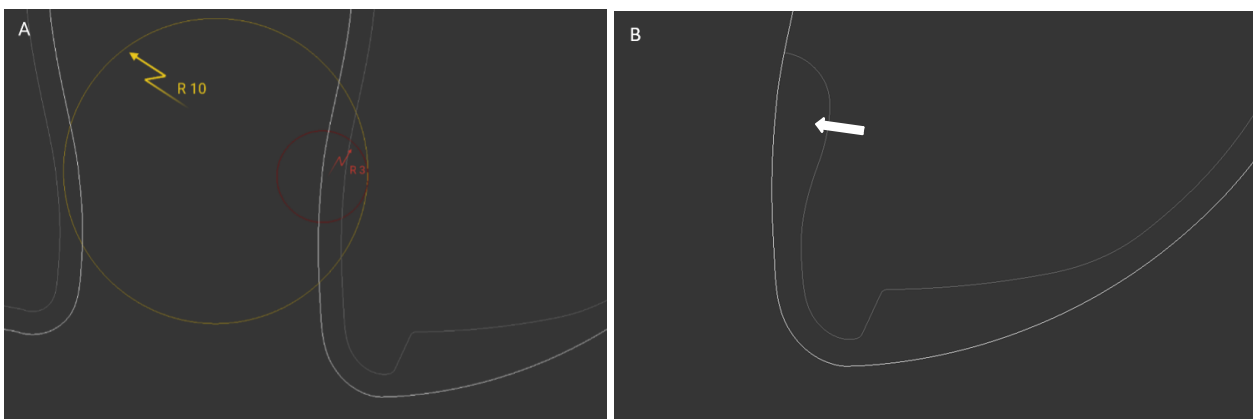


**Figure 57:** top view of the construction circles of posterior-medial dovetail locking detail (A). The bigger circle (yellow) was used for the opening radius (10 mm), while the smaller circle (red) for the closing transition (3 mm) with the outer tibial contour (white). Image B shows instead the final dovetail lock profile, indicated by the white arrow, after trim-weld-fillet operation. Values in mm.

Once the posterior locking profile was completed, an anterior lip was introduced. Firstly, the 1,5 mm medial outline upper curvature was continued anteriorly by a 24,77 mm radius circle centred in (13,764; 0,025; 0). This curve was aimed to produce the approx. 3 mm max anterior recess profile. The closing transition was provided by a 2 mm radius circle centred in (12,415; -0,9; 0) (Fig. 58 A). Trim-weld-fillet operation was finally applied (Fig. 58 B).

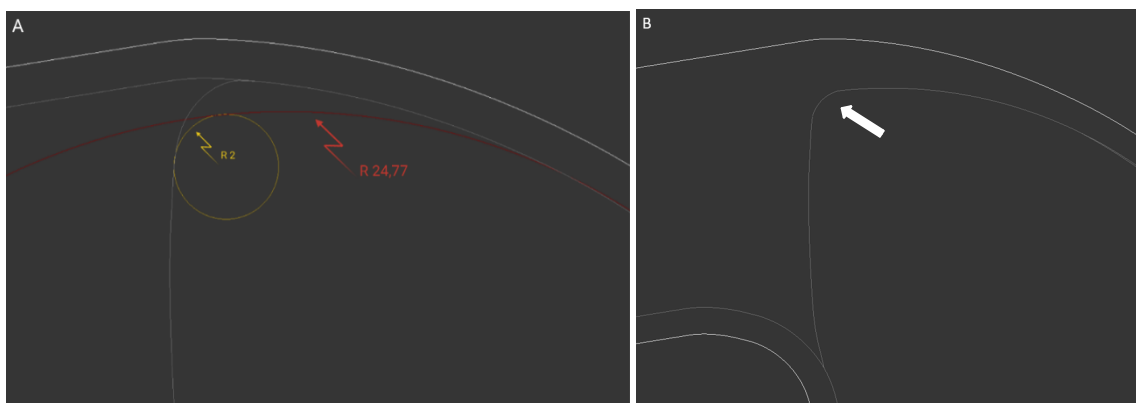


**Figure 58:** top view of the construction circles of anterior-medial lip (A). The bigger circle (red) was used for the recess profile (24,77 mm), while the smaller circle (yellow) for the closing transition (2 mm) with the locking outline

(grey). Image B shows instead the final result, indicated by the white arrow, after trim-weld-fillet operation. Values in mm.

The following step was to close the locking profile in the proximity of the central cruciate cutout. In order to do this, the anterior medial locking contour curvature was extended by a 150 mm radius circle centred in (159,293; 21,343; 0) and finally closed towards the cruciate notch outline by a 5 mm radius circumference centred in (5,014; 6,454; 0) (Fig. 59 A). As always, trim-weld-fillet operation was ultimately applied to the 2D geometries (Fig. 59 B).

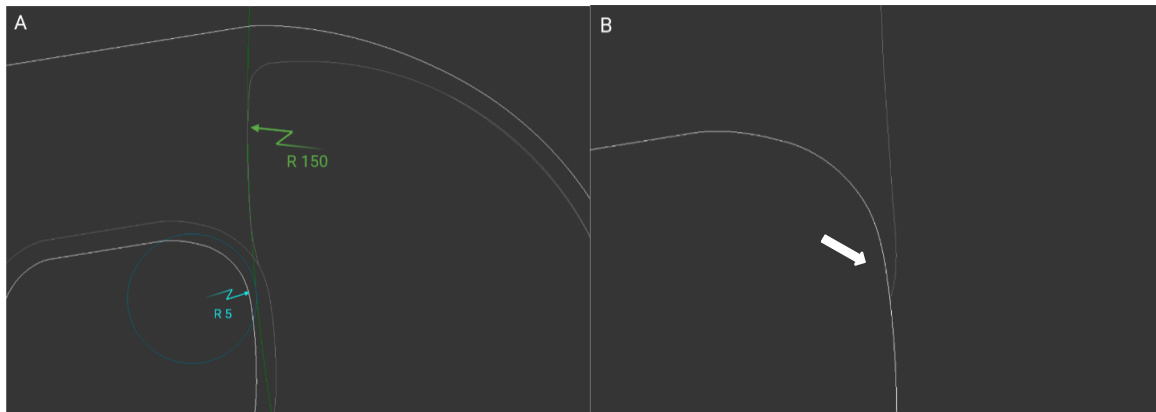


**Figure 59:** top view of the construction circles of the closing transition in correspondence of the central notch (A). The bigger circle (green) was used to extend the locking profile, while the smaller circle (light blue) for the closing transition (5 mm) with the cutout contour (grey). Image B shows instead the final result, indicated by the white arrow, after trim-weld-fillet operation. Values in mm.

The really last stride for the medial locking mechanism design was to create two symmetrical non-stark endings of the locking profile ensuring the partiality of the peripheral capture interface. With this goal, an inner outline of 0,75 mm was drawn from the tibial baseplate contour at a first stage. Two oblique lines (inclination angle of  $\pm 10^\circ$ ) were then sketched on both anterior and posterior regions of the locking profile, roughly around  $y = 20$  mm (anterior) and  $y = -20$  mm (posterior). These lines were employed to bridge the 1,5 mm outline (Fig. 61, black line) followed by the locking contour (with the exception of the more recessed lips and dovetail lock) to the 0,75 mm new one (Fig. 61, red line). In order to smooth these transitions, trim-weld-operation was performed at a final stage (Fig. 61). The area between the two oblique changeovers was thought not to host any locking mechanism, but rather a vertical delimiting wall, that should interface the medial insert without grooves or captures. This partial withdrawal was aiming for a simplified bearing surgical insertion, while still providing a robust and reliable locking mechanism, taking inspiration from Zimmer Unicompartmental Knee (ZUK) System (Fig. 60). ZUK implant, indeed, as could be directly seen within the

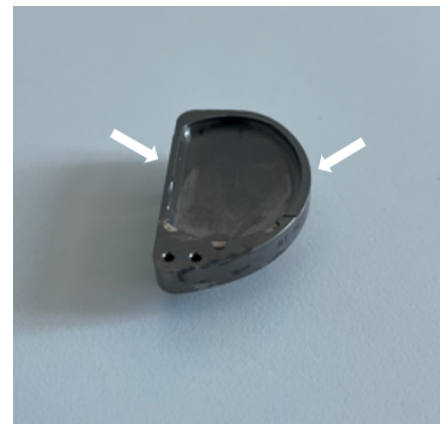


**Figure 60:** the two locking withdrawal

at region  
 clinics, presents a secure locking mechanism that interrupts on both sides in at middle region,  
 indicated by the white arrows,  
 the middle region, leaving just a bounding wall with decreased width in ZUK implant.  
 Picture taken at Tarabichi centre.  
 compared to the capture interface.<sup>91</sup>

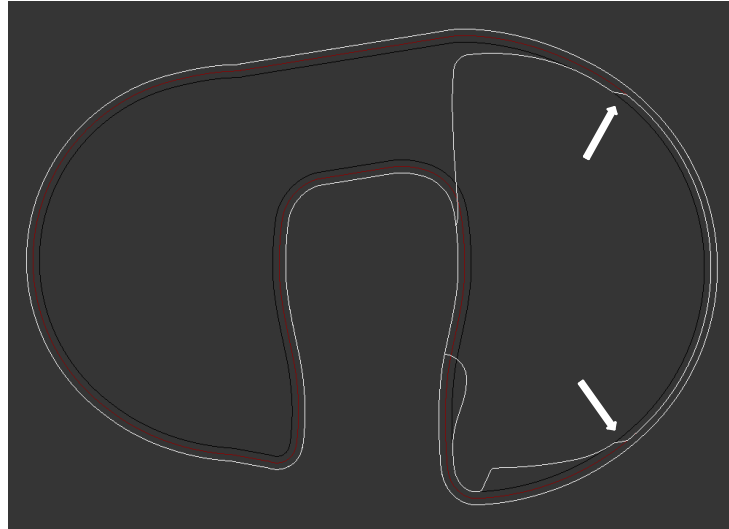


**Figure 60:** the two white arrows highlight the anterior and posterior transitions between 1,5 mm (black) and 0,75 mm (red) outlines which suppress the locking detail in the middle medial region.

### *Lateral compartment*

Moving to the lateral condyle, no locking mechanism was pursued as a mobile bearing configuration was aimed here. Instead, influenced by the worldwide successful design<sup>92,93</sup> of Oxford Unicompartmental Knee System, a simple guiding medial wall was developed. The latter should direct the AP translation of the bearing and minimize medial dislocation risk. After accurately analysing the Oxford prosthesis at Tarabichi center, the lateral wall design was initiated. In alignment with the medial counterpart, a minimum 1,5 mm wide wall profile was sketched in top view. In order to do this a vertical line, 1,5 mm spaced from the most lateral point of the cutout profile ( $x = -10$  mm) was plotted. However, unlike Oxford design, an anterior lip was attached to the AP wall (Fig. 61 B) for two purposes. First, additional thickness in the most anterior-lateral corner of the anterior bridge was required, as this area was not reinforced by the hemisphere and therefore it could have been turned into a vulnerable spot for fatigue stresses. Second, this lip was intended for an anterior constraint in the AP insert translation. This rounded rim was created using a 5 mm radius circle centred in  $(-16,673; 18,597; 0)$  (Fig. 61 A). Finally, trim-weld-fillet operation was executed.

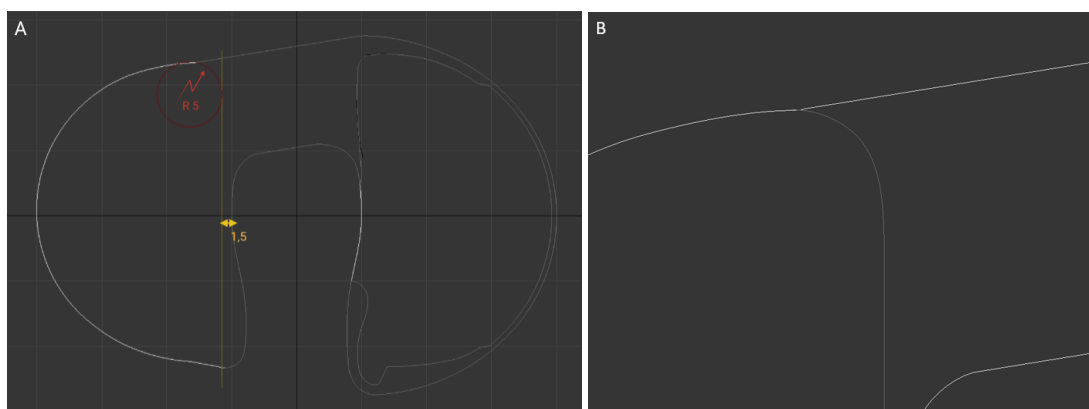


**Figure 61:** top view of the vertical line (yellow) and construction 5 mm radius circle (red) used for the lateral wall and anterior lip (A). Close-up of the anterior rim after trim-weld-fillet operation (B). Values in mm.

To sum up, the novel “hybrid” locking profile was designed with a proper partial peripheral capture interface in the medial side, featuring a medial dovetail lock and an anterior and a posterior more pronounced lip, while consisting of a simple guiding wall in the lateral compartment, concluded

anteriorly by a 5 mm radius lip (Fig. 62). This configuration reflects the revolutionary concept of bearing mobility decoupling, introduced by our BCR TKA design, with a fixed medial pivot bearing and a mobile lateral bearing, recreating the natural disparity of the human knee.

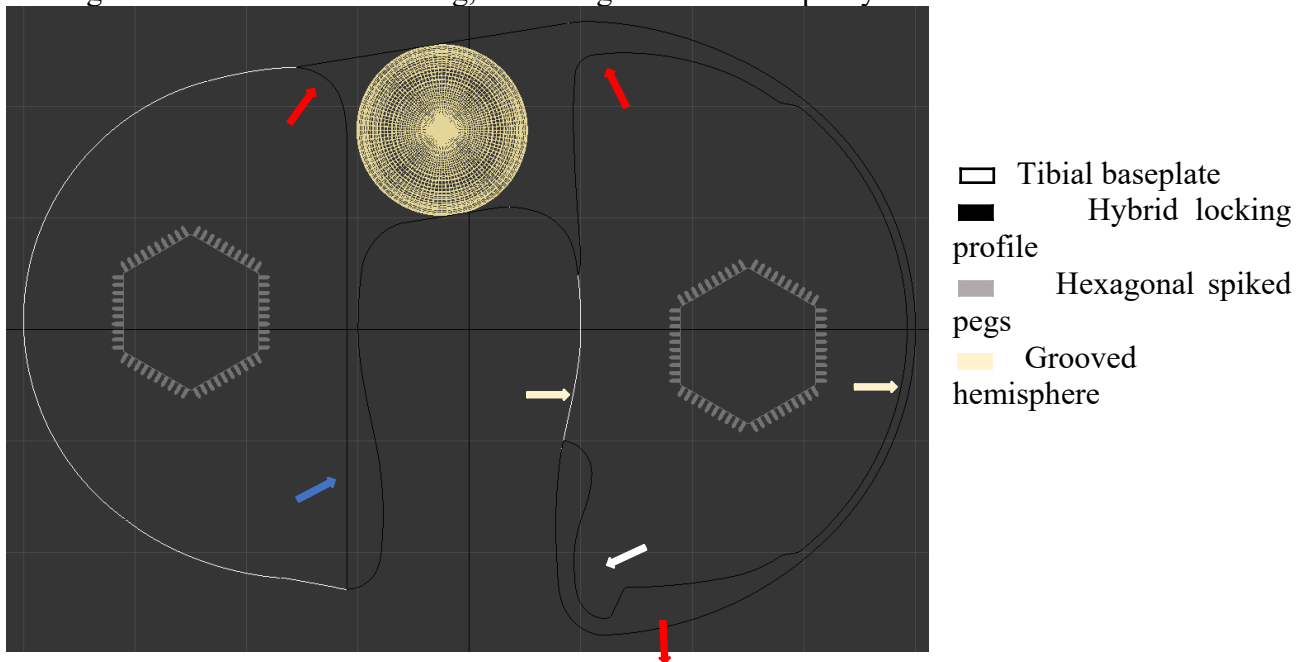


**Figure 62:** top view of the complete 2D profile of tibial component and fixation elements. The white arrow points to the dovetail detail, red arrows to the lips in both medial and lateral compartments, yellowish arrows to the medial regions where no locking mechanism was designed and finally the blue arrow to the guiding medial wall in the lateral compartment.

### 3D extrusion

The hybrid locking profile was initially elevated to  $z = 2,5$  mm to result on top of the tibial baseplate. Thereafter, a 2,5 mm upper extrusion was applied on it (Fig. 63). This value was reputed sufficient to guarantee a stable lock on medial side and a reliably high wall on lateral side, limiting at the same time the amount of metal implanted in the joint space.



**Figure 63:** the 2,5 mm upper extrusion of the “hybrid” locking profile.

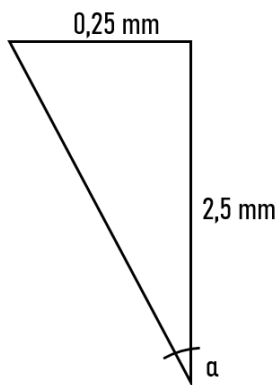
## Cruciate notch modelling

No current BCR TKA design offers a “cruciate-friendly” central notch, to our knowledge. In our conception, a cruciate-friendly means an asymmetrical, chamfered and outwards inclined implant interface with the retained cruciate ligaments. The sharp edges and the vertical walls of the currently available BCR TKAs notches represent a possible threat to the integrity and functionality of the ACL and PCL over time. On the contrary, a smooth and inclined cutout superior border should reasonably prevent high stresses at the soft tissues-implant interface that might lead to cruciate tears and microdamages over time, with tremendous consequences on implant stability. Additionally, inwards (to the implant) directed walls together with an asymmetrical anterior profile and a wider anterior aperture are thought to guarantee more working space for both PCL and ACL throughout the knee ROM, resulting in a more physiological intercondylar design than the straight one of current BCR implants.

## Cutout inclination

An inner 0,25 mm outline of the tibial contour was sketched and moved to  $z = 2,5$  mm at a first stage. The bottom vertices of the locking mechanism facing the central notch, along with the top ones of the tibial baseplate were then manually translated to this outline, exploiting vertex snap tool (Fig. 64). This resulted in a  $5,71^\circ$  inwards inclination as can be easily seen using trivial trigonometric laws (equation 1).

**Equation 1:**



$$\alpha = \tan^{-1}(0,25/2,5) = 5,71^\circ$$

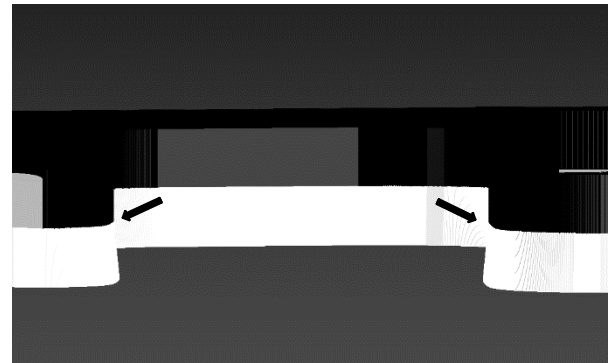


**Fig. 64:** the  $5,71^\circ$  inwards inclination (black arrows) applied to the top cutout-facing border of the tibial baseplate (white) and bottom edges of the hybrid locking mesh (black). Front view.

This angle was agreed after several trials performed on the mesh. At the end, it resulted that an angle between  $4^\circ$  and  $7^\circ$  was ideal for our design because it didn't overturn the geometry and consequent functionality on the lateral wall and the medial dovetail lock providing at the same time a notable inclination.

The next step was then to continue this inward inclination on hybrid locking mechanism. Since its height was 2,5 mm and the same angle of  $5,71^\circ$  was pursued, an additional inward 0,25 mm outline was required for the upper locking border. Such spline was drawn at  $z = 5$  mm and all the top vertices of the hybrid locking mechanism facing the central cutout were manually moved onto it, exploiting vertex snap tool.

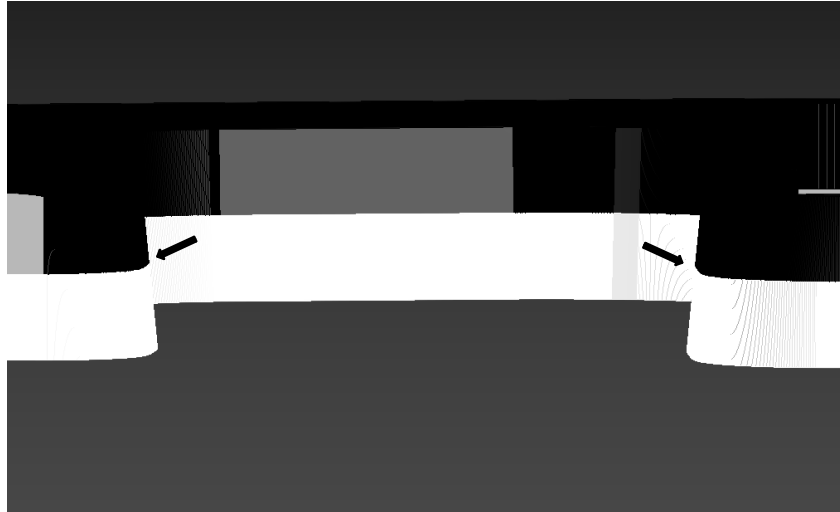


**Figure 65:** front view of the completed inclination highlighted by the black arrows.

### Notch top rim chamfer

The notch top border chamfer step can be divided in two parts: a constant 0,5 mm radius chamfer applied to rim 1 (Figure 66, white arrow) and a variable radius chamfer applied to rim 2 (Fig. 66, black arrow)

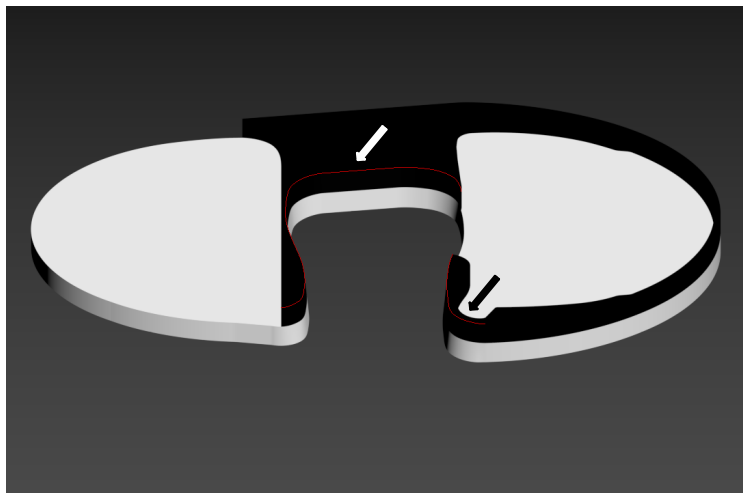


**Figure 66:** the white arrow indicates the highlighted rim 1, while the black one rim 2.

The rim 1 was initially selected and a radial chamfer operation was applied to it. The chamfer radius was set to a constant 0,5 mm and a 0,5 edge depth was assigned. The segments number was set to 8 resulting in a blunt and rounded border (Fig. 67).

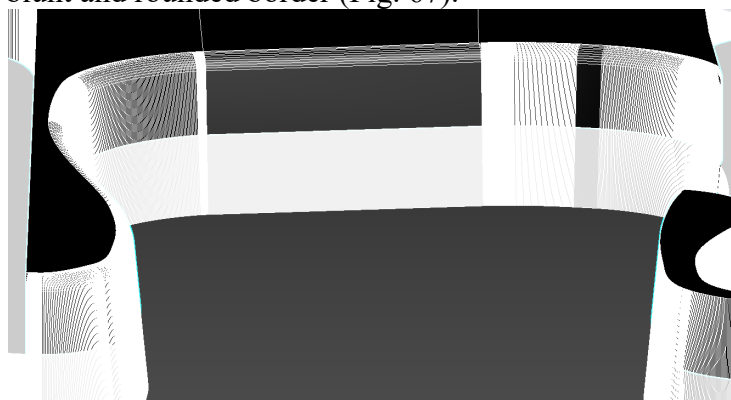
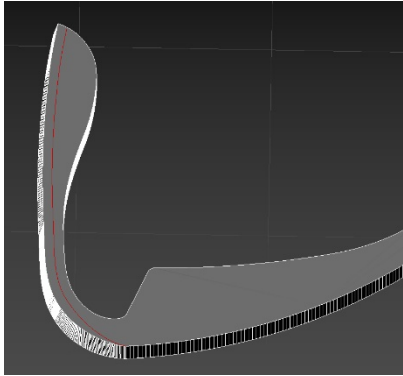


**Figure 67:** close-up of the constant 0,5 mm radius chamfer applied to rim 1.

The rim 2, instead, necessitated a gradually decreasing radius chamfer from a maximum of 0,5 mm at the anterior extremity to a total chamfer suppression ( $R = 0$  mm) at the posterior end. This radial transition required two designing steps. The first one was to draw an inward 0,5 mm outline of the rim 2 profile and then move its posterior end to the one of rim 2. This necessarily changed the spline curvature, that was smoothly adjusted by fillet operation. The second consisted in using the resulting spline as a reference for the introduction of a new edge on the top face of the locking mesh. This was done by the combination of cut tool and vertex snap mode until the red-highlighted edge in figure 68 was created. This new border was employed as an upper constraint for the chamfer that, although set to 0,5 mm it couldn't exceed this edge, resulting in a constant 0,5 mm radius curvature below the rim and



the upper chamfer gradually collapsing into the top border of the medial locking mechanism (Fig. 69). A 0,5 mm radius radial chamfer

was therefore applied with 0,5 mm edge depth and 1,5 edge end and radial bias. upper chamfer in red.

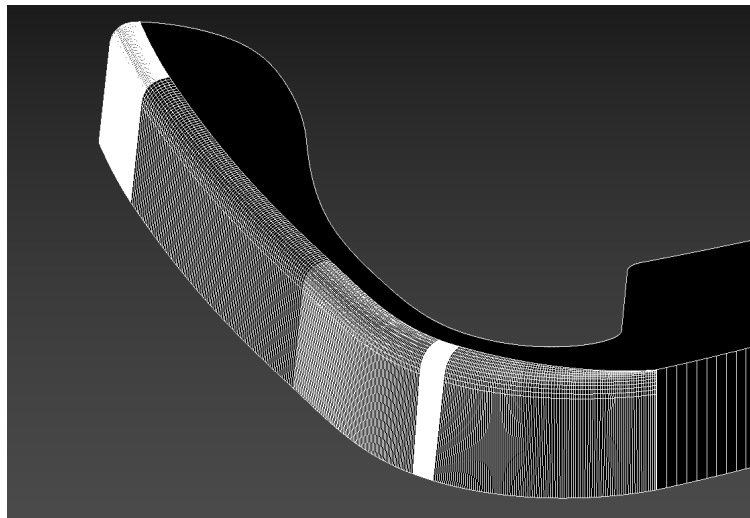


**Figure 69:** gradually collapsing chamfer of rim 2.

### **Inclination of the lateral wall**

The polyethylene inserts should ideally reflect the notch inclination for the same abovementioned reasons and to provide a continuous interface without any abrupt angulation changes. This necessarily implies that the bearing-facing lateral wall should be inclined as well. The lateral inclination was aimed to follow the notch one of  $5,71^\circ$ . Applying the same trigonometric law as before, a 0,25 mm inward outline of the lateral wall edge was determined for the 2,5mm high mesh (Fig. 70 A, red line). At this stage, the vertices constituting such edge were translated to the outline, leading to the wanted inclination angle. The posterior chamfer vertices were finally adjusted manually exploiting again simple geometric laws. The final result can be seen in Figure 70 B.

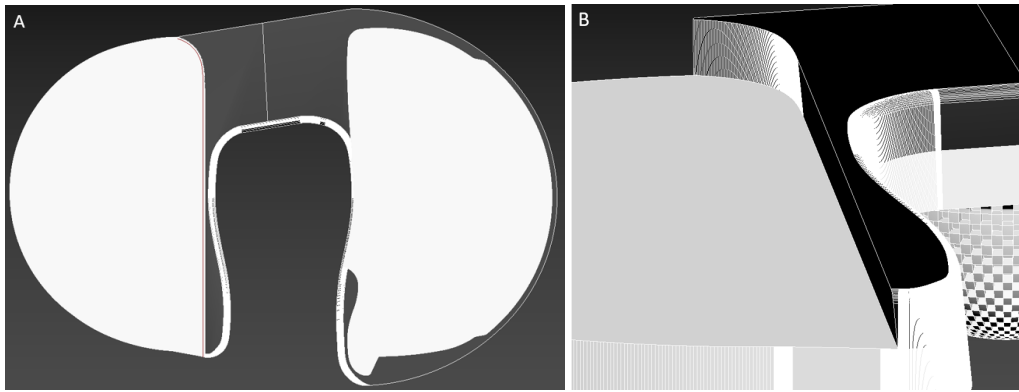


**Figure 70:** 0,25 mm inward outline (red) utilized for the lateral inclination of the wall (A) and final result with adjusted posterior chamfer (B).

### **First version of tibial component**

With the 3D modelling of the hybrid locking mesh done, the initial version of the novel BCR TKA tibial component was completed. It's important to pinpoint that, at this stage, the locking mechanism was not entirely finished, but was missing the locking semi-peripheral groove. Yet, this 3D modelling step was planned from the beginning as a boolean subtraction of the medial bearing mesh from the locking one and therefore it is intended for the inserts designing phases. Here below, different views of this preliminary design are presented. However, as will be deepened in the next chapter, a new decisive modification in the tibial baseplate was introduced to the first version, by mutual agreement with drs. Tarabichi and Elfekky, resulting in the really final version of the implant design.



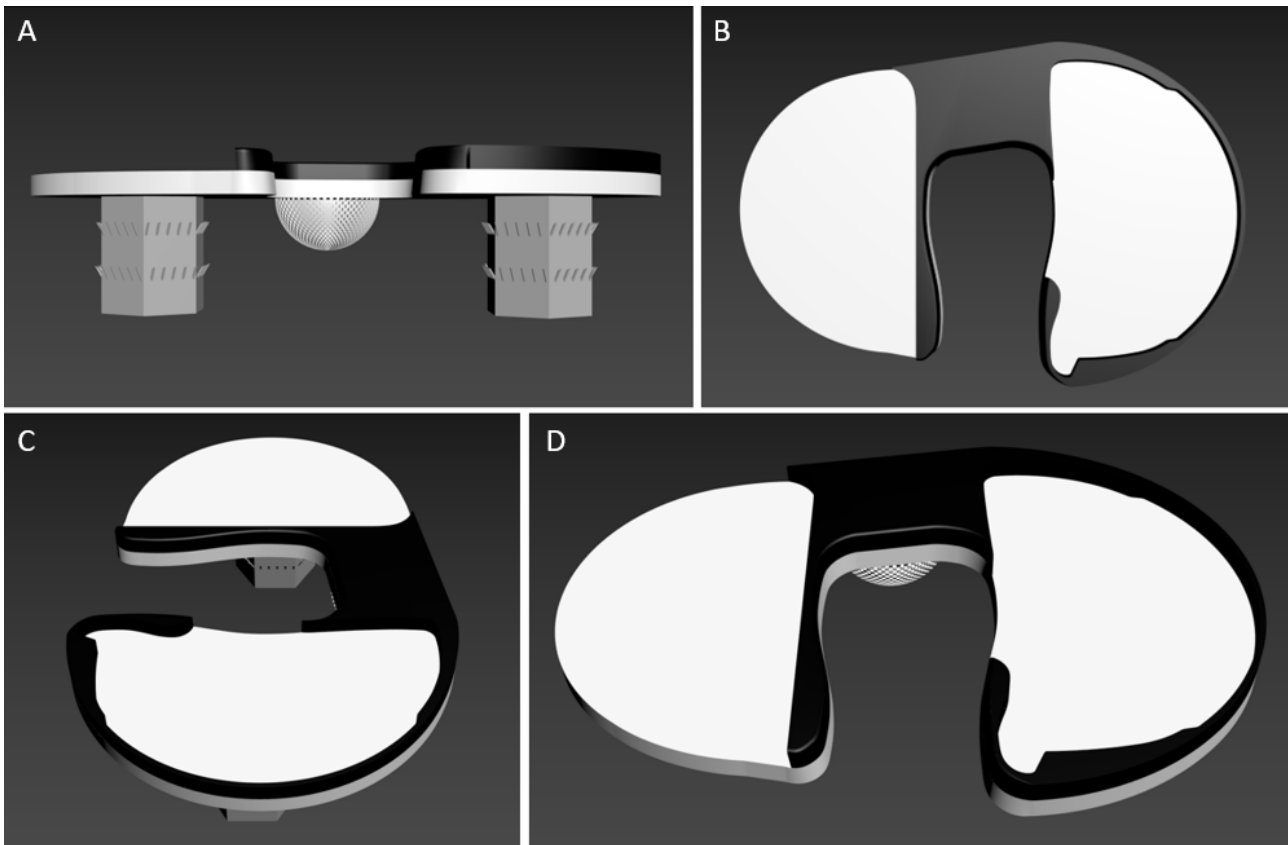


**Figure 71:** Different views of the initial version of the novel BCR TKA tibial component. In order: front view (A), top view (B), right-top view (C) and front-top view (D).

**Domed lateral tibial plateau modification.**

The tibial version showed above was theoretically a robust and promising solution, offering a medial ZUK-like fixed bearing replacement and a lateral Oxford-like mobile bearing one. Given the global clinical success of the two mimicked UKA prosthesis, high confidence was placed in this design by the author and the doctors. However, one crucial aspect was not taken into account until this stage: the Oxford Unicondylar Knee offers a reliable and well proven replacement when applied to the medial compartment, but is associated to disappointing results in the lateral one.<sup>94-97</sup>

It's 80% survival at 10 years and unacceptably high early rate of dislocation, forced several surgeons not to recommend MB UKA for the lateral compartment.<sup>95,98</sup> Somehow, the high mobility of the lateral condyle that should justify the application of a mobile bearing design, led to the opposite result, being source of insert dislocation and implant failure. Barè et al. attributed the cause of these unsatisfactory results to a suboptimal Oxford design, not reflecting the lateral condyle anatomy.<sup>99</sup> Indeed, the flat or slightly concave surface of Oxford UKA, while matching the medial plateau, it does not replicate the convexity of the lateral one. For this reason, a modification to the standard Oxford Knee was required for the lateral



**Figure 72:** The new Oxford domed lateral component.<sup>104</sup>

After several morphological studies, a new convex tibial baseplate

replacemen

articulating against a biconcave PE bearing for lateral UKA was recently introduced and today is available on the market as “Oxford® Domed Lateral Partial Knee (Biomet, Bridgend UK)” (Fig.72).<sup>100</sup> This new configuration aims to finally restore the complex kinematics of the lateral compartment and, at the same time, significantly reduce the lateral bearing dislocation rate. The first, because only a convex plateau can allow the physiological roll-back and posterior displacement of the lateral femoral condyle on the tibia without impingement, during flexion (Fig. 53).<sup>99,102</sup> The second, because a spherically domed tibial surface together with a corresponding biconcave bearing substantially increases the AP and ML inlay entrapment and therefore the amount of distraction needed to dislocate.<sup>101,99,103</sup> Last but not least, the double concavity of the bearing provides full congruency with both femoral and tibial surfaces throughout ROM, minimizing polyethylene wear.

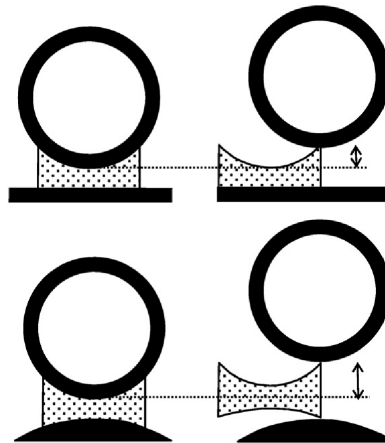


**Figure 73:** schematic representation of the increased entrapment (7 mm) of lateral bearing guaranteed by a domed tibial baseplate (bottom), with respect to the flat plateau present in standard Oxford Knee (top).<sup>103</sup>

Given the recent market release of this new domed tibial implant, a limited number of clinical reports is present in literature. However, among these, highly promising results are disclosed by Pandit<sup>103</sup> and Altuntas<sup>105</sup>. The first reported no primary bearing dislocations at 4 years and significantly improved ROM and clinical scores when the Oxford Domed Lateral Partial Knee was inserted and a modified surgical technique was employed. The second revealed comparable functional results to TKA approaches and, most importantly, no bearing dislocations for the domed Oxford Knee at an average follow-up of 3 years. Although these are early results, there is evidence that most reported dislocations occurs in the first 2 years post-operation and are unlikely after this period.<sup>103</sup>

Convinced by the theoretical and clinically proven advantages introduced by this novel domed tibial implant, it has been agreed to edit our prosthesis baseplate accordingly. Following the directives of the Oxford domed knee designer team, an upper spherical convexity with a radius in the range of 75 mm was applied to our old flat lateral tray.<sup>99</sup> Indeed, these attributes were found to result in the highest bearing entrapment and in the closest to normal joint kinematics. Hence, a 75 mm radius sphere was initially designed in 3Ds Max. At first sight, it was immediately clear that this radius was too small to fit our tibial lateral contour. In fact, Barè<sup>99</sup> highlighted that the dome radius is directly proportional to the AP tibial lateral plateau dimension. Since our AP length (46 mm) was notably higher than the average one of Barè’s study (43,3 mm), an  $R > 75$  mm was expected. Several trials were attempted with radius increments of 1 mm. Among these, the best solution was found to be  $R = 85$  mm because it ensured a fully covered flat tibial lateral plateau and a final lateral condyle maximum height between 2 and 3 folds the initial one, as it was calculated for the Oxford domed knee. The sphere was placed with its superior vertex in (-25,67; -0,959; 6,724). The x coordinate assured a symmetrical convexity in x dimension with  $z_{max}$  on lateral border equivalent to  $z_{max}$  on notch border being 5,525 mm. The y coordinate was determined by moving the sphere until it perfectly matched both posterior and anterior lateral plateau ends contemporarily.

After having placed the sphere correctly, a slice modifier was applied to it with the slicing horizontal plane being at  $z = 2,5$  mm. Only the portion of the sphere higher than this level “survived” to the modifier in this way (Figure 74).

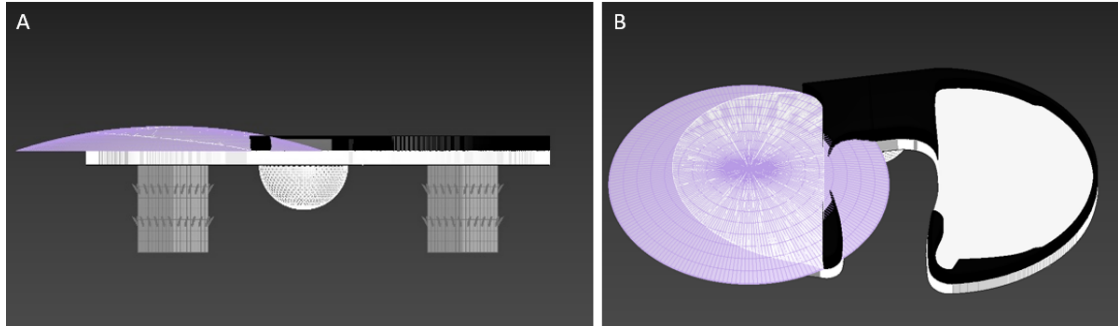


**Figure 74:** front view (A) and top-front view (B) of the sliced 85 mm radius sphere in purple. From image B is clear the perfect baseplate (white) AP coverage by the sphere.

At this stage, a spline following the lateral plateau contour was created. This was keeping the tibial profile until the lateral wall posteriorly and the lip anteriorly. After these points, the spline followed the hybrid lateral locking profile as could be seen in Figure 75.

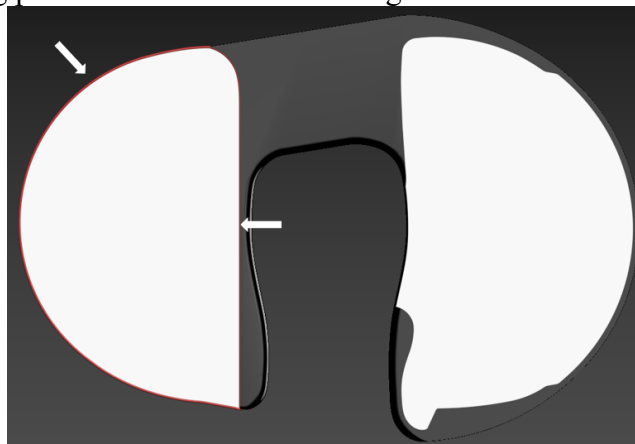


**Figure 75:** the red contour highlighted by the white arrows represents the lateral plateau spline designed.

The abovementioned spline was then extruded upwards by 5 mm (the spline at  $z = 2,5$  mm) and a boolean intersection between this geometry and the sliced sphere was performed resulting in a domed, spherical mesh perfectly fitting the asymmetric lateral plateau contour (Fig. 76).

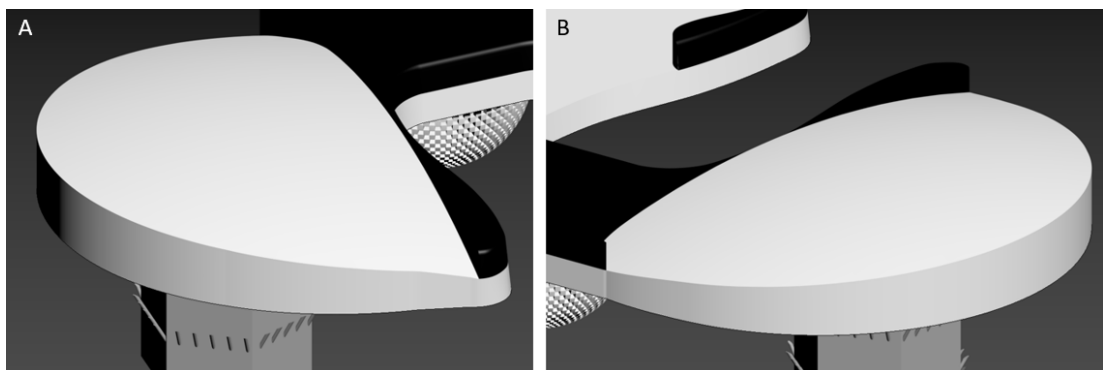


**Figure 76:** perspective views of the 85 mm radius convex lateral tibial plateau, with a focus on the posterior region (A) and anterior one (B).

### Lateral wall convexity

It was immediately clear that the plateau modification was not isolated, but it was necessarily bringing along some substantial adjustments in the lateral wall geometry. Indeed, if a convexity is introduced in the mobile bearing lateral baseplate, the guiding wall should follow this new curvature as well (Fig. 77 A). If instead a flat wall is maintained, plateau standing out over the wall will happen in the middle region and the insert interface will not be sufficiently high to prevent medial dislocation for the majority of the wall length (Fig. 77 B). Therefore, the exact convexity of the lateral tibial condyle was aimed for the lateral wall of the hybrid locking mesh as well.

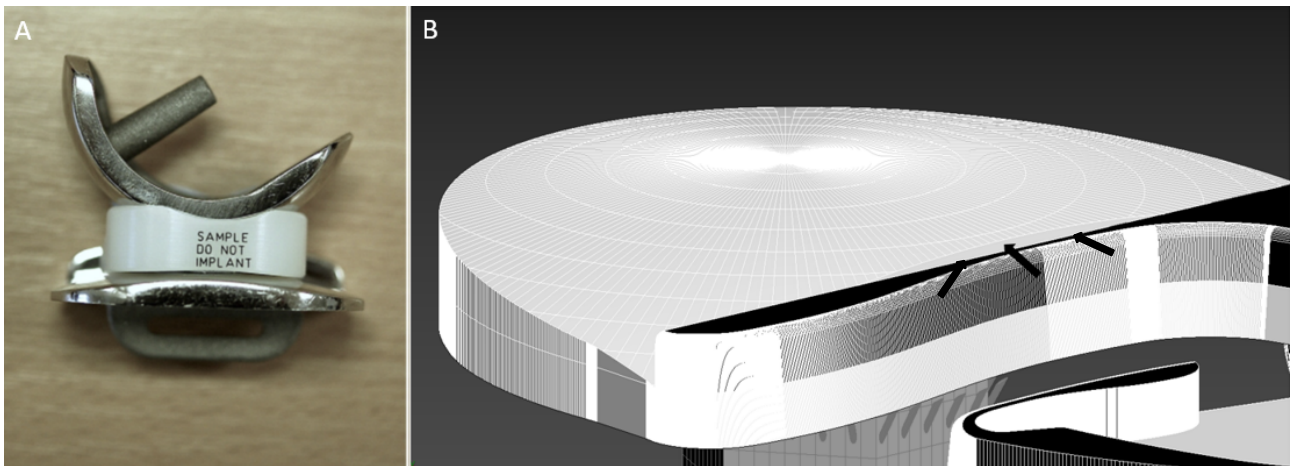


**Figure 77:** lateral condylar convexity followed by the guiding wall of an Oxford® Domed Lateral Partial Knee (A). Black arrows in image B point to the tibial tray overhang above the middle area of the flat lateral wall. This suggests that a domed guiding wall is required as well, to provide a reliable and constant interface with the mobile bearing.

In order to reproduce the plateau convexity on the lateral wall, a copy of the dome mesh was made and elevated to a minimum height of 5 mm. This was then used as a reference profile for the wall convexity modelling in lateral view. Indeed, each superior vertex of the wall was manually translated in z direction such that it perfectly overlapped with the dome mesh clone outline (Fig. 78).

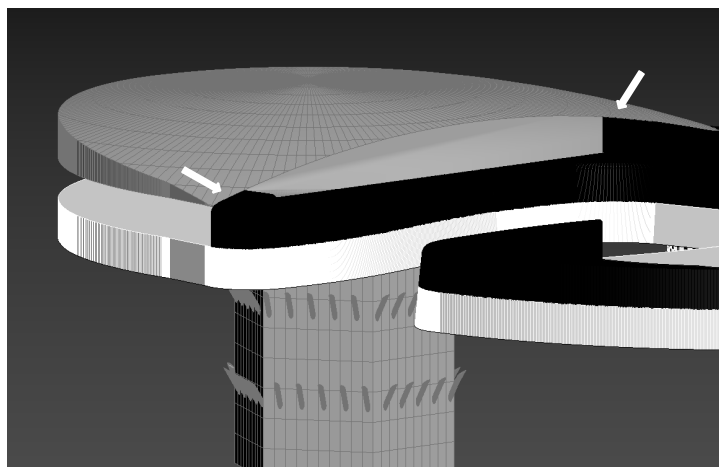


**Figure 78:** the dome copy (on top, grey) utilized as a reference for the lateral wall convexity. The arrows indicates regions that were already translated onto the dome contour in lateral view.

This was leading to a wall convexity that starting from a minimum z of 5 mm (2,5 mm of the proper wall plus 2,5 mm of the tibial tray) at posterior and anterior ends, reached its maximum height of 8,025 mm ( $z_{\max} + \text{locking mesh height}$ ) in the middle wall region. Although such profile was correct

for the bearing interface of the lateral wall, some adjustments were required on the notch side (Fig. 79).

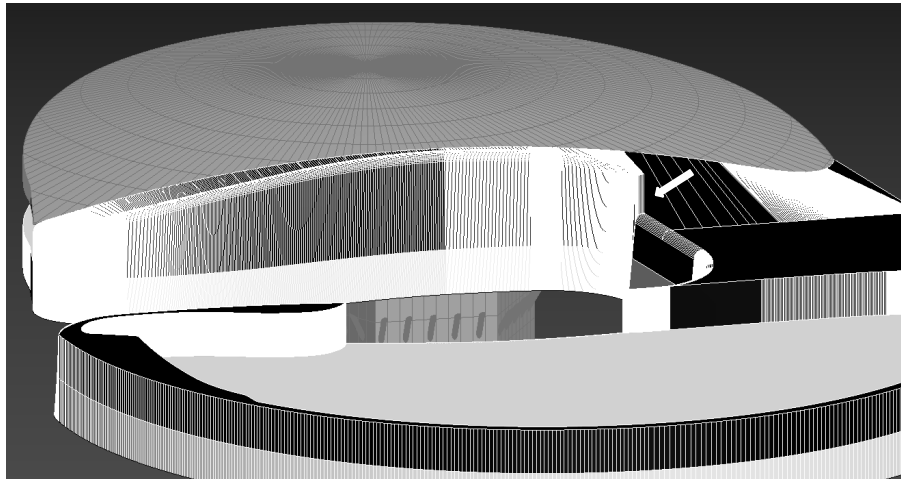


**Figure 79:** if the exactly same plateau convexity had been applied to the notch-facing wall side a discontinuous changeover between elevated lateral wall and flat medial locking mechanism would have been present, as pinpointed by the white arrow.

Here, the goal was to gradually collapse the wall height from its maximum point to the anterior border of the cruciate cutout at  $z = 5 \text{ mm}$ , in order to create a smooth transition between the lateral elevated and the medial flat compartments of the hybrid locking mesh. In order to create this height collapse a multi-radius transition spline was designed in right view and utilized as a reference path. Three different circles were utilized. The changeover can be seen as a decreasing radius passage, which started at the top with the biggest circumference ( $R = 50 \text{ mm}$ ), proceeded with the intermediate ( $R = 30 \text{ mm}$ ) and closed the transition at the bottom with the smallest ( $R = 20 \text{ mm}$ ) (Fig.80).

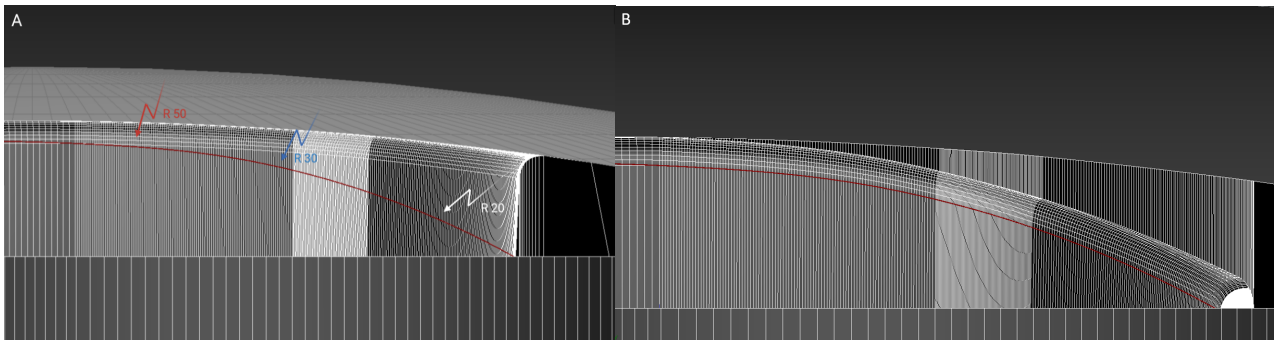


**Figure 80:** right view of the lateral wall before (A) and after (B) the decreasing-radius transition to the central notch. Red curve represents the reference spline made of three radii of curvatures (A). Values in mm.

Once the transition was completed, the junction between lateral wall and central cutout was refined following some reference 2D elementary geometries. In order:

- An oblique line (Fig. 81 A) was exploited to lower the wall in the proximity of the anterior cutout border.
- A 5 mm radius circle centred in  $(-8,486; 0; 0,097)$  was used to give a slight convexity to the initial part of the junction (Fig. 81 B).
- A 1 mm radius circle centred in  $(-5,892; 0; 5,501)$  was employed to reverse the curvature of the previous circumference conferring a S shape profile to the wall-notch attachment (Fig. 81 C).

It's important to finally highlight that additional edges were created on the anterior cutout chamfer (Fig.81 B) by the swift-loop tool in order to continue the concave curvature of the 1 mm radius

circle to some extent, avoiding any abrupt shift to the completely flat geometry of the anterior notch rim.

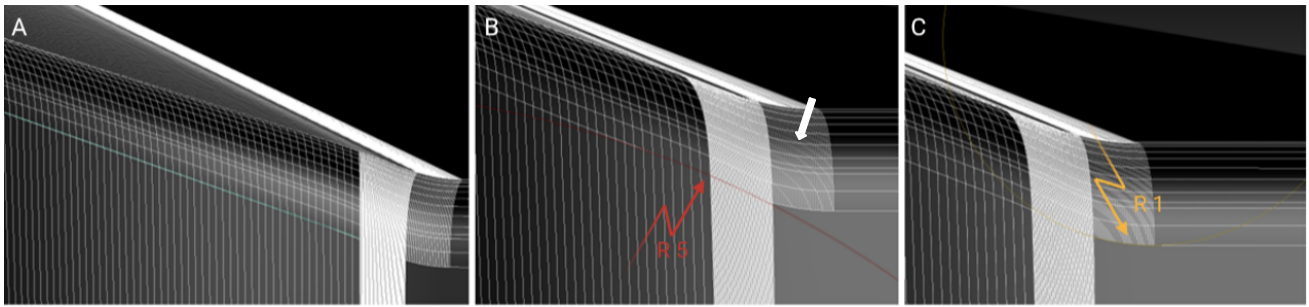


**Figure 81:** wall-junction transition explained by the reference geometries sequentially used. On the left (A), the oblique initial line (green); in the middle (B), the 5 mm radius circle (red) and on the right (C), the 1 mm radius circle (yellow). The white arrow in image B indicates the additional geometry introduced on the anterior notch chamfer.

Different views of the final, convex lateral guiding wall are showed below.

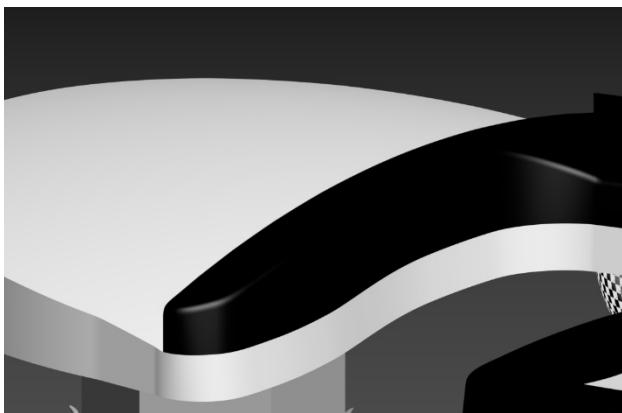


**Figure 82:** front-right view of the convex lateral wall.

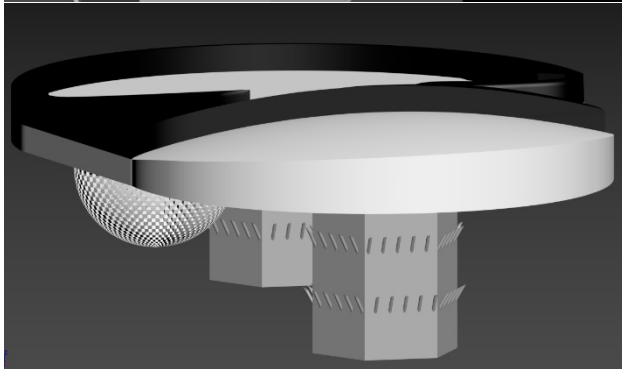


**Figure 83:** back-left view of the lateral wall following the same convexity of the domed tibial lateral plateau.

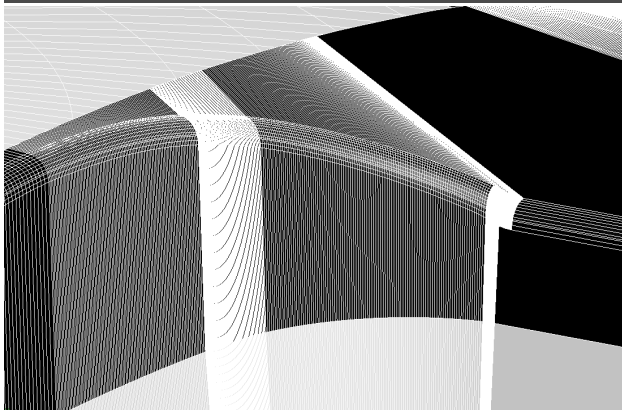
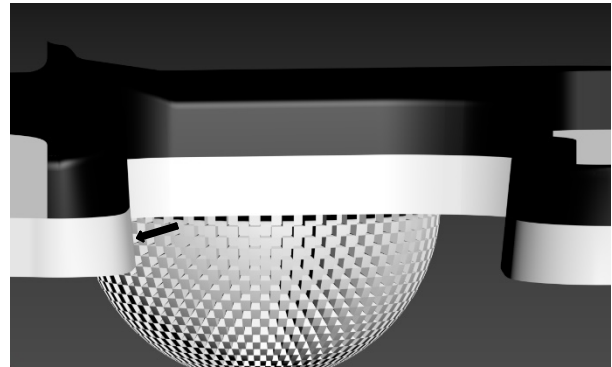


**Figure 84:** close-up of the wall height smooth collapse into the anterior notch rim. Image in edged faces mode to show the inner mesh geometry.

## Lateral wall inclination

The previous lateral wall inclination both on notch and bearing side, conceived for a constant 2,5 mm wall height, was not suitable anymore, as the structure height has been certainly altered by this new dome shape (Fig. 85).

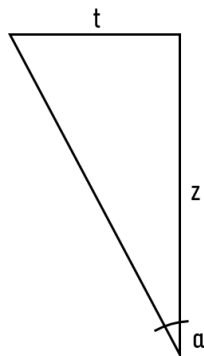
Regions higher than 2,5 mm should therefore feature a xy translation (representing the minor cathetus) greater than 0,25 mm in order to maintain the 5,71° inclination angle (equation 1,2). However, this was not an easy task to perform, as each superior vertex of the convex wall has a specific z and therefore should feature a specific xy translation.



In order to do this point-specific translation, a guiding spline path was designed and exploited as a background reference. Since the posterior and anterior ends of the convex wall featured the minimum height of 2,5 mm, the starting curve should be a 0,25 mm inward outline of the lateral wall, given by the introduced convexity.

The same outline used for the notch inclination in chapter .... Was utilized for this purpose. For convenience, we will refer to the z coordinates from now on, so a 2,5 mm wall height will be described by a 5 mm z (baseplate thickness considered as well). At the same time, the 0,25 mm notch outline will be referred to the bottom tibial contour and therefore considered as a 0,5 mm inwards outline. Moving then towards the middle wall region, the z is rising until the maximum of 8,025 mm is reached. If one wanted to stick to the 5,71° inclination angle, a rough 0,8 mm xy translation (t) should be applied to this point ( $t = 0,1 \cdot 8,025$ ).

### Equation 2



$$t = \tan(\alpha) \cdot x = 0,1 \cdot x$$

Since the z increase was gradual and pretty regular on both anterior and posterior sides, it was not necessary to compute t for each single superior wall vertex (that would have required days at the same time), but only for some key z steps. Within the range [0,5 ; 0,8], where 0,5 outline is associate to the minimum wall height and 0,8 to the maximum, additional outlines with 0,025 mm increments were designed, resulting in this sequence of splines (in mm):

- 0,5
- 0,525
- 0,55
- 0,575
- 0,6
- 0,625
- 0,65

- 0,675
- 0,7
- 0,725
- 0,75
- 0,775
- 0,8

These outlines were then translated on top of the lateral wall (Fig. 86).

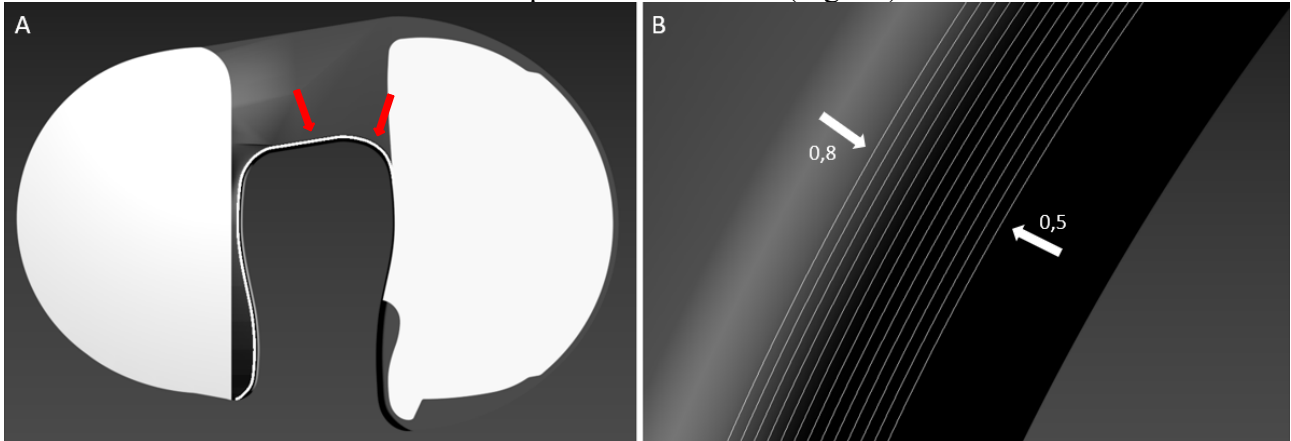


**Figure 86:** the outlines set utilized as reference for the lateral wall inclination (A) and a close-up of the outline succession from 0,5 mm to 0,8 mm with 0,025 mm increments (B). Note that the height of the central and medial regions of the anterior notch rim (red arrows in image A) was not influenced by the wall convexity and therefore kept their initial inclination.

The next step was to design a sinuous and continuous spline, that starting from the 0,5 mm outline at both ends reached the 0,8 mm one at the highest region of the wall, passing by all the intermediate 0,025 mm steps. It was important that the curvature reflected the convexity profile of the wall, such that, for instance, when the reference inclination spline was on the 0,65 mm outline, the underneath wall region was 6,5 mm high. This was not a trivial task and required several tools like refine, trim, weld and fillet, but at the end it resulted in a smooth and precise contour as can be seen in Figure 87.

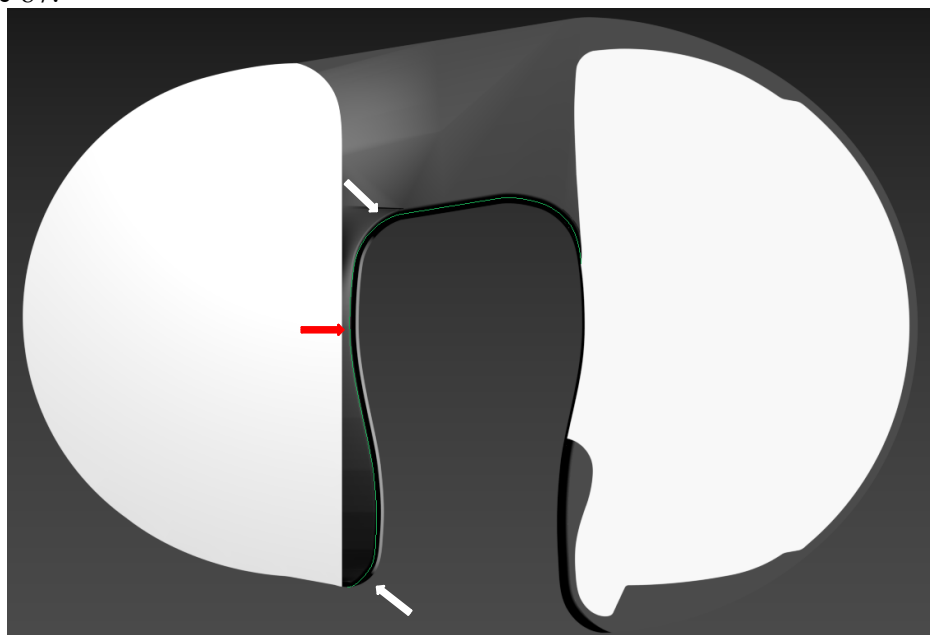


**Figure 87:** final gradual transition spline from the 0,5 (white arrows) to 0,8 (red arrow) mm outline (green).

Having this spline as a top reference the wall chamfer points were translated onto it accordingly and the lateral wall inclination on notch side was therefore completed (Fig. 88).



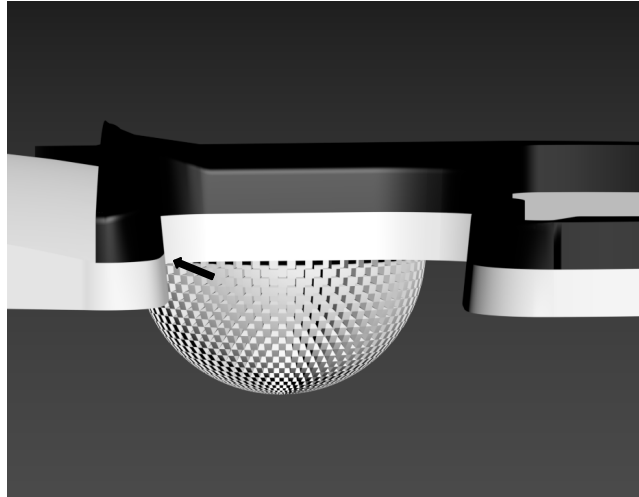


**Figure 88:** restored  $5,71^\circ$  lateral inclination of the notch-facing side of the wall (arrow).

The really last step was to apply the same lateral inclination to the bearing-facing side of the wall. However, for the latter, a trick was exploited in order to simplify the modelling step. Indeed, the bearing interface is not represented by the whole wall lateral height, but just by the portion above the domed plateau. Only this region should be inclined, while the one below should have a vertical interface with the dome mesh. Importantly, this upper region keeps a constant height of 2,5 mm, as the wall convexity is followed by the dome curvature on the lateral side. Hence, a constant 0,25 mm xy translation is required here, contrarily to the point-specific one of the medial side.

Initially the no more suitable previous inclination modifier was deleted. After that, in order to keep the region below the dome intersection vertical, a new edge following the plateau lateral contour on the lateral face of the wall was drawn by cut tool in snap vertex mode (Fig. 89).

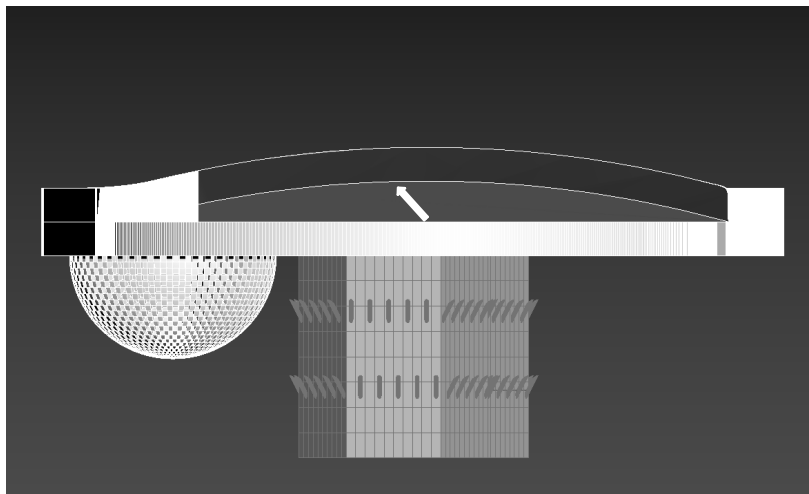


**Figure 89:** convex lateral plateau contour drawn on the lateral face of the wall (white arrow).

The next step was to select the lateral wall border as a whole edge and click on “create shape” in the edit edges panel. This will produce a spline out of the selected border. A 0,25 mm lateral outline was then created from such 2D profile and exploited as a reference for the xy translation of the bearing-facing wall border (Fig. 90A). Each point was therefore manually moved onto the outline by vertex snap tool, until a  $5,71^\circ$  inclination was conferred to the whole lateral wall face (Fig. 90 B). At the end, the posterior chamfer vertices were manually adjusted in x-y direction exploiting again simple geometric laws, as done for the initial tibial implant version (Fig. 90 C).

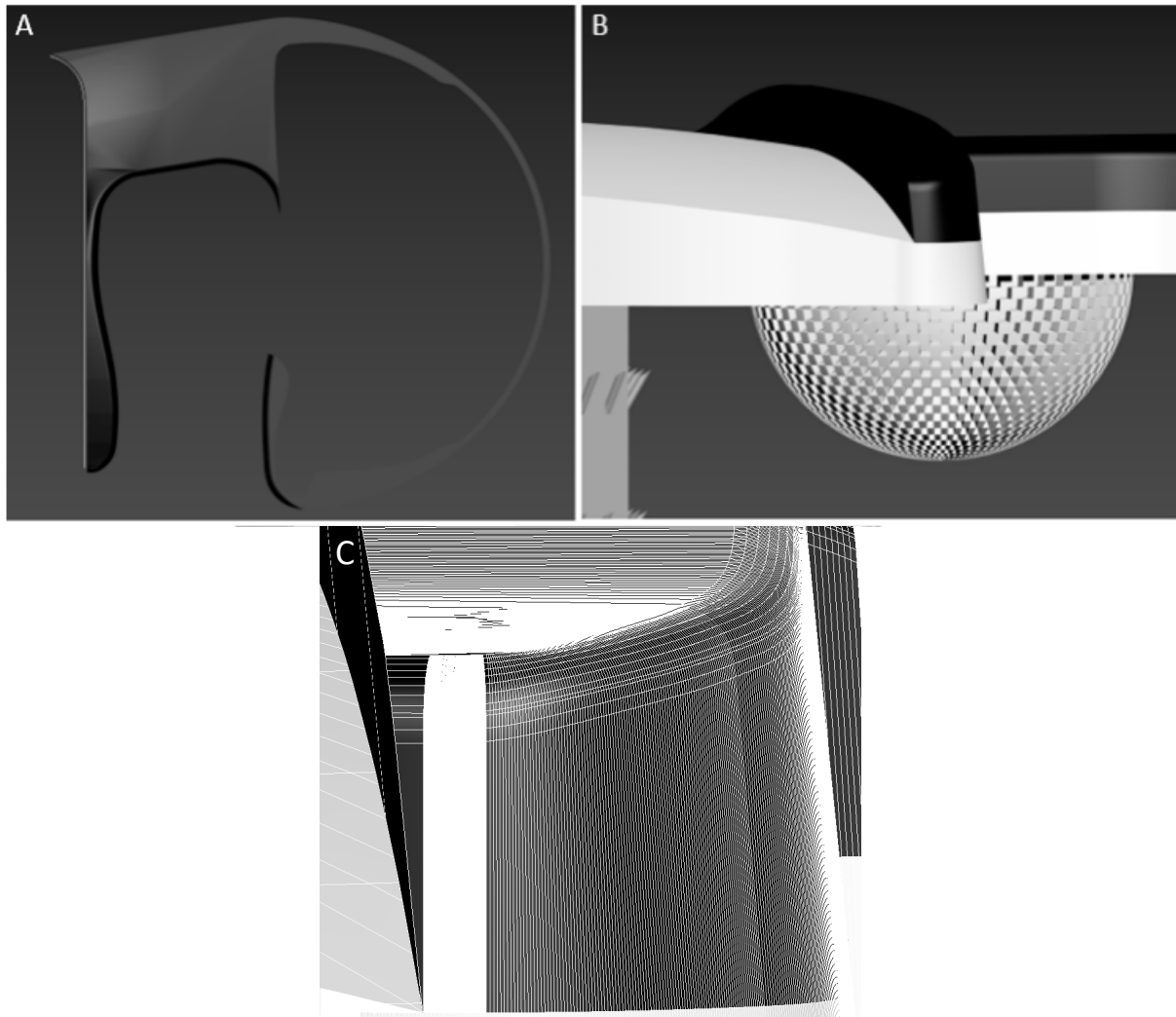


**Figure 90:** 0,25 mm reference inclination outline (A, light grey), translated lateral superior border of the wall resulting in a 5,71° inclination equal to the one on the notch side (B) and a close-up of the manually adjusted wall posterior chamfered edge (C).

A close-up of the convex, inclined lateral wall is showed here below.

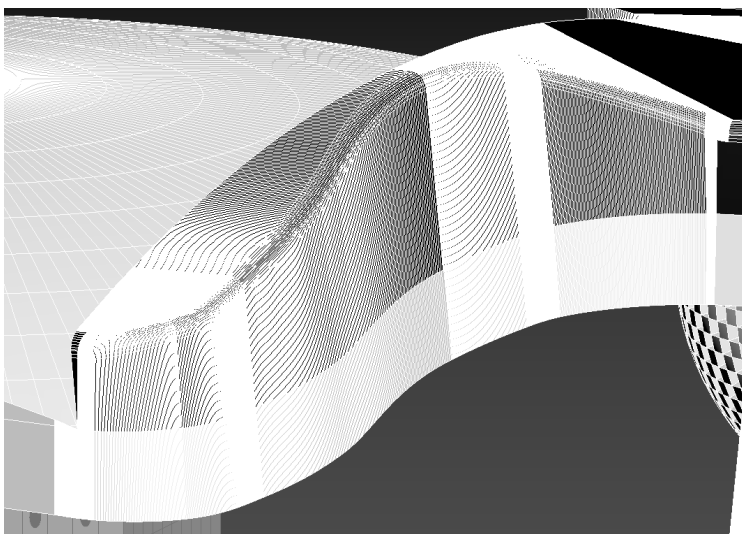


**Figure 91:** the introduced convexity and lateral inclination of the lateral wall, in edged faces mode.

The final tibial component version of our novel “hybrid” BCR TKA design is shown here below from different perspectives.

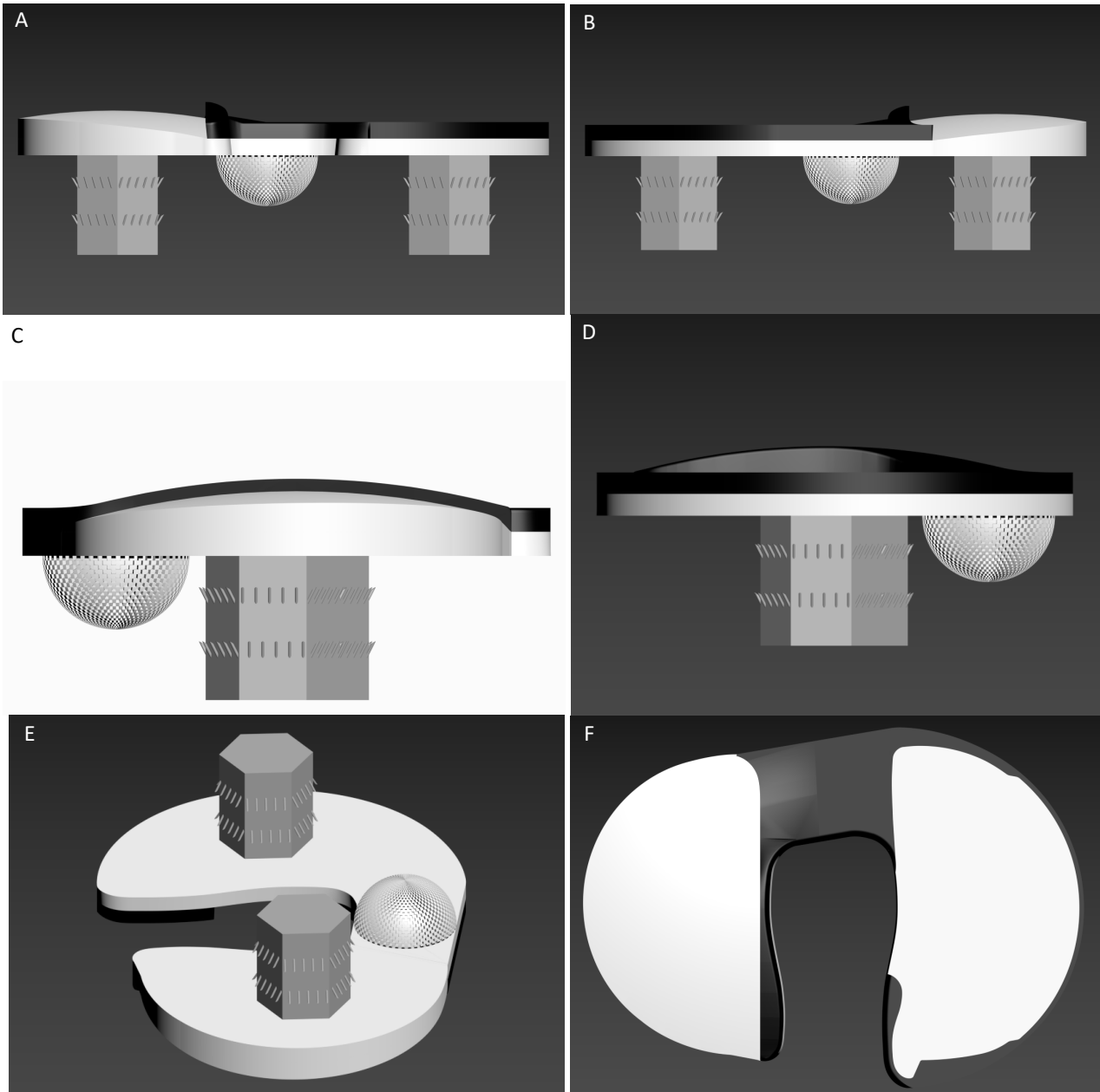


**Figure 92:** Different views of the final version of the novel “hybrid” BCR TKA tibial component design. In order: front (posterior) view (A), back (anterior) view (B), left (lateral) view (C), right (medial) view (D), bottom view (E) and top view (F).

1. <https://drtarabichi.com/> webpage
2. THE PERSONALIZED KNEE® MEDIAL CONGRUENT® BEARING DESIGN RATIONALE. <https://www.zimmerbiomet.com/content/dam/zimmer-biomet/medical-professionals/knee/persona-knee-system/persona-medial-congruent-bearing-design-rationale.pdf>
3. Hofmann AA, Plaster RL, Murdock LE. Subvastus (southern) approach for primary total knee arthroplasty. *Clin Orthop Relat Res.* 1991;269:70–7. [[PubMed](#)] [[Google Scholar](#)]
4. Bindelglass DF, Vince KG (1996) Patellar tilt and subluxation following subvastus and parapatellar approach in total knee arthroplasty – implication for surgical technique. *J Arthroplasty* 11: 507–511
5. Faure BT, Benjamin JB, Lindsey B, Volz RG, Schutte D (1993) Comparison of the subvastus and paramedian surgical approaches in bilateral knee arthroplasty. *J Arthroplasty* 8:511–516
6. Hofmann AA, Plaster RL, Murdock LE (1991) Subvastus (southern) approach for primary total knee arthroplasty. *Clin Orthop* 269: 70–77
7. <http://hofmannarthritisinstitute.com/knee/knee-muscle-sparing-approach/>
8. Bert Parcels TKA BONE CUTS February 24, 2017 knee basics Hip and Knee Book.
9. <https://www.barrons.com/articles/shares-of-hip-replacement-giant-could-gain-25-1458970055>
10. <https://symbios.ch/it/professionisti-del-settore-medico/prodotti-e-soluzioni/origin/>
11. <https://www.orthalign.com/kneealign/>
12. Oktas, B., & Vergili, O. (2018). The effect of intensive exercise program and kinesiotaping following total knee arthroplasty on functional recovery of patients. *Journal of orthopaedic surgery and research*, 13(1), 233. <https://doi.org/10.1186/s13018-018-0924-9>
13. Pozzi, F., Snyder-Mackler, L., & Zeni, J. (2013). Physical exercise after knee arthroplasty: a systematic review of controlled trials. *European journal of physical and rehabilitation medicine*, 49(6), 877–892.
14. Petterson, S. C., Mizner, R. L., Stevens, J. E., Rasis, L., Bodenstab, A., Newcomb, W., & Snyder-Mackler, L. (2009). Improved function from progressive strengthening interventions after total knee arthroplasty: a randomized clinical trial with an imbedded prospective cohort. *Arthritis and rheumatism*, 61(2), 174–183. <https://doi.org/10.1002/art.24167>
15. Bade, M. J., & Stevens-Lapsley, J. E. (2011). Early high-intensity rehabilitation following total knee arthroplasty improves outcomes. *The Journal of orthopaedic and sports physical therapy*, 41(12), 932–941. <https://doi.org/10.2519/jospt.2011.3734>
16. Stevens-Lapsley, J. E., Balter, J. E., Wolfe, P., Eckhoff, D. G., & Kohrt, W. M. (2012). Early neuromuscular electrical stimulation to improve quadriceps muscle strength after total knee arthroplasty: a randomized controlled trial. *Physical therapy*, 92(2), 210–226. <https://doi.org/10.2522/ptj.20110124>
17. <https://www.dell.com/it-it/shop/notebook-dell/inspiron-15-notebook/spd/inspiron-15-5502-laptop>
18. <https://www.prosoftweb.it/post/autodesk-3ds-max>
19. <https://www.autodesk.it/products/3ds-max/overview>

20. <https://area.autodesk.com/all/tutorials/3ds-max/>
21. <https://forums.autodesk.com/t5/3ds-max/ct-p/area-c1>
22. <https://www.poliigon.com/>
23. <https://www.chaosgroup.com/blog/understanding-metalness>
24. <https://www.arnoldrenderer.com/arnold/>
25. <https://knowledge.autodesk.com/support/3ds-max/learn-explore/caas/CloudHelp/cloudhelp/2019/ENU/3DSMax-Rendering/files/GUID-DDD521BE-16A3-4E43-AE40-6B38E588C13A-htm.html>
26. <https://knowledge.autodesk.com/support/3ds-max/learn-explore/caas/CloudHelp/cloudhelp/2017/ENU/3DSMax/files/GUID-31E5AF23-A661-46BB-BA7A-6520C325145E-htm.html>  
NB: the same reference as 25??
27. <https://hdrihaven.com/>
28. Geoffrey H. et al. (1995) Resection Specimen Analysis of Proximal Tibial Anatomy Based on 100 Total Knee Arthroplasty Specimens. *The Journal of Arthroplasty Vol. 10 No. 1*
29. Yifei Dai et al. (2014) Anatomic tibial component design can increase tibial coverage and rotational alignment accuracy: a comparison of six contemporary designs. *Knee Surg Sports Traumatol Arthrosc* 22:2911–2923
30. Sam Tarabichi, M.D. (year?) Unmet Needs in Total Knee Replacement, *PPT presentation for Persona<sup>R</sup>, Zimmer. Tarabichi Joint Replacement Center Dubai*
31. Martin, et al. (2014) Maximizing Tibial Coverage Is Detrimental to Proper Rotational Alignment. *CORR*.
32. Insall JN (1984) Total knee replacement, p. 587. In *Insall JN (ed): Surgery of the knee. Churchill Livingstone, New York, 1984*
33. Bindelglass D, Cohen J, Dorr L (1991) Current principles of design for cemented and cementless knees. *Tech Orthop* 6:80–85
34. Chau R, Gulati A, Pandit H, Beard DJ, Price AJ, Dodd CA, Gill HS, Murray DW (2009) Tibial component overhang following unicompartmental knee replacement—does it matter? *Knee* 16:310–313
35. Burstein AH (1984) Biomechanics of the knee. p. 21. In *Insall JN (ed): Surgery of the knee. Churchill Livingstone, New York.*
36. Colombet, P., Robinson, J., Christel, P., Franceschi, J. P., Djian, P., Bellier, G., & Sbihi, A. (2006). Morphology of anterior cruciate ligament attachments for anatomic reconstruction: a cadaveric dissection and radiographic study. *Arthroscopy : the journal of arthroscopic & related surgery : official publication of the Arthroscopy Association of North America and the International Arthroscopy Association*, 22(9), 984–992.  
<https://doi.org/10.1016/j.arthro.2006.04.102>
37. Girgis, F. G., Marshall, J. L., & Monajem, A. (1975). The cruciate ligaments of the knee joint. Anatomical, functional and experimental analysis. *Clinical orthopaedics and related research*, (106), 216–231. <https://doi.org/10.1097/00003086-197501000-00033>
38. Stäubli, H. U., & Rauschning, W. (1994). Tibial attachment area of the anterior cruciate ligament in the extended knee position. Anatomy and cryosections in vitro complemented by magnetic resonance arthrography in vivo. *Knee surgery, sports traumatology, arthroscopy : official journal of the ESSKA*, 2(3), 138–146.  
<https://doi.org/10.1007/BF01467915>
39. Dijk R van (1983) The behaviour of the cruciate ligaments in the human knee. *Radopi, Amsterdam, pp 1-163*
40. Gandhi, S., Singla, R. K., Kullar, J. S., Suri, R. K., & Mehta, V. (2014). Morphometric analysis of upper end of tibia. *Journal of clinical and diagnostic research : JCDR*, 8(8), AC10–AC13. <https://doi.org/10.7860/JCDR/2014/8973.4736>

41. Jacobsen K. (1974). Area intercondylaris tibiae: Osseous surface structure and its relation to soft tissue structures and applications to radiography. *Journal of anatomy*, 117(Pt 3), 605–618.
42. Servien, E., Saffarini, M., Lustig, S., Chomel, S., & Neyret, P. (2008). Lateral versus medial tibial plateau: morphometric analysis and adaptability with current tibial component design. *Knee surgery, sports traumatology, arthroscopy : official journal of the ESSKA*, 16(12), 1141–1145. <https://doi.org/10.1007/s00167-008-0620-0>
43. Deen, J. T., Clay, T. B., Iams, D. A., Horodyski, M., & Parvataneni, H. K. (2017). Proximal tibial resorption in a modern total knee prosthesis. *Arthroplasty today*, 4(2), 244–248. <https://doi.org/10.1016/j.artd.2017.10.005>
44. Martin, J. R., Watts, C. D., Levy, D. L., Miner, T. M., Springer, B. D., & Kim, R. H. (2017). Tibial Tray Thickness Significantly Increases Medial Tibial Bone Resorption in Cobalt-Chromium Total Knee Arthroplasty Implants. *The Journal of arthroplasty*, 32(1), 79–82. <https://doi.org/10.1016/j.arth.2016.06.007>
45. Martin JR, Watts CD, Levy DL, Kim RH. Medial tibial stress shielding: a limitation of cobalt chromium tibial baseplates. *J Arthroplasty* 2017;32(2):558.
46. Smith and Nephew. GENESIS II Design Rationale Materials Section-Fulfill. 7128-0438 Section G7.
47. Pijls, B. G., Van der Linden-Van der Zwaag, H. M., & Nelissen, R. G. (2012). Polyethylene thickness is a risk factor for wear necessitating insert exchange. *International orthopaedics*, 36(6), 1175–1180. <https://doi.org/10.1007/s00264-011-1412-6>
48. Stress Raiser, *from: Introduction to Aerospace Materials*, 2012. <https://www.sciencedirect.com/topics/engineering/stress-raiser>
49. Sam Tarabichi M.D. (year?) Cementless TKA. Just do it ! PPT presentation for Burjeel Hospital for Advanced Surgery (BAHS). Tarabichi Joint Replacement Center Dubai
50. <https://www.zimmerbiomet.com/content/dam/zimmer-biomet-OUS-Surg-techniques/knee/97-5954-002-00%20Rev%203%20NexGen%20TM%20Modular%20Tibia%20SurgTech-FINAL%20DIGITAL.pdf>
51. Hanzlik J.A., Day J.S., Rinnac C.M., Kurtz S.M., Ingrowth Retrieval Study Group Is there a difference in bone ingrowth in modular versus monoblock porous tantalum tibial trays? *J Arthroplasty*. 2015;30:1073.
52. <https://www.zimmerbiomet.com/content/dam/zimmer-biomet/medical-professionals/000-surgical-techniques/knee/97-5026-027-00%20Rev%205%20PERSONA%20Trabecular%20Metal%20Tibia%20SurgTech-digitalFINAL.pdf>
53. Stilling, M., Madsen, F., Odgaard, A., Rømer, L., Andersen, N. T., Rahbek, O., & Søballe, K. (2011). Superior fixation of pegged trabecular metal over screw-fixed pegged porous titanium fiber mesh: a randomized clinical RSA study on cementless tibial components. *Acta orthopaedica*, 82(2), 177–186. <https://doi.org/10.3109/17453674.2011.566139>
54. Cementless PSI TKA: Optimizing efficiency. Michael A. McShane, MD
55. Persona. The Personalized Knee System. TM Tibia Peg Location – Persona Vs. NexGen. PPT presentation May 1, 2015, Zimmer Biomet.
56. INITIAL FIXATION STABILITY OF TWO TYPES OF CEMENTLESS TKA FEMORAL IMPLANTS Bo Gao (2018) Orthopaedic Proceedings Vol. 98-B, No. SUPP\_1
57. Papas, P. V., Congiusta, D., & Cushner, F. D. (2019). Cementless versus Cemented Fixation in Total Knee Arthroplasty. *The journal of knee surgery*, 32(7), 596–599. <https://doi.org/10.1055/s-0039-1678687>
58. Capella, M., Dolfen, M., & Saccia, F. (2016). Mobile bearing and fixed bearing total knee arthroplasty. *Annals of translational medicine*, 4(7), 127. <https://doi.org/10.21037/atm.2015.12.64>
59. Komistek, R. *et al.* “In Vivo Fluoroscopic Analysis of the Normal Knee.” *Clinical Orthopaedics and Related Research*. 410: 69–81, 2003.

60. Freeman, M. *et al.* "The Movement of the Knee Studied by Magnetic Resonance Imaging." *Clinical Orthopaedics and Related Research*. 410: 35–43, 2003.
61. Persona, THE PERSONALIZED KNEE MEDIAL CONGRUENT<sup>®</sup> BEARING DESIGN RATIONALE
62. TIBIO-FEMORAL MOVEMENT IN LIVING KNEE WITH FULL FLEXION AFTER TKA, Sam Tarabichi *et al.* PPT presentation for American Hospital, Dubai, UAE.
63. Von Keudell, A., Sodha, S., Collins, J., Minas, T., Fitz, W., & Gomoll, A. H. (2014). Patient satisfaction after primary total and unicompartmental knee arthroplasty: an age-dependent analysis. *The Knee*, 21(1), 180–184. <https://doi.org/10.1016/j.knee.2013.08.004>
64. Ode, Q., Gaillard, R., Batailler, C., Herry, Y., Neyret, P., Servien, E., & Lustig, S. (2018). Fewer complications after UKA than TKA in patients over 85 years of age: A case-control study. *Orthopaedics & traumatology, surgery & research : OTSR*, 104(7), 955–959. <https://doi.org/10.1016/j.otsr.2018.02.015>
65. Pinskerova V, Iwaki H, Freeman MA. The shapes and relative movements of the femur and tibia at the knee. *Orthopade* 2000;29(Suppl. 1):S3–5.
66. Hill PF, Vedi V, Williams A, Iwaki H, Pinskerova V, Freeman MA. Tibiofemoral movement 2: the loaded and unloaded living knee studied by MRI. *J Bone Joint Surg Br* 2000;82(8):1196–8.
67. Iwaki H, Pinskerova V, Freeman MA. Tibiofemoral movement 1: the shapes and relative movements of the femur and tibia in the unloaded cadaver knee. *J Bone Joint Surg Br* 2000;82(8):1189–95.
68. O'Connor JJ, Shercliff TL, Biden E, Goodfellow JW. The geometry of the knee in the sagittal plane. *Proc Inst Mech Eng [H]* 1989;203–4:223–33.
69. Nakagawa S, Kadoya Y, Todo S, Kobayashi A, Sakamoto H, Freeman MA, *et al.* Tibiofemoral movement 3: full flexion in the living knee studied by MRI. *J Bone Joint Surg Br* 2000;82-8:1199–200.
70. N. Poirier, P. Graf, F. Dubrana, Mobile-bearing versus fixed-bearing total knee implants. Results of a series of 100 randomised cases after 9years follow-up, *Orthopaedics & Traumatology: Surgery & Research*, Volume 101, Issue 4, Supplement, 2015, Pages S187-S192, ISSN 1877-0568, <https://doi.org/10.1016/j.otsr.2015.03.004>.
71. Huang, C. H., Liao, J. J., & Cheng, C. K. (2007). Fixed or mobile-bearing total knee arthroplasty. *Journal of orthopaedic surgery and research*, 2, 1. <https://doi.org/10.1186/1749-799X-2-1>
72. Łapaj, Ł., Mróz, A., Kokoszka, P., Markuszewski, J., Wendland, J., Helak-Łapaj, C., & Kruczyński, J. (2017). Peripheral snap-fit locking mechanisms and smooth surface finish of tibial trays reduce backside wear in fixed-bearing total knee arthroplasty. *Acta orthopaedica*, 88(1), 62–69. <https://doi.org/10.1080/17453674.2016.1248202>
73. Li S, Scuderi G, Furman BD, Bhattacharyya S, Schmieg JJ, Insall JN. Assessment of backside wear from the analysis of 55 retrieved tibial inserts. *Clin Orthop Relat Res*. 2002;404:75–82.
74. Wasielewski RC, Parks N, Williams I, Surprenant H, Collier JP, Engh G. Tibial insert undersurface as a contributing source of polyethylene wear debris. *Clin Orthop Relat Res*. 1997;345:53–59.
75. <file:///C:/Users/DIEGO/Desktop/PE%20fixed%20medial%20bearing/Persona%C2%AE%20Medial%20Congruent%E2%84%A2%20Bearing.htm>
76. O'Rourke MR, Callaghan JJ, Goetz DD, Sullivan PM, Johnston RC. Osteolysis associated with a cemented modular posteriorcruciate- substituting total knee design: five to eight-year followup. *J Bone Joint Surg Am*. 2002;84:1362–1371.
77. Robinson EJ, Mulliken BD, Bourne RB, Rorabeck CH, Alvarez C. Catastrophic osteolysis in total knee replacement: a report of 17 cases. *Clin Orthop Relat Res*. 1995;321:98–105.

78. Engh GA, Ammeen DJ. Session II: Polyethylene wear. *Clin Orthop Relat Res.* 2002;404:71–74.
79. Rodriguez JA, Baez N, Rasquinha V, Ranawat CS. Metal-backed and all polyethylene tibial components in total knee replacement. *Clin Orthop Relat Res.* 2001;392:174–183.
80. Conditt MA, Stein JA, Noble PC. Factors affecting the severity of backside wear of modular tibial inserts. *J Bone Joint Surg Am.* 2004;86:305–311.
81. Engh GA, Koralewicz LM, Pereles TR. Clinical results of modular polyethylene insert exchange with retention of total knee arthroplasty components. *J Bone Joint Surg Am.* 2000;82:516–523.
82. Costa L, Luda MP, Trossarelli L, Brach del Prever EM, Crova M, Gallinaro P. Oxidation in orthopaedic UHMWPE sterilized by gamma-radiation and ethylene oxide. *Biomaterials.* 1998;19:659–668.
83. Kurtz SM, Muratoglu OK, Evans M, Edidin AA. Advances in the processing, sterilization, and crosslinking of ultra-high molecular weight polyethylene for total joint arthroplasty. *Biomaterials.* 1999;20:1659–1688.
84. Pang HN, Jamieson P, Teeter MG, McCalden RW, Naudie DD, MacDonald SJ. Retrieval analysis of posterior stabilized polyethylene tibial inserts and its clinical relevance. *J Arthroplasty.* 2014;29:365–368.
85. Wasielewski RC. The causes of insert backside wear in total knee arthroplasty. *Clin Orthop Relat Res.* 2002;404:232–246.
86. Wasielewski RC, Galante JO, Leighty RM, Natarajan RN, Rosenberg AG. Wear patterns on retrieved polyethylene tibial inserts and their relationship to technical considerations during total knee arthroplasty. *Clin Orthop Relat Res.* 1994;299:31–43.
87. Kurtz SM, Gawel HA, Patel JD. History and systematic review of wear and osteolysis outcomes for first-generation highly crosslinked polyethylene. *Clin Orthop Relat Res.* 2011;469:2262–2277.
88. Conditt MA, Stein JA, Noble PC. Factors affecting the severity of backside wear of modular tibial inserts. *J Bone Joint Surg Am.* 2004;86:305–311.
89. Sisko, Z. W., Teeter, M. G., Lanting, B. A., Howard, J. L., McCalden, R. W., Naudie, D. D., MacDonald, S. J., & Vasarhelyi, E. M. (2017). Current Total Knee Designs: Does Baseplate Roughness or Locking Mechanism Design Affect Polyethylene Backside Wear?. *Clinical orthopaedics and related research*, 475(12), 2970–2980. <https://doi.org/10.1007/s11999-017-5494-3>
90. <https://www.smithnephew.com/global/assets/pdf/anthem%20total%20knee%20system%20design%20rationale.18%2016392%20v3.pdf>
91. Zimmer® Unicompartamental High Flex Knee System, brochure.
92. <https://www.zimmerbiomet.com/content/dam/zimmer-biomet/medical-professionals/knee/oxford-partial-knee/why-oxford-partial-knee-key-points-clinical-rationale.pdf>
93. <https://www.zimmerbiomet.com/medical-professionals/knee/product/oxford-partial-knee.html>
94. Goodfellow JW, Kershaw CJ, Benson M.K, O'Connor JJ. The Oxford Knee for unicompartamental osteoarthritis. The first 103 cases. *J Bone Joint Surg Br* 1988;70-5:692 – 701.
95. Gunther TV, Murray DM, Miller R, Wallace DA, Carr AJ, O'Connor JJ, et al. Lateral compartment arthroplasty with the Oxford Meniscal knee. *Knee* 1996;3:33–9.
96. Murray DW, Goodfellow JW, O'Connor JJ. The Oxford medial unicompartamental arthroplasty: a ten-year survival study. *J Bone Joint Surg Br* 1998;80-6:983 –9.
97. Svard UC, Price AJ. Oxford medial unicompartamental knee arthroplasty. A survival analysis of an independent series. *J Bone Joint Surg Br* 2001;83-2:191 –4.
98. Newman JH. Unicompartamental knee replacement. *Knee* 2000;7: 63– 70.



99. Baré, J. V., Gill, H. S., Beard, D. J., & Murray, D. W. (2006). A convex lateral tibial plateau for knee replacement. *The Knee*, 13(2), 122–126. <https://doi.org/10.1016/j.knee.2005.09.001>
100. <https://www.oxfordpartialknee.net/content/dam/zb-minisites/oxford-partial-knee-hcp/documents/oxford-domed-lateral-pkr-brochure.pdf>
101. B.J. Robinson et al. Dislocation of the bearing of the Oxford Lateral Unicompartmental arthroplasty. A Radiological Assessment. *JBJS Vol 84-B*, No.5, July 2002
102. Duren et al. A new domed tibial lateral component provides improved range of movement & retains normal kinematics for the Oxford UKR. Presentation. EFORT 2007
103. Pandit, H., Jenkins, C., Beard, D. J., Price, A. J., Gill, H. S., Dodd, C. A., & Murray, D. W. (2010). Mobile bearing dislocation in lateral unicompartmental knee replacement. *The Knee*, 17(6), 392–397. <https://doi.org/10.1016/j.knee.2009.10.007>
104. Streit, M. R., Walker, T., Bruckner, T., Merle, C., Kretzer, J. P., Clarius, M., Aldinger, P. R., & Gotterbarm, T. (2012). Mobile-bearing lateral unicompartmental knee replacement with the Oxford domed tibial component: an independent series. *The Journal of bone and joint surgery. British volume*, 94(10), 1356–1361. <https://doi.org/10.1302/0301-620X.94B10.29119>
105. Altuntas, A. O., Alsop, H., & Cobb, J. P. (2013). Early results of a domed tibia, mobile bearing lateral unicompartmental knee arthroplasty from an independent centre. *The Knee*, 20(6), 466–470. <https://doi.org/10.1016/j.knee.2012.11.008>

### **Use this in the rendering results section.**

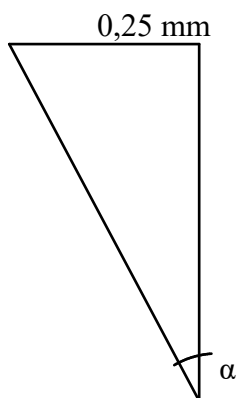
Three physical cameras, with the target directed towards the centre of the implant, were applied to the scene resulting in a front view, a top-front view and a bottom-right view. An exposure gain of 8 EV gave the best rendering results, while the focal length was kept as the default 40mm.

Among these, the best result was given by “Photo\_Studio\_01”, as it was providing a wide, white studio image for photoshoot with a few objects in it, therefore producing the perfect lighting of the scene without too much reflection on the highly polished metal product. Indeed, this material was created with a highly reflecting surface and therefore when an outdoor image or an indoor one full of objects were applied as environment, the original light-grey colour of the polished metal gave way to the blue of the sky or the surrounding things colours. Only a clean environment with a neutral white colour as a background preserved the metallic colouring and a few realistic reflections on it, without going too far. Finally, a spherical environmental mapping and an offset of 0,22 and -0,06 in U and V direction respectively of the HDRI guaranteed the optimal positioning of the background image around the rendered prosthesis

Acta Orthopaedica 2011; 82 (2): 177–186 179 by a peripheral locking mechanism. The NexGen trabecular metal (TM) monobloc (Zimmer) has 2 hexagonal trabecular metal pegs for direct press-fit fixation in the tibial cancellous condyle surface (Figures 2 and 3). Trabecular metal consists of tantalum with 75–80% porosity, a mean pore size of 430  $\mu\text{m}$ , and an elastic modulus similar to that of subcondral bone (Bobyne et al. 1999a, Rahbek et al. 2005a).

Table 1: AP Dimensions (mm)  
(Mean  $\pm$  Standard Deviation)

$AP_{\text{medial}} 10\%$	$37,9 \pm 4,2$
$AP_{\text{medial}} 20\%$	$47,4 \pm 4,8$
$AP_{\text{medial}} 30\%$	$50,6 \pm 5,8$
$AP 50\%$	$42,9 \pm 6,8$
$AP_{\text{lateral}} 10\%$	$34,8 \pm 4,5$
$AP_{\text{lateral}} 10\%$	$41 \pm 4,9$
$AP_{\text{lateral}} 10\%$	$41,6 \pm 5,4$



$\alpha$   
2,5 mm

$$= \tan^{-1} (0,25/2,5) = 5,71^\circ$$

ok

